Louisiana State University

LSU Scholarly Repository

LSU Doctoral Dissertations

Graduate School

January 2020

Experimental Evaluation of How Mineralogy and Microstructure Impact Micro-Geomechanics of Shale Rocks

Hui Du

Louisiana State University and Agricultural and Mechanical College

Follow this and additional works at: https://repository.lsu.edu/gradschool_dissertations

Part of the Petroleum Engineering Commons

Recommended Citation

Du, Hui, "Experimental Evaluation of How Mineralogy and Microstructure Impact Micro-Geomechanics of Shale Rocks" (2020). *LSU Doctoral Dissertations*. 5134.
https://repository.lsu.edu/gradschool_dissertations/5134

This Dissertation is brought to you for free and open access by the Graduate School at LSU Scholarly Repository. It has been accepted for inclusion in LSU Doctoral Dissertations by an authorized graduate school editor of LSU Scholarly Repository. For more information, please contactgradetd@lsu.edu.

EXPERIMENTAL EVALUATION OF HOW MINERALOGY AND MICROSTRUCTURE IMPACT MICRO-GEOMECHANICS OF SHALE ROCKS

A Dissertation

Submitted to the Graduate Faculty of the
Louisiana State University and
Agricultural and Mechanical College
in partial fulfilment of the
requirements for the degree of
Doctor of Philosophy

in

The Craft & Hawkins Department of Petroleum Engineering

by
Hui Du
B.S., China University of Petroleum, Beijing, 2011
B.S., University of Alaska Fairbanks, 2011
M.S., Missouri University of Science and Technology, 2013
May 2020

ACKNOWLEDGMENTS

I would like to express the deepest appreciation to my advisor, Dr. Yuanhang Chen, for graciously serving as my doctoral research committee chair. I also want to appreciate my former advisor, Dr. Mileva Radonjic, who is my mentor in both research and life. It would not be possible to finish my Ph.D. journey without them.

My sincere gratitude also goes to my committee members: Dr. Amitava Roy, Dr. Barbara Dutrow, Dr. Shengli Chen, Dr. Seung Kam, and the graduate school Dean's Representative Dr. Junhong Liang for their invaluable contributions, criticisms, and cooperation.

I would like to thank Dr. Clayton Leohn and Dr. Dongmei Cao of the LSU Material Characterization Center for their help and training with the imaging equipment, sample preparation, and image interpretation. I wish to acknowledge Mr. Fenelon Nunes and Ms. Janet Dugas from the Craft and Hawkins Department of Petroleum Engineering for helping with purchases, maintenance, reservations, and paperwork. I also thank Dr. Radisav Vidic, Dr. Daniel Hill, Dr. Chunxiao Li, Halliburton and LaFarge companies, for providing the necessary rock and cement materials. I am appreciative of friends and colleagues with whom I co-authored publications, shared and gained useful ideas, including Arome Oyibo, Darko Kupresan, Abiola Olabode, Kristen Carpenter, Alan Didier, and Ruixuan Guo.

I am grateful to my parents and parents-in-law for their unrelenting support. Special thanks to my beloved wife, Dr. Shuang Cao, for her help, encouragement, and great patience throughout my Ph.D. journey. To our daughter, Anna Du, thanks for being the beaming light and making this part of our lives enriching.

TABLE OF CONTENTS

LIST OF TABLES

LIST OF FIGURES

NOMENCLATURE

A, Contact area (nm^2)

a, Impression length (nm)

c, Average length of the radial cracks (nm)

E, Young’s Modulus (GPa)

Ei, Young’s Modulus of the indenter (GPa)

Er, Reduced modulus (GPa)

Gm, Medium mineral grains

Gr, Rigid mineral grains

Gs, Soft mineral grains

H, Hardness (GPa)

h, Penetration depth (nm)

Kc, Fracture toughness (MPa m$^{1/2}$)

l, Average length of a Palmqvist crack (nm)

P, Indentation load (mN)

S, Slope of the unloading curve (mN nm^{-1})

ν, Poisson’s Ratio

νi, Poisson’s Ratio of the indenter tip

ξ , Constant depending on the indenter geometry

ABSTRACT

Shales play an essential role in petroleum exploration and production because they can occur either as unconventional reservoir rocks for hydrocarbon extraction via hydraulic fracturing or as caprocks for conventional reservoirs and subsurface gas/ waste storage. For both extraction and storage applications, the success rate is directly depending on the rigorous candidate selection. Conventional rock characterization techniques normally measure rock properties by seismic/logging at the reservoir scale, and on drilled/outcrop cores at the core scale. However, shales are highly heterogeneous in composition, containing a large number of reactive minerals in micro/nanoscale with significantly different properties. The structural features and properties of these minerals at the micro/nanoscale can impact the durability performance of rock materials at the macroscale.

This study compares properties of several types of shales measured at mineral scale, with the intent to predict the rock susceptibility to fracturing at a larger scale since all fractures are initiated at atomic scale imperfections. Indentation tests were conducted at micro and nanometer scales on sections cut from drilled core samples to obtain the mechanical properties of the bulk and individual mineralogical phases. Their durability performances under stress were combined with the differences observed in depth, lamination, composition, as well as microstructure to give the final conclusion. High-resolution microscopy and Energy Dispersive X-Ray Spectroscopy (EDS) analysis were combined to provide a spatial link between geochemistry and geomechanics at micro and nano scale.

Results from this study indicated 1). Shale caprocks had the higher bulk mechanical properties, more uniform grain size, higher rigid grain content, and lower degree of anisotropy than the shale reservoir rocks; 2) Fractures were more likely initiated at the boundary of two mechanically different mineral grains, and the fracture/deformation within the caprocks can be self-healed within few months.

This study provides a time and cost efficient way for rock geomechanical evaluation to help the identified the optimal target/candidate for subsurface applications by evaluating the mechanical properties of shale and their susceptibility to fracturing. Also, the non-destructive nature of testing makes it possible for the dynamic study of the rock in contact with different fluids and dry/wet cycling conditions.

1. INTRODUCTION

1.1.PROBLEM STATEMENT

Shales play an essential role in petroleum exploration and production because they can occur either as unconventional reservoir rocks for hydrocarbon extraction via hydraulic fracturing or as caprocks for conventional reservoirs and subsurface gas/ waste storage. In general, shale formations in which permeability can be significantly enhanced by the formation of hydraulic fractures can be the target for hydrocarbon extraction, while the ones with low permeability and resilient to the formation of fractures are ideal for underground storage (CO_2 sequestration, waste disposals). Hydraulic fracturing has been used to produce hydrocarbons from shales for a number of years, but the fundamental mechanism to initiate and propagate these fractures remains unclear. The non-productive perforation clusters percentage range from 21% (Eagleford shale) to 32% (Woodford shale) with an average of 29.6% [Miller et al., 2011]. As for carbon capture and storage (CCS), although it is by far the only technology which can reduce emissions on a significant scale and CO_2 storage in oil and gas reservoirs is not likely to lead to technological difficulties, the CCS projects have been limited to a few industrial applications and still be in waiting for large scale industrial application [Global CCS Institute, 2015; 2019], due to the concern of potential gas leakage to water aquifers or atmosphere.

For both applications, the success rate is directly depending on rigorous candidate selection. Unfortunately, there has not been a well-defined and unified approach to address this process up to now. In order to the evaluation of subsurface resources as well as the safety assessment of waste disposals and CO_2 sequestration, it is desirable to have detailed characterization of the shale and establish the following properties in order to estimate whether or not they are suitable hydrocarbon resources/subsurface seals: mineralogical composition, petrophysical properties (porosity and permeability), mechanical properties (compressive and tensile strength, Young's modulus and/or hardness). Basically, all subsurface shale formations can be divided into these two end members based on petrophysical and geomechanical properties: caprocks or reservoir rocks.

The common practice for rock characterization in the literature is screening the formations based on influencing variables such as skin factor, permeability, porosity, etc. [Samsuri et al., 2012]. Rock properties are measured by seismic/logging at reservoir scale, on drilled/outcrop cores at core scale, the microscopic scale is done on drilling cuttings or rock fragments/polished thin sections and lately on the nanoscale. However, shales are highly heterogeneous in composition, containing a large number of reactive minerals in micro/nanoscale with significantly different properties. The structural features and properties of these minerals at the micro/nanoscale can impact the durability performance of rock materials at the macroscale.

Since the shale properties are controlled by the rock mineralogical composition and the internal structure of different types of minerals, this study is focused on these two most fundamental aspects of the rock: mineralogy and microstructure. This study compares properties of several types of shales measured at mineral scale, with the intent to predict the rock susceptibility to fracturing at a larger scale, since all fractures are initiated at atomic scale imperfections (crystal defects such as impurities or deformations).

1.2.THESIS SCOPE AND OBJECTIVES

For the evaluation of subsurface resources as well as the safety assessment of waste disposals and CO_2 sequestration, it is desirable to have a detail characterization of rock petro-physically, mechanically and mineralogically. The utilization of shale formation depends on its petrophysical and geomechanical properties. The mechanical properties of the rock are the key factors that determine the likelihood of rock failure (fracture initiating and propagating), while the petrophysical properties (porosity and permeability) control the fluid migration within the rock. Both of these properties are controlled by the rock mineralogical composition and the internal arrangement of different types of minerals known as the microstructure.

The main objective of this study is to relate the mechanical property differences of the rocks to their mineralogical composition and microstructure alterations to link between geochemistry and geomechanics of shales, so that the rock behavior can be better understood at the subsurface condition, the knowledge on shale mineralogy /microstructure and its impact on rock behavior can be used to guide the candidate selection for different shale applications.

The second objective is to draw analogies with shales and cement behavior as effective hydraulic barriers in subsurface conditions. The main engineered hydraulic barrier in wellbores, the cement sheath, can be subjected to many types of failures during the well life, while shale caprocks are natural materials that have superior hydraulic barrier characteristics to cement. The goal is by investigating the similarities of hydraulic barrier features to help improve the subsurface application of engineered hydraulic barriers in zonal isolation.

2. BACKGROUND AND LITERATURE REVIEW

2.1. FUNDAMENTALS OF SHALES

2.1.1 Definition, Classification, Mineralogical Composition

Shale is the most abundant of the sedimentary rock. It is deposited and formed by squeezing excess formation water and mineralogical transformations at different temperatures and pressures. Shales have distinct laminated layering characteristics and high clay and/or silt content. There are two main chemical processes responsible for these formations, with two fundamental mechanisms: 1) neoformation – precipitation from solution; and, 2) transformation – a new clay mineral inherits part of its silicate skeleton from preexisting materials such as phyllosilicate [Diaz-Perez et al., 2007]. Shales are typically laminated and fissile. In order for fine clay and silt particles to form, larger organic pieces must be broken down and deposited in environments conducive to shale formation. The processes that break down these larger pieces into clay or silt sized particles include chemical weathering in soils, the formation of authigenic minerals at the sediments depositional sit, the formation of diagenetic minerals after deposition, and clay minerals formed by hydrothermal alteration [Diaz-Perez et al., 2007; Du et al., 2017a].

Shales are predominantly composed of clay minerals. They might also have other silica and carbonate based minerals that contribute to their geomechanical strength, the most commonly seen minerals in shale are listed in Table 2.1 below together with their general formulae. In 1965, Shaw and Weaver documented the average mineralogical composition of shales from three hundred rock samples showing: 30.8 percent quartz, 4.5 percent feldspar, 3.6 percent carbonate, <0.5 percent iron oxides, 60.9 percent clay minerals, 1 percent organic material, and 2 percent other materials [Shaw and Weaver, 1965]. The shale with high clay content showed low permeability, high absorption capacities, and slow dissolution kinetics [Tournassat et al., 2015], which made it remarkably stable as a barrier material at the subsurface condition.

Table 2.1. Mineralogical composition of shale and their general formula [Drever, 1982; Hussain et al., 1996; Bergaya and Lagaly, 2013; Yu et al., 2017]

Category	Minerals	General Formula*
tectosilicates	Quartz	SiO_2
	K-feldspar	$KAlSi_3O_8$
	Plagioclase	$NaAlSi_3O8 – CaAl_2Si_2O_8$
phyllosilicates (clays)	Chlorite	$(Mg,Fe)_3(Si,Al)_4O_{10}(OH)_2 \cdot (Mg,Fe)_3(OH)_6$
	Illite	$(K,H_3O)(Al,Mg,Fe)_2(Si,Al)_4O_{10}[(OH)_2,(H_2O)]$
	Kaolinite	$Al_2Si_2O_5(OH)_4$
	Smectite (Montmorillonite)	$(Na,Ca)_{0.33}(Al,Mg)_2(Si_4O_{10})(OH)_2 \cdot nH_2O$
other minerals (primarily carbonates)	Calcite	$CaCO_3$
	Dolomite	$CaMg(CO_3)_2$
	Pyrite	FeS_2
	Halite	NaCl
	Hematite	Fe_2O_3
	Ankerite	$Ca(Fe,Mg,Mn)(CO_3)_2$
	Siderite	$FeCO_3$
	Fluorapatite	$Ca_5(PO_4)_3F$

*Chemical composition is idealized. Minerals in natural rocks are rarely found separately (especially for clays), they are usually mixed with each other.

Clays, as the major constituent of shales, have currently attracted great interest and are subjected to an intensive examination because of their extraordinary properties. Clay minerals are classified as “silicates”. Natural clays are highly heterogeneous in composition and contain impurities in the form of associated minerals, their chemical composition typically includes more oxygen than Si, Al, or Mg, so many arguably consider them as (hydr)oxides of silicon, aluminum, or magnesium [Bergaya and Lagaly, 2013]. Shales are predominantly composed of clay such as kaolinite, smectite, and illite. Bourg [2015] documented different shale formations showing the relationship between their utility and composition. Clay mineral content was identified as a very important variable that controls the key material properties of these formations. Shale formations with high clay content (> 35%) are utilized as seals (shale caprock) for carbon capture and storage (CCS) and nuclear waste storage, because of their low permeability and resilience to the formation of fractures[Du et al., 2017a]; while shale formations with low clay content are more suitable for unconventional hydrocarbon extraction as their permeability can be significantly enhanced by the formation of hydraulic fractures [Bourg, 2015.]

2.1.1.1. Structure of clay

Clay minerals are one of the major constituents of natural geomaterial, they are mostly composed of oxygen, silicon, hydrogen, aluminum as well as calcium, sodium, potassium, magnesium, and iron [Mitchell and Soga, 2005]. Most clay minerals are made of two distinct building blocks: tetrahedrons (T) and octahedrons (O) as shown in Figure 2.1. The tetrahedral and octahedral sheet may condense in either a 1:1 or 2:1 proportion to form a layered structure. The 1:1 layer structure consists of the repetition of one tetrahedral and one octahedral sheet (T-O), such as in kaolinite, while in the 2:1 layer structure one octahedral sheet is sandwiched between two tetrahedral sheets (T-O-T), such as in smectite. The schematics of the T and O building blocks, as well as the 1:1 and 2:1 layer structures, are shown in Figure 2.1 below. The layer structures showed here is simplified, in fact, the lateral dimension of the T sheet is usually greater than the O sheet, causing a lateral misfit between the two sheets, adjustment is required in one or both sheets to match of the lateral dimensions, this is known as Layer Distortion [Brindley and Brown, 1980; Moore and Reynolds, 1989; Bergaya and Lagaly, 2013]

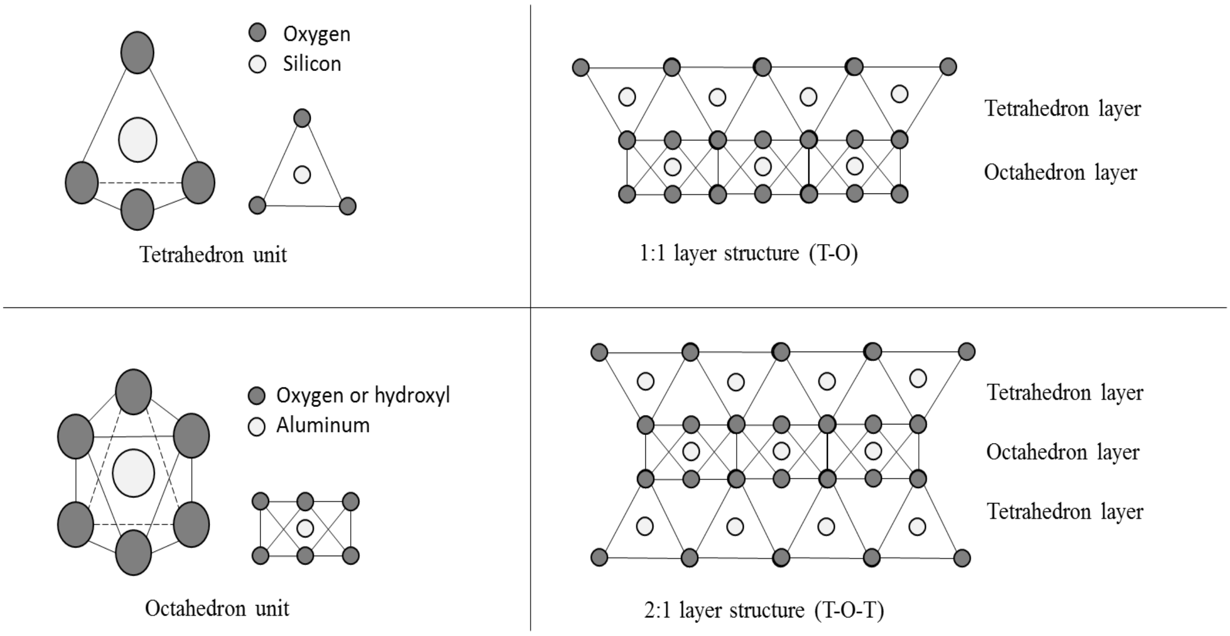

Fig. 2.1. Schematics of the tetrahedrons and octahedrons building blocks (left) and the basic layer structures of clay minerals, the bonding between sheet is covalent bond (right) [Figure redraw from Nelson, 2015]

The assembly of these sheets makes clay particles, the arrangement of these particles leads to different morphologies, such as plates, tubules, laths, and fibers. All the clay minerals are therefore porous, containing pores of varied size and shape (interlayer, inter-particle /inter-aggregate pores) [Bergaya and Lagaly, 2013]. Figure 2.2 below showed the schematic of structures of the four most commonly seen clay minerals as well as their dimensions. The porous microstructure gives clay minerals a significantly larger surface area than other minerals because of the internal and external surfaces [Van Olphen, 1963; Van Olphen and Fripiat, 1979; Drever, 1982]. The approximately surface areas of these four clay minerals as well as their Cation Exchange Capacities (CEC) are listed in Table 2.2 below. CEC describes the capacity of minerals to hold exchangeable cations, which will be further discussed later. The surface area and CEC of clay are also compared with the most commonly seen mineral in sedimentary rock, quartz [Katsube et al., 2003; Bergaya and Lagaly, 2013; Ag Source Laboratories, 2017]. As shown from Table 2.2, clay minerals not only have a magnitude larger surface area, they also have a much higher surface charge, which leads to the next part, the charge of the clay.

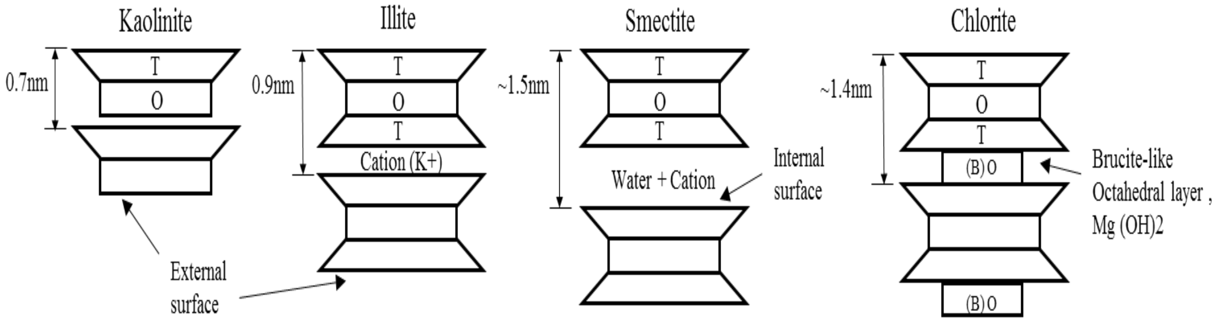

Fig. 2.2. Schematic of structures of different types of clay and their dimensions, from left to right are: 1) 1:1 layer (T-O) kaolinite; 2) 2:1 (T-O-T) layer non-expandable illite; 3) 2:1 layer expandable smectite; 4) 2:1:1 (T-O-T-B) chlorite. Illite has cations (commonly K+) between two layers and smectite has both water molecules and cations between the layers. Illite and smectite commonly exist in natural rock as a mixture known as I-S mixed layers. [Figures redraw from Mitchell, 1993]

Table 2.2. Approximately surface area of common clay minerals and their Cation Exchange Capacities (CEC) [Katsube et al., 2003; Bergaya and Lagaly, 2013; Ag Source Laboratories, 2017]

Clay	Surface Area (m^2/g)			CEC (meg/100g)
	internal	external	Total	
Smectite	750	50	800	80-150
Illite	0	15	15	15-40
Kaolinite	0	15	15	3-10
Chlorite	5	25	30	<10
Quartz			~3	1-2

2.1.1.2. Charge of clay

The net charge of the clays is a sum of permanent charge and pH-dependent charge. Permanent charge, also known as structural charge, is commonly a negative charge because of the isomorphous substitution. Lower charge cations replace higher charge cations as central cation leaves a net negative charge. Common examples include Al for Si in the tetrahedral sheet and Mg for Al in the octahedral sheet. When Al substitutes for Si, local distortions occur because of the bond length difference between Si–O and Al–O [Nemecz, 1981], leaving the clays a negative charge. The strength of a bond is proportional to the difference in atoms' electronegativities, following the order of:

$$\text{H-O} < \text{Si-O} < \text{Al-O} < \text{Mg-O} < \text{Li-O}$$

This is also why it was named permanent charge, once Al replaced Si, AL-O bond has higher strength than Si-O, making it hard to be reversed. As a consequence of the ion substitution, the charge of clay increase in the same order(Si < Al < Mg <Li) [Bergaya and Lagaly, 2013]. Besides the isomorphous substitution, the Layer Distortion can also contribute to the permanent charge.

The origin of pH-dependent charges is due to the chemical reaction happened at the mineral surfaces, it can be either positive or negative depending on the type of metal ion and the pH of the surrounding solution [Schoonheydt and Johnston, 2006]. The pH dependent charges provide the major proportion of total net charge for 1:1 layer clay such as kaolinite, but it only accounts for a small proportion of the total charge for 2:1 layer clays like smectite. The pH value where the net surface charge equals to zero is referred to as the point of zero charge (ZPC). Table 2.3 below list the ZPC values of some common minerals from different works of literature:

Table 2.3. Zero Point of Charge of some minerals [Somasundaran and Agar, 1967; Drever, 1982; Hussain et al., 1996; Yin et al., 2013]

Minerals	pH
SiO_2 (Quartz)	2
SiO_2 (Gel)	1.0-2.5
Calcite	8-9.5
Feldspars	2.0-2.4
Kaolinite*	3.5-4.6
Illite	2.5
Montmorillonite	<2.5
Chlorite	3-5.5
Albite	2

2.1.1.3. Diffuse Double Layer (DDL) and Cation Exchange Capacity (CEC) of clay

Clay surfaces have negative charges, when placed in a solution, they will attract the cations from the solution to the clay surfaces to maintain electrical neutrality, which results in a higher cation concentration near the clay surface than the bulk solution. The high cation concentration tends to diffuse away towards the bulk solution until it reaches the same level of the bulk solution [Mojid, 2011]. This cation diffuse layer and the negatively charged clay surface together form the diffuse double layer. The thickness of this double layer depends on both clay surface charge and the solution salinity.

The diffuse double layer theory explains the interaction between the clay surfaces and the surrounding solution. It is based on the Gouy-Chapman Model [Gouy, 1910; Chapman, 1913] Then Otto Stern refined the model and came up with Stern's Model by taking consideration of that some of the ions may be selectively adsorbed on the clay surface form a Stern layer. The Stern layer together with the diffuse layer balanced out the total negative charge of the clay surface [Stern, 1924; Sposito, 1989; Santamarina et al., 2001]. The schematic of the DDL is shown in Figure 2.3 below.

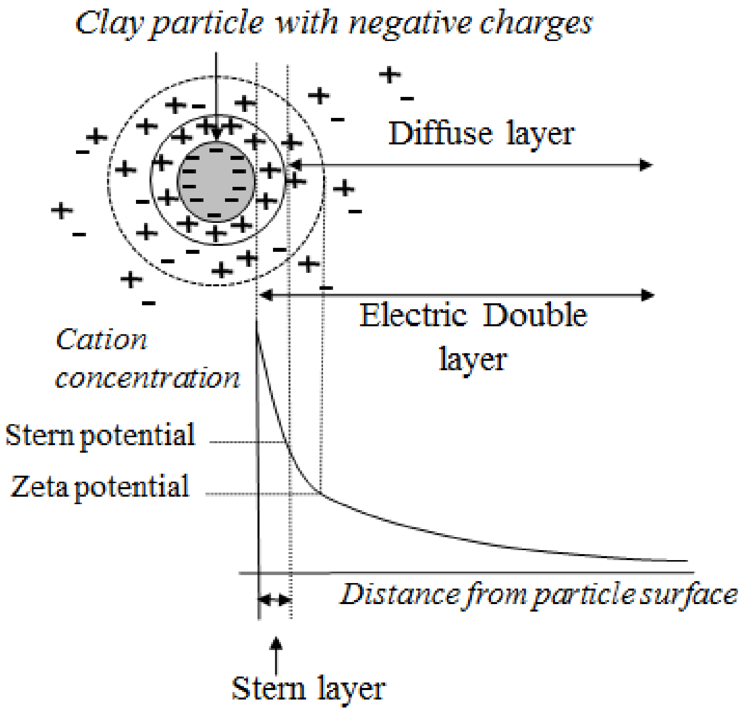

Fig. 2.3. Schematic showing the cation distribution of a negatively charged clay particle according to Stern Model. The cation concentration tends to diffuse away from the clay surface towards the bulk solution. Stern Model considered some of the ions may be selectively adsorbed on the clay surface form a Stern layer. [Figure redraw from Chilingar et al., 2014]

Cation Exchange Capacity (CEC) is a commonly measured value of minerals, or rocks containing clays. It tells the capacity of clay to hold exchangeable cations, which is the concentration of unfixed cations in the diffuse layer. The exchangeable cations hold by the clay to balance the negative surface charge are reversible and diffusion-controlled, in some cases, there is the selectivity of one cation over another [Gast, 1977]. Because the total surface charge is influenced by pH, the CEC also varies with pH [Meier and Kahr, 1999].

Clays with high CEC has the potential to be long-term storage of high-level long-lived nuclear wastes as they can adsorb a large number of ions [Cosenza et al., 2007; 2008; 2015].

The CEC of shale is proportional to its clay content and has been shown to be related to its geomechanical properties [Dewhurst et al., 2008]. The existence of this double layer can also reduce effective porosity, resulting in a decrease in permeability. The thickness of the double layer is dominated by the clay mineralogy, increasing from chlorite to kaolinite to illite to smectite and is influenced by the salt concentration in the pore fluid [Mesri and Olson, 1971]. Therefore, the type and amount of clay content are the key factors affecting shale sealing capacity, as both of them control the CEC, which determines the mechanical and petrophysical properties of the rock [Du et al., 2017a].

2.1.2. Shale Depositional Environment

2.1.2.1. Clay behaviors in colloidal systems (DLVO theory)

The DLVO theory is named after Boris Derjaguin and Lev Landau, Evert Verwey and Theodoor Overbeek It is largely applied for the prediction of the stability of many colloidal systems, including the clay behaviors [Missana' and Adell, 2000]. This theory describes the force between charged surfaces interacting through a liquid medium. It combines the effects of the van der Waals attraction and the electrostatic repulsion due to the double layer. Figure 2.4 (a) indicates the van der Waals attraction, double layer energy of interaction, and the combination of the two opposite potentials as a function of distance from the surface of a spherical particle. Figure 2.4 (b) shows an example of the qualitative variations of with distance of separation at different salt concentrations [Khilar and Fogler, 1998]. The DLVO theory was used to explain the mechanism of low salinity water flooding which has been in the center of attention in the oil industry as a cost-effective technique to improve oil recovery. Low salinity water can cause the double layer expansion to trigger positive disjoining pressure in the rock fluid system. Xie et al. [2016] also suggested that it can be applied to discuss the low recovery of hydraulic fracturing fluid during the implementation of hydraulic fracturing. [Xie et al., 2016]

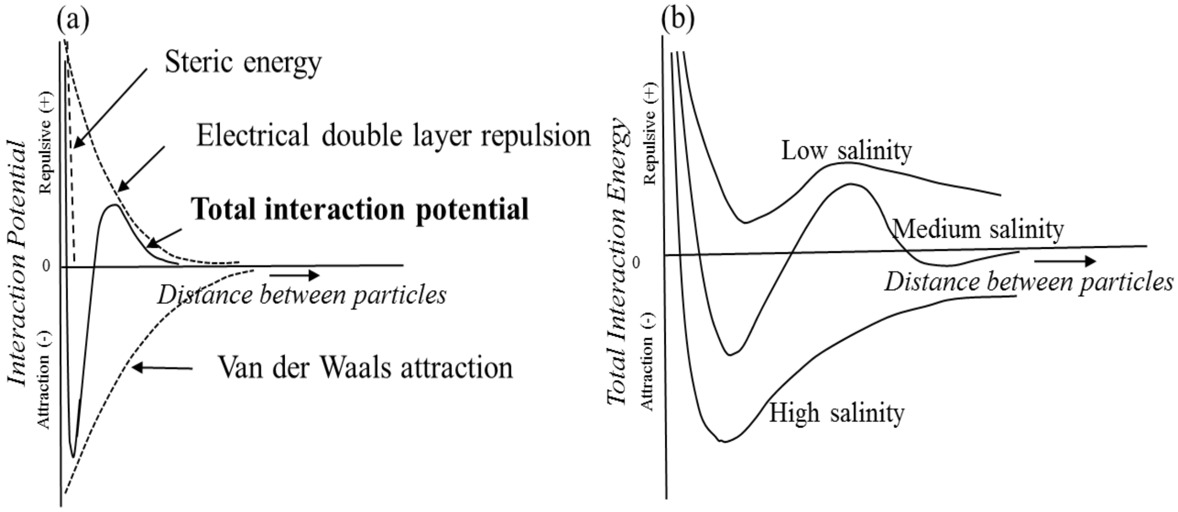

Fig. 2.4. Repulsive and attractive forces as a function of distance (a) The combination of the steric energy, van der Waals attraction and double layer energy of interaction as a function of the particles distance (b) The qualitative variations of total interaction energy with distance of separation at three different salt concentrations [Derjaguin and Landau, 1941; Verwey and Overbeek, 1948; Khilar and Fogler, 1998].

2.1.2.2. Clay minerals stability and conversion

Clay minerals of relatively young (Late Tertiary) shales are expandable smectites while in older shales illites are predominate. The smectite illitization is a common but most volumetrically important mineralogical reaction occurring during the burial diagenesis of shales, and it correlates with hydrocarbon maturation [Perry and Hower, 1970; 1972]. The reaction progress was characterized by the simultaneous increase in the illite content in the illite-smectite mixed layers (IS) following mineralogical sequence:

Smectite →high smectite contents IS →high illite contents IS→ illite.

Other reactions accompany the smectite transformation are the alteration of K-feldspar and plagioclase to clays, silica, and/or albite [Lynch, 1997]. The general equation is written as:

$$\text{Smectite} + Fe^{3+} + K^{+} = \text{illite} + Si^{4+} + Na^{+} + Mg^{2+} + Fe^{2+} + H_2O$$

The transformation of smectite to illite needs the addition of iron and potassium then produces silica, sodium, calcium, magnesium, iron, and water. The iron and potassium are provided by K-feldspar and plagioclase, the released elements form quartz, chert, calcite, dolomite, ankerite, hematite, and albite, which are common minor minerals found in shale. Therefore, this smectite to illite reaction connects nearly all of the minerals found in shale. Studies from different researchers also show the released Si^{4+} from this reaction is an important source of silica for sandstone cement [Towe, 1962; Hower et al., 1976; Howard, 1981; Lynch, 1997; Van de Kamp, 2008] Furthermore, the smectite illitization is also the reason causes overpressure zones in shales which drive the expulsion of hydrocarbons and water to more permeable rocks [Burst, 1969; Bruce, 1984].

Minerals have opposite charges will attract each other while minerals with the same charges will repel one another. This phenomenon is believed to be important for the transportation of clay minerals within the rock [Ryan and Gschwend, 1992]. Neasham overserved a strong influence of commonly occurring dispersed clay minerals on sandstone porosity and permeability. He defined three categories of dispersed clays within the hydrocarbon-bearing sandstones, 1) Pore-filling kaolinite, 2) Pore-lining chlorite, and 3) Pore-bridging illite. Basically, all clays would fill the pores in sandstone causing reduction of permeability and porosity, the differences is kaolinite is not attached to the wall and acting as migrating fines but chlorite and illite would be attached to the wall and form a coating or bridge to block the pores [Neasham, 1977]. This happened when ZPC quartz < Reservoir pH< ZPC clays, the clays and the pore wall (mainly quartz in sandstone) have opposite charge resulting clays attached to the pore wall while kaolinite is normally electrically neutral, which makes it a migrating fine instead of attaching. Although, the phenomenon of the clays in sandstones can be explained by these minerals ZPC properties differences, but this only applied to sandstone when quartz is a major phase.

2.1.3. Shale Texture

2.1.3.1. Microstructures

The shale is a multi-phase material with a multi-scale internal structure, although shale is highly heterogeneous in chemical compositions, it has low permeability primarily due to compaction and clay dehydration during the diagenetic evolution of the rock in the subsurface. The tight packing structure obtainable in shale occurred resulting from million years of tectonic compaction [Iverson et al., 2008; Jennings et al., 2007; Thomas and Jennings, 2003].

Due to the small particle size, the interstitial spaces of shale are very small which makes the hydrocarbons and water difficult to flow through or move within the rock. Therefore, shale can act as a cap rock for oil and natural gas reservoirs, because it isolates or limits the fluid flow. Although the interstitial spaces within shale are small, they can still add up to a significant volume of the rock. The large volume of space within the rock allows the shale to hold significant amounts of water, gas, or oil without migrations due to the low permeability. The oil and gas industry overcomes these limitations of shale by combining the horizontal drilling and hydraulic fracturing technologies to create artificial interconnected pathways (porosity and permeability) within the rock [King, 2019].

2.1.3.2. Anisotropy

Macro and microstructure of shales are dominated by distinct laminated layering characteristics which caused the anisotropy in petrophysical and mechanical properties. Elastic anisotropy of shales is understood to be the result of 1) the anisotropic fabric created by the preferred orientation of minerals (platy clay), 2) the anisotropic properties of the clay minerals itself due to their layered structures, and 3) the amount of organic content [Vernik and Nur, 1992; Vernik and Liu, 1997; Suarez-Rivera and Fjær, 2013].

The preferred orientation of plate-shaped clay minerals is caused by slow sedimentation/compaction and mechanical rotation that leads platelets parallel to the sediment surface. This pattern is further modified by dissolution and recrystallization of neoformed minerals perpendicular to the principle effective stress during compaction and diagenesis [Ho et al., 1995; Worden et al., 2005; Lonardelli et al., 2007; Day-Stirrat et al., 2012]. Most clay minerals are made of two distinct building blocks: tetrahedrons (T) and octahedrons (O). The T and O sheets may be condensed in either a 1:1 or 2:1 proportion to form a layered structure, and the arrangement of these layers leads to different morphologies, as well as anisotropic properties. [Bergaya and Lagaly, 2013]. The degree of anisotropy of the shale was found to increase with clay and organic content because solid organic materials are anomalously compliant compared with the surrounding minerals [Ahmadov et al., 2009; Kumar et al., 2012; Sone and Zoback., 2013]

2.2. SHALES AS RESERVOIRS

Shale has become an important resource of hydrocarbons over the last decade. It has the potential to become a rich hydrocarbon source rock as well as a reservoir rock. As reservoir rock, shale typically includes relatively large amounts of organic material, fine grain size, and low permeability compared with other rock types. In the shale reservoir, the permeability of shale is several orders of magnitude less than a conventional sandstone reservoir [Williams, 2012]. Various clay types and pore volumes affect the reservoir quality from the petrophysical and geomechanical perspectives. In detail, the shale reservoir quality depends on their thickness, extent, organic content, thermal maturity, depth, pressure, temperature, fluid saturations, porosity and permeability [Zhao et al., 2007; Curtis et al., 2012].

2.2.1. Petrophysical Properties

For shale reservoir rock, the pore size and structure provide important information in understanding gas and oil storage and transport mechanisms and their controls [Ross and Bustin, 2009]. The petrophysical properties emphasize those properties relating to the pore system, its fluid distribution and flow characteristics. To characterize the petrophysical properties of the shales, it is necessary to determine the capability of the rock to accumulate and transport reservoir fluids which are defined as porosity and permeability.

The definition for porosity is the void space within rock volume, and it is a function of the grain texture. The porosity determines the volume of reservoir fluids accumulated by rock. It means the volume of void spaces in the rock that are filled with oil, gas, and water. Two types of porosities are distinguished, which are total porosity and effective porosity. In general, effective porosity has direct implications for oil and gas productivity. However, it is significant to investigate the pore structure and total porosity of shale gas reservoirs, as both affect gas sorption processes and total gas storage capacities. The evaluations are conducted by the structurally heterogeneous nature of fine-grained strata and their intricate pore networks, which are interdependent on the total organic carbon (TOC) content, mineralogy, maturity and grain-size [Ross et al., 2008].

Shale reservoirs are grouped as unconventional because the hydrocarbon is trapped in part by sorption processes in the low permeability strata [Naik, 2007]. Permeability is associated with the presence of natural discontinuities (fracture/cracks) within the rock. These discontinuities enable the flow of reservoir fluids through/between pore spaces. The permeability enables the flow of natural gas or oil into production, it is dependent on the size of pores, the configuration of the rock grains, grain grading, and cementation, as well as the rock fracturing patterns [Zendehboudi, and Bahadori, 2016]. Shale is characterized by low permeability and it prevents any unrestrained flow of hydrocarbons.

In general, both permeability and porosity are highly dependent on the mineral composition, organic matter distribution, and organic contents with information on thermal maturity [Curis et al., 2012]. To characterize petrophysical properties, specific methods have used which include low pressure CO_2 and N_2 isotherm analyses, high pressure Hg porosimetry, and relevant geochemical analyses [Anovitz and Cole, 2015]. On the other hand, the petrophysical properties of shale can be described at different scales, which include micro/nano scale, macron scale, and lithological scale. Due to the small pore size of shale, it has been quite a challenge to use more advanced techniques to understand and measure the petrophysical properties of shale, especially in micro/nano scale.

2.2.2. Hydrocarbon Extraction and Hydraulic Fracturing

As mentioned before, the individual interstitial space of shale is small but can add up to a significant volume where it can hold significant amounts of water, gas, or oil but not be able to effectively transmit them because of the low permeability. Horizontal drilling and hydraulic fracturing techniques are combined and used by the oil and gas industry to overcome this problem by creating artificial conductivity within the rock to extract the hydrocarbons from the rock. The hydraulic fracturing treatment pumps a specifically designed fracturing fluid downhole at high pressures to initiate fractures in the rock, once the fracture is wide enough, a propping material (sand or ceramic beads) is pumping into the rock matrix to keep the created fractures open.

The two key components here are the fracturing fluid and proppant. Chemicals are often added to the water and used as fracturing fluid. Different additives served a variety of purposes. The gel is added to thicken the water to make it more effective at opening fractures and carrying proppants deep into the fractured matrix. Other chemicals are used to reduce friction, prevent corrosion, keep rock debris suspended in the liquid, kill bacteria, control pH and many other functions [King, 2019]. The commonly used proppant is simply sand grains, while man-made ceramic proppant is used in higher pressure environments in case of the sand grain itself start to fracture and producing fines when subject to higher closure stresses [Jansen, 2014].

Although hydraulic fracturing has been used to produce hydrocarbons from shales for more than a decade, the fundamental mechanism to initiate and propagate these fractures remains unclear. Rickman et al. [2008] demonstrated the key factors for a successful fracture treatment, including mechanical properties, mineralogy, and other petrophysical characteristics of the shale. He suggested that the target rock with high Young's Moduli and low Poisson's Ratios was beneficial for treatment successful treatment. Li et al. [2013] agreed with Rickman et al. that shale with a higher Young's Modulus and a lower Poisson's ratio resulted in greater fracture treatment success. Bourg [2015] concluded that the shale formations with lower clay content are more suitable for unconventional hydrocarbon extraction because these rocks' permeability can be significantly enhanced by the formation of hydraulic fractures.

2.3. SHALES AS CAPROCKS AND BARRIERS

The exploration of shale has not only limited to the resource and reservoir shales but also extends to the caprock due to its high sealing ability. Caprocks are essentially defined as low permeability formations, and sometimes, but not necessarily, with low porosity. More than 60% of effective seals for geologic hydrocarbon bearing formations as natural hydraulic barriers constitute of shale caprocks. The effectiveness of cap rock depends on its ability to immobilize fluids, which includes a low permeability and resilience to the in-situ formation of fractures as a result of the pressurized injection. The alteration in the sealing properties of shales is directly related to the differences in its mineralogical composition and microstructure [Du et al., 2017a]. Caprock is the rock that prevents the hydrocarbon flow fluid at a certain geological condition. It stops the migration paths for oil and gas. Their ability to exhibit good sealing characteristics arises from shale's small and water-wet pores properties. These small pore throats are responsible for generating high capillary pressures so that can exclude the hydrocarbons from the reservoir [Bruno, et al., 2013; Al-Bazali et al., 2017]. Moreover, a range of mineralogical compositions and bulk physical properties of shales are associated with the sealing ability of the barrier.

2.3.1. Fluid- Rock Interaction

Shale formation behaves uniquely when it in contact with injected fluids. The interaction of shales with fluids is a not well-understood but very important aspect for the drilling, completion, as well as production optimization process. Fluid-rock interactions can affect reservoir and seal rocks properties. The precipitation and dissolution of minerals can change in the petrophysical and mechanical properties of the rock. Mineral dissolution can result in an increase of porosity and enables the creation of pathways for fluid migration; Mineral precipitation leads to a decrease in porosity which increases the sealing effect of the rock. Another example of fluid-rock interaction is that in contact with water can cause a smectite-rich shale to swell. [Emmanuel et al., 2015, Koteeswaran et al., 2018]

Three of the most common and significant mechanisms for shale–fluid interaction are summarized as follows [Van Oort et al., 1995; Lal, 1999; Van Oort, 2003;]:

1) Darcy flow, the interaction is governed by the hydraulic gradient between surrounding fluid and shale pore fluid, and the water is driven into the shale when the fluid pressure is greater than shale pore pressure;

2) Diffusive flow, it is governed by the chemical potential gradient. The fluid ion concentration and shale cation exchange capacity decide the direction of the ion movement. The water flows into the shale when the surrounding fluid has higher ion concentration. Additives such as salts can be used to change the water activity by altering its ion concentration;

3) Osmotic flow, it also plays a significant role in the fluid-rock interaction. The flow direction and interactions depend on factors such as membrane efficiency of shale and water ion concentration of the injected fluids [Koteeswaran et al., 2018].

2.4. CURRENT GAPS IN KNOWLEDGE

Hydraulic fracturing has been proved to be effective to produce hydrocarbons from shales, but a lot of related problems still remain unclear. First of all, is that the fundamental mechanism to initiate and propagate these fractures in shale remains unclear. Although the horizontal drilling with hydraulic fracturing has been operated for a number of years with favorable economics, there are still a large number of wells are failing to meet the production expectations. Figure 2.5 below is the data documented from different unconventional shale reservoirs showing the percentage of perforation clusters that are not producing [Miller et al., 2011]. As shown in Figure 2.5 below, from 21% to 32% of the perforation clusters are not contributing to the production.

The second problem is the fluid-rock interaction. Shales are reactive, the chemical added in the fracturing fluid can alter the properties of the rock such as wettability, mineralogy, and mechanical properties. It is an important but not well-understood aspect, the fracturing fluid compatibility for a given shale formation needs to be quantified with experiment test before and after water exposure [George, 2016]. Although the fluid-rock interaction was not the main focus here, using the same tools and techniques of this study seems promising for this problem, because they are non-invasive rock characterization method and can be used for the dynamic study.

The third problem is the treatment needs large volumes of water, as well as a variety of chemicals for different purposes. Hydraulic fracturing with large volumes of water works, but where all these fracturing fluid goes after injection is not clear. This may lead to other problems such as reduce fracture conductivity, causing casing damage or even pollutions [Zhang, 2014].

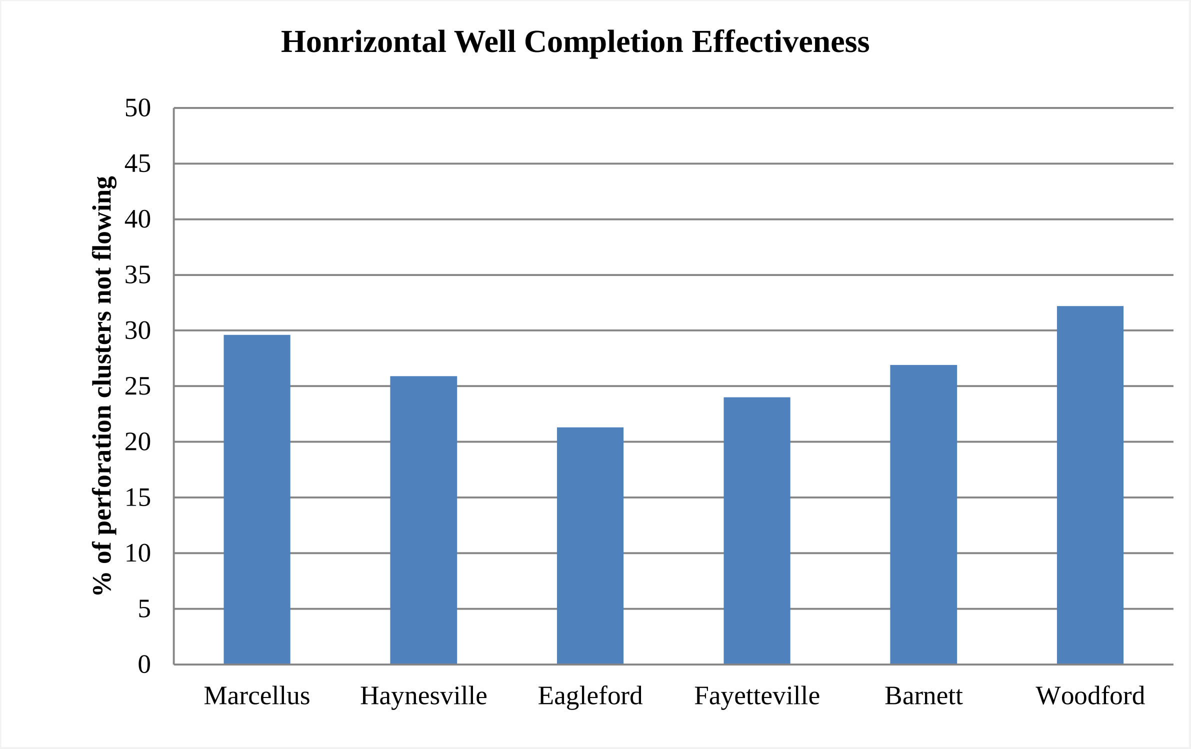

Fig. 2.5. Percentage of perforation clusters that are not producing from different unconventional shale reservoirs [data from Miller et al., 2011]. Among which, Eagleford has the best performance with 21% of perforation cluster not flowing, while Woodford has the worst performance with about 32% not contributing.

This study is focused on establishing how indentation data can be used in evaluating the mechanical properties of shale and their susceptibility to fracturing using a non-invasive method, which is fast and requires only a small volume of rock. The value of this approach is a reduction of time and cost in geomechanical evaluation, as indentation could be done on drill cuttings instead of core samples. Also, the non-destructive nature of testing makes it possible to conduct the dynamic studies, by having rock samples in contact with different fluids and dry/wet cycling conditions, temperature change and geochemically different fluids (pH, salinity). In addition, when combined with SEM/EDS/BSE microstructural characterization, geochemical and geomechanical changes can be monitored in an interdependent manner.

3. MATERIALS AND METHODOLOGY

3.1. MATERIALS

Three different types of materials were studied in this research, including shale, lab-made samples, and wellbore cement, of which shales were the main focus, the lab-made sample results and wellbore cement are mentioned to get some fundamental understanding of the multiphase composites. Shales from different formations with different mineralogy compositions were tested to see the effect of depths, mineral content, and property anisotropy, then finally the deformations under stress. Since the natural samples are complicated multiphase composite found in the varied depositional environment, the lab samples were made with a controlled environment and exact mineralogical composition as well as constant mineral ratios through the given design. Thus, the impact of mineralogical composition variation on mechanical properties and microstructures can be systematically quantified and compared. Finally the wellbore cement, as an engineered hydraulic barrier material, was compared with natural rocks to find the similarities to help improve the subsurface application of engineered hydraulic barriers in zonal isolation

3.1.1. Sealing Shales and Reservoir Shales

Shales play an essential role in petroleum exploration and production. Shales can occur either as unconventional reservoir rocks for hydrocarbon extraction via hydraulic fracturing or as caprocks for conventional reservoirs and subsurface gas/ waste storage. The utilization of a shale depending on its ability to immobilize fluids: in general, shales that exhibit low permeability and resilient to the formation of fractures are ideal for underground storage (CO_2 sequestration, waste disposals); Shale formations which permeability can be significantly enhanced by the formation of hydraulic fractures can be the target for hydrocarbon extraction. Carbon capture and storage (CCS) is, by far, the only technology which can reduce emissions on a significant scale from fossil fuel power plants and industrial sources [Global CCS Institute, 2015]; On the other hand, the ability to produce gas from rocks previously considered caprocks is an unprecedented and innovative feat, resulting in an over-supply of natural gas to the North American market in recent years [Clarkson et al., 2016; Du and Radonjic, 2018]. Two types of shale as representatives of shale caprock and source rock (Pottsville and Marcellus shale) were mainly focused on in this study. Both rocks have similar tectosilicates content (quartz and feldspar) around 50%. Pottsville shale has 46% of clay minerals and no carbonate content, while Marcellus shale is carbonate-rich (~27%) with a clay content of 22% [Olabode and Radonjic, 2017].

The Pottsville shale core samples used in this experiment were obtained from three monitoring wells in the Black Warrior Basin, Alabama. The wells were for the CO_2 Enhanced Coal Bed Methane (ECBM) Project from the Southeast Regional Carbon Sequestration Partnership (SECARB). Core samples were from the depth of 10,800-11,000ft, the porosity of the rock is from 1% to 9%. The Pennsylvanian Pottsville Formation is a mapped bedrock unit in Pennsylvania, western Maryland, West Virginia, Ohio and Alabama. The Pottsville formation consists of a gray conglomerate, fine to coarse-grained sandstone, the formation also contains siltstone, shale, limestone as well as anthracite and bituminous coal. The Black Warrior basin from which the core samples were collected, is a late Paleozoic foreland basin with a regional dip toward the southwest. The eastern part of the basin is the broad Alleghanian folds together with numerous northwest-striking normal faults

[University of Alabama, 2009]. “The Pottsville formation is exposed at the surface and overlain with angular unconformity in the western two-thirds of the area by poorly consolidated Mesozoic and Cenozoic strata of the Gulf coastal plain and Mississippi Embayment.” [USGS, 2007]. In the Early Permian, the Pottsville Formation was buried at maximum depths of approximately 2–3 km [Pitman et al., 2003; Olabode, 2017]

The Marcellus shale core samples used in this experiment are from an active production well in Washington County, PA, the U.S. from depths of 6,300-6,450ft, with porosity around 10%. The Marcellus shale is found in the Appalachian Basin of eastern North America. Like most Devonian Appalachian shales, it contains more than 2% (by volume) of organic materials and tends to be black and classified as shales/mudrocks [Ettensohn and Barron, 1982]. The Marcellus Shale is made of dark-gray to black, fissile, pyritic shale. It is interbedded with dark-gray argillaceous limestone or calcareous shale [Cate, 1963; Avary, 2019]. Some areas also contain a fossiliferous layer of limestone which is the Purcell Member of the Marcellus Shale [Cate, 1963] and prominent zones of calcareous concretions ranging in diameter from several centimeters to more than 1 m (3.3 ft). The clay minerals in this Devonian-aged shale from the Appalachian basin are illite, chlorite, kaolinite, and two types of mixed-layer clay. Mixed-layer clay minerals result from the random interlaying of two or more clay minerals, including random interlaying of illite and an expandable mineral such as smectite, (I-S mixed-layer clay) and a random mixture of illite and either degraded chlorite or a vermiculite [Fisher et al., 1970; Hosterman and Whitlow, 1983]. The Marcellus formation is an especially interesting shale because not only is it considered for carbon capture and storage (CCS) compatibility, but the latest advances in hydraulic fracturing technology enabled its use in the production of natural gas [Du et al., 2017b].

Apart from Marcellus and Pottsville shale, a few more shale samples from Eagleford, Wilcox, Mancos, and Bakken formations are also included for comparison as their composition are significantly different. The age, depth, location, and lithology of the shale samples used in this experiment were listed in Table 3.1 below in the order of their clay content: Eagle ford has the least amount of clay(~15%) and Wilcox has the most amount of clay content (~50%). The indentation results from Woodford and Wolfcamp shale formations measured by Shukla et al were also included for comparison [Shukla et al., 2013].

Table 3.1. Comparison of shale samples used in the experiment [MacFarlane, 1890; Nordquist, 1953; Hentz et al., 2014; Olabode, 2017]

Formation	Age	Depth	Location	Lithology
Eagleford	Late Cretaceous	Outcrop	Texas	calcareous fissile fossiliferous
Mancos	Upper Cretaceous	~2,500ft	Colorado/ Utah	calcareous silty
Marcellus	Middle Devonian	~6,500ft	Pennsylvania	calcareous fissile fossiliferous
Bakken	Late Devonian to Early Mississippian	~11,000ft	North Dakota	siliceous fissile fossiliferous
Pottsville	Upper Pennsylvanian	~11,000ft	Alabama	quartz rich silty
Wilcox	Upper Cretaceous	>10,000ft	Louisiana	swelling clay-rich

All of the samples used in this study were cut by a diamond saw into small specimens of approximately 1 x 0.5 square inch in area with a thickness of around 0.5 inches. The specimens were then ground, polished down to 1 μm and ultrasonically cleaned. Finally, the specimens were oven-dried for at least 24 hours to avoid the difference caused by moisture content [Du et al., 2017b].

3.1.2. Most Common Minerals of Shales

Shale primarily contains quartz, plagioclase, K-feldspar, carbonates, and clay minerals in varying proportions, as well as several other minerals in minor proportions. Minerals in natural rocks are rarely found separately (especially for clays), they are usually mixed with each other, the mineralogical compositions vary even from the same formation. Therefore, in order to have controlled and exact mineralogical composition as well as a constant mineral ratio, artificial samples were made in the lab. The XRD data of different shale formations are obtained from the literature as references to choose the starting materials for making lab-made samples. These shales are shown in Table 3.2.

Quartz, calcite, kaolinite, illite, and smectite are identified as the common component in natural shale which is used to generate the artificial rock (lab-made composites) and study the effect of each component. Quartz and calcite are the major components in their categories; as for clay minerals, all clay minerals are made of two distinct building blocks: tetrahedrons (T) and octahedrons (O), illite represent 2:1 layer (T-O-T) non-swelling clay, smectite represent 2:1 layer swelling clay and kaolinite are 1:1 layer (T-O) clay. In natural rock, clays are rarely found separately, they are usually mixed not only with other clays but also with other minerals like carbonates, feldspars, micas, and quartz. In order to limit the effect from other impurities, the materials used in this study were purified minerals collected from different manufacturers. Purified natural minerals were mixed at different ratios, allowing us to observe the impact of the mineralogical composition on mechanical properties and obtain a systematically quantified comparison between samples [Du and Radonjic, 2016].

Table 3.2. Mineralogical composition of shale from the literature [Mutschler et al., 2009; Alemu et al., 2011; Angeli et al., 2009; Mbia et al., 2014; Bereskin and McLennan., 2008; Lynch, 1997; Heath et al., 2011; Heath et al., 2012]

Category	Minerals	Keuper claystone	Janusfjellet shale	Draupne shale	Fjerritslev shale	Chimney shale	Anahuac shale	upper Kirtland	lower Kirtland
Tecto-silicates	Quartz	9	13	35.7	40	25	20.7	5	21
	K-feldspar			2.5	1	3	3.1	11	10
	Plagioclase	3	6	1.6	1	4	3.9	18	13
Phyllo-silicates (clays)	Chlorite	19	19	3.4	1	2	1.8	19	12
	Illite + mica	35	26	9.2	23	19	12.5	22	
	Kaolinite			12.3	27		16.8	7	9
	Smectite							23	3
	Illite + Smectite	25		14.6		19	41.3	4	28
Other minerals (primarily carbonates)	Calcite	6	29		3	12			1
	Dolomite			14.6	2	9			
	Pyrite			6.1	2	5			1
	Halite	3							
	Hematite	3							
	Ankerite		7			2		1	1
	Siderite					1			
	Fluorapatite					1			

Kaolinite has 1:1 layer structures (T-O) with a general composition of $Al_2Si_2O_5(OH)_4$. It is built up by stacking of identical layers with a predominance of Al^{3+} in the O layer and Si^{4+} in the T layer, while some isomorphous substitution of Mg^{2+}, Fe^{3+}, Ti^{4+}, and Fe^{2+} for Al^{3+} can occur in the O layer. Kaolin minerals have a well-known tendency to form a wide variety of ordered and disordered polytypes, and the diffraction patterns showed a significant difference between ordered and disordered kaolinite (Ordered kaolinite shows sharper and narrower peaks). The variety is caused by a series of stacking faults or defects, which also explained the poor structural order commonly observed in kaolin minerals [Dornberger-Schiff and Durovic, 1975; Plancon et al., 1989; Zvyagin and Drits, 1996]. Kaolinite is commonly used in ceramics, rubber, and plastics. The paper industry uses kaolinite to produce a glossy paper such as is used in most magazines [Wayne et al., 1991]

Illite has a 2:1 layer structure (T-O-T) with a general formula of $(K, H)Al_2(Si, Al)_4O_{10}(OH)_2 - xH_2O$, It is a micaceous clay mineral that occurs widely in soils and sediments. The structure of illite is two tetrahedrons layers sandwiching an octahedrons layer in between, the common isomorphous substitution is Al^{3+} for Si^{4+} in the tetrahedron layers and Mg^{2+}, Fe^{3+} for Al^{3+} in the octahedron layer [Brigatti, and Guggenheim, 2002]. Variable amounts of water molecules can lie between two T-O-T Illite particles, as well as different ions. Illite samples from diverse genetic environments have different chemical compositions because of the isomorphous substitution and inter-particle 'impurities" [Lindgreen et al., 1991]. Like kaolinite, illite is also used in the preparation of mixtures for traditional ceramics [Ferrari and Gualtieri, 2006]

Montmorillonite is used in this experiment as a representative of smectite. The structure of montmorillonite is similar to the 2:1 layer of illite, but the layer charge and hydration of the interlayer cations are different. The general formula of montmorillonite is $(Na,Ca)_{0.33}(Al,Mg)_2(Si_4O_{10})(OH)_2\ nH_2O$, and like other clay minerals, the chemical composition mostly differs from the formula because of the ion isomorphous substitution. Commonly Si^{4+}, Al^{3+}, and Fe^{3+} are found in the tetrahedral (T) layer while Al^{3+}, Fe^{3+}, Fe^{2+}, Mg^{2+}, Ni^{2+}, Zn^{2+}, and Li^{+} generally occupy the octahedral (O) layer. The isomorphous substitution in both T and O layers changes the total charge of mineral, which is the key factor for many physical properties of Montmorillonite (smectite) such as swelling and rheological behavior [Bergaya, and Lagaly, 2013]. Montmorillonite is used in the oil drilling industry as a standard additive of drilling mud, because of its unique rheological properties.

Adding montmorillonite makes the mud slurry viscous, which helps in keeping the drill bit cool and removing drilled solids [Hosterman and Patterson, 1992]. Montmorillonite is also effective as an adsorptive phase for heavy metals [Bhattacharyya and Gupta, 2008], which play a key role in the nuclear waste storage site.

Chlorite is not used in this experiment, although the mineralogical composition table shows they widely exist in all samples, because the chlorite group is not well understood, and so far, no known industry uses. The structure of the group is similar to illite, but between each 2:1 (T-O-T) layer, there is an additional O layer forming a 2:2 layer structure with the sequence of (T-O-T) O (T-O-T) O. The O layer in clays are normally Al-based, but the additional O layer in chlorite is usually is composed of $(Mg^{2+}, Fe^{3+})(OH)_6$, so, it was also classified as a 2:1:1 layer structure. Not only in structure, but he mechanical properties of chlorite also has a significant difference from other clays (much higher mechanical properties comparing to other clays), therefore, it is not always considered a part of the clay minerals and sometimes left alone as a separate group within the phyllosilicates [The clay mineral group, 2018].

3.1.3. Wellbore Cement as an Engineered Sealing Material

The primary functions of wellbore cement are to primarily provide zonal isolation, mechanical support of the metal pipe and prevent corrosion of wellbore system metal components. During the well life this main artificial hydraulic barrier in wellbores, cement sheath, can be subjected to many types of failures. The integrity of the wellbore cement sheath is a function of the petrophysical and mechanical properties of the hydrated cement, the geometry of the cased well and the properties of the drilled formation [Thiercelin et al., 1998]. During cementing operations, insufficient mud removal and improper cement placement might lead to weak bonding on both interfaces of the cement sheath and eventually gas channeling and poor zonal isolation [Agbasimalo and Radonjic, 2014]. Debonding at cement/rock and cement/metal casing can be caused by operational casing movement, cement shrinkage, and pressure and/or temperature changes. The completion and production operations can cause pressure and temperature oscillations which contribute to the development of fractures and micro annuli within the cement matrix [Nelson and Guillot, 2006]. Cement fractures, resulting from internal pressurization of the casing, generally cause loss of annular zonal isolation in the lower one quarter to one-third of the well, while large temperature changes cause cement sheath fracturing in the upper one-third to half of the well [Goodwin and Crook, 1992]. Both tensile and shear failures of the cement sheath have been shown to strongly relate to the wellbore pressure and temperature [Jo and Gray, 2010]. Initial casing expansion and contraction can create a micro-annulus which significantly increases the hydraulic conductivity of the wellbore, while further casing loading can cause initiation of the radial cracks in the cement matrix, once the tensile stresses exceed the tensile strength of the material, also resulting in compromised zonal isolation of the wellbore cement [Boukhelifa et al., 2004].

Mechanical properties of hydrated cement, such as hardness and compressive strength, are primarily influenced by the water to cement (w/c) ratio since the rate of cement hydration dictates the amount of porosity versus solid phases. Glinicki and Zielinski [2004] found that the Vickers hardness measured by indentation had a linear relationship with the w/c ratios. Based on their results, after 28 days, the 0.3 w/c ratio hydrated cement had a hardness of over

550 MPa, the 0.5 w/c ratio cement had a hardness of 375 MPa, while the cement with highest w/c ratio of 0.7 produced a hardness of 200 MPa, this result clearly showed an inverse relationship. Water to cement ratio, given the same curing conditions such as hydration time, temperature and pressure, also dictates petrophysical properties of hydrated cement, which is crucial for compressibility of the porous medium.

Different designs of cement were used in this study to see the effect of water to cement ratio, salinity, and mechanical compression. For the mechanical compression evaluation, two cement designs were used: 1.56 g/cm^3, 0.87 w/c ratio cement slurry, and 1.96 g/cm^3, 0.38 w/c ratio cement slurry. The lightweight cement slurry (tail cement) is most commonly used in shallower formations while the heavier cement slurry (head cement) is used for cementing operations in deeper formations with high pore pressures. Both of the cement slurries were prepared in a four liter, 3.75 horsepower laboratory blender at 20,800 rpm. The samples were cured in a water bath for a minimum period of 28 days with the water pH being kept between 12 and 13 by mixing the water with $Ca(OH)_2$. Defoaming agent and bentonite were used as additives for the API Class H cement [API Recommended Practice 10B]. These samples were first designed and prepared by Darko Kupresan for a study on the application of expandable casing technology. His previous study was focused on the unique approach to the usage of expandable casing technology as a new remediation operation for micro-annular gas migration. For this study, the effect of compression had on cement microstructure and its mechanical properties were reported. The mini wellbore model was designed to represent the cemented casing in the wellbore, the cement was initially placed in the annular space represented by “pipe-inside-pipe” physical model. After cement hydration was completed, the inner diameter of the pipe was expanded causing cement compression as shown in Figure 3.1 below. [Kupresan et al., 2013; Kupresan et al., 2014].

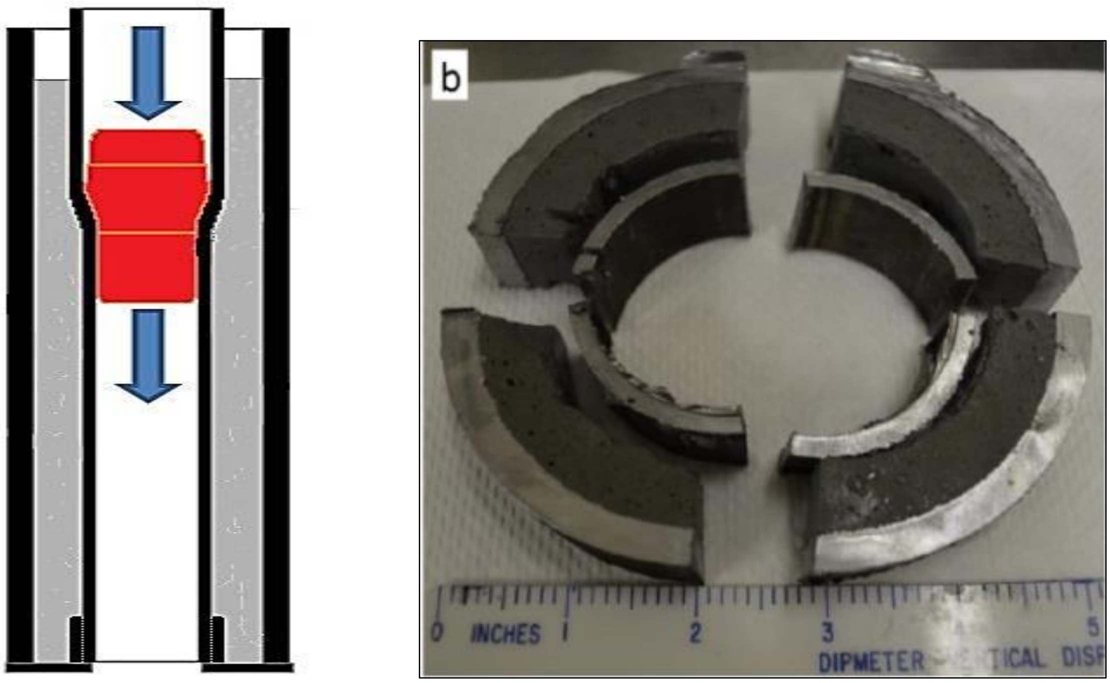

Fig. 3.1. Left: schematic of pipe-in-pipe expansion (compression) process; Right: 16ppg cement sample [Kupresan, 2014]; Inner pipe represents the casing, outer pipe represents the formation, Expansion cone (red) was pulled through the inner pipe casing an expansion of the inner pipe and compression of the cement sheath.

For the evaluation of the effect of water to cement ratio, cement the slurries were mix at w/c of 0.3, 0.4, 0.6, 0.8, and 0.9 with deionized (DI) water; while for the salinity effect, cement slurries were mixed at w/c=0.4 with variations in salinity of 0, 35,000, and 180,000 parts per million (ppm). The 35,000 ppm solution was close to the seawater salinity to represent the condition when cement was placed at offshore wells, and 180,000ppm represented the condition when cement was placed next to a salt dome. Sodium chloride was used for the adjustment of salinity. All of these cement samples were prepared in the same procedure of the mechanical compression cement following the American Petroleum Institute (API) standard.

3.1.4. Lab-made Sample to Represent the Simplified Shale

Lab-made samples were generated and tested in the lab for this study because natural shales are heterogeneous and their mineralogical composition varies even from the same formation. To simplify the rock, the lab-made samples were generated with controlled and exact mineralogical composition as well as a constant mineral ratio through the given design. Thus, the impact of mineralogical composition variation on mechanical properties and microstructures can be systematically quantified and compared between samples [Du et al., 2017a].

Lab-made samples are prepared by one-dimensionally consolidating a dilute slurry of the materials in a rigid ring container as shown in Figure 3.2. The procedure includes three main stages: mixing, consolidation, and sample preparation. Materials with different ratios were mixed thoroughly with water using an electric blender to produce a homogenous slurry. The water used includes de-ionized (DI) water, low/high salinity water (2,000 / 35,000 ppm) with sodium chloride. The mixing water content was approximate twice the liquid limit of the clays in order to get a stable slurry with no free water present. After mixing, the slurry was kept in ambient condition for at least 24 hours to remove the excess water and large entrapped air bubbles within the slurry. Afterward, the slurry was deposited in a rigid ring container with porous stones placed on both the top and bottom of the sample allowing double drainage. The whole sample container set up is submerged in water which has the same salinity of mixing water. Then, the slurry was loaded from top incrementally until no further displacement at the maximum force. After the re-sedimentation, the sample was removed from the container, dried in the oven at a regulated temperature (70^0C) and polished for indentation analysis and SEM imaging [Du et al., 2017a].

Different samples were created to represent low, mid and high clay content shale with 15%, 45%, and 75% of clay minerals. The quartz to carbonate ratio is approximately 1.5 to 1. The mixing water salinity was set as 2,000ppm and 35,000ppm to represent low salinity formation water and high salinity seawater. One sample with 45% clay content and 0 ppm salinity was made as the control sample to see the effect of salinity. Natural rocks were also included for comparison [Du et al., 2017a].

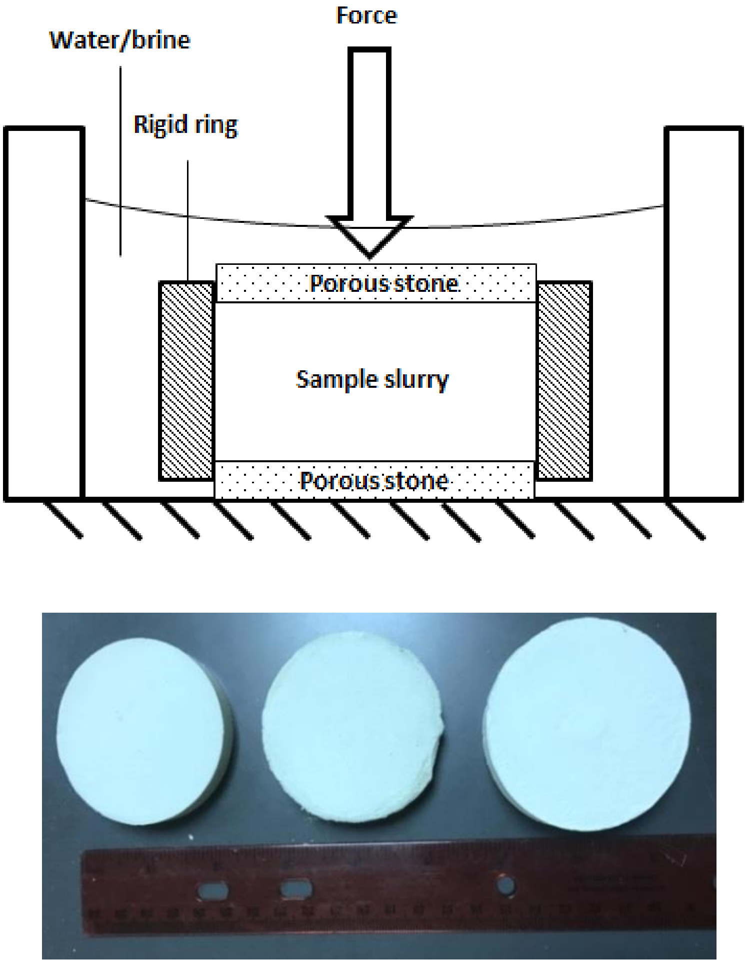

Fig. 3.2. Schematic of the experiment design (top) Examples of the lab-made samples (bottom), from left to right are the samples of 35000 ppm salinity with a clay content of 15%, 45%, and 75%. [Du et al., 2017a]

The advantages and disadvantages of these three materials used in this experiment can be summarized in Table 3.3 below:

Table 3.3. Comparison of the lab-made sample, shale, and cement

	Lab-made sample	Shale	Cement
Advantages	Composition; mineral ratio; deposition environment	low permeability; durability & integrity at various temperature, pressure, chemical attack; self-healing	low permeability; can be modified; self-healing with confinement
Disadvantages	loose structure; lack of time, temperature, pressure, interaction between particles	complexity in composition	compatibility (high pH); interfaces; tensile failure

3.2. METHODOLOGY

3.2.1. Imaging Techniques for Materials Characterization

Rocks are heterogeneous multiphase composites. From deposition to burial, the natural sediments undergo a series of progressive transformations then diagenesis within the Earth's crust, giving each rock unique physical properties and microstructures. Due to the heterogeneity, when subject to a load, the stress inside the material is not uniform, resulting in local stress concentrations which can lead to microcracking within the material. The growth of these microcracks can lead to critical cracking and eventually cause the failure of the material [Lukovic et al., 2015]. Therefore, visualizing the microstructure of the sample becomes an important part of the rock characterization. For this study, both optical and electrical microscopes were used for the visualization of rock at different scales.

3.2.1.1. Optical microscopy

Several different microscopes were used throughout this study, including 1) the Leica® DM2500-P modular polarization optical microscope; 2) Keyence VHX-6000 digital microscope, 3) Echo Revolve optical microscope. The Leica microscope had multiple levels of magnification provided by ocular lenses. The Keyence and Echo microscopes were able to image on surfaces with high roughness which can be used to show the rock sample surface after indentation. The Keyence microscope could also measure and draw a surface profile, and the Echo microscope helped to image the samples from different angles.

3.2.1.2. Scanning Electron Microscopy (SEM)

Scanning Electron Microscopy uses a focused beam of high energy electrons to generate signals at the surface of a solid object, revealing information about the texture and structure of the composition [Goldstein et al., 2003]. Inside a vacuum chamber, an electron gun directs a stream of electrons vertically down a set of electromagnetic lenses, the field emission gun produces a strong electric field to stimulate electrons out of their atoms. The lenses were also placed in the vacuum chamber to help direct the electrons towards the sample and avoid obstruction /contamination by other particles. In SEM, two types of electrons are primarily detected: secondary electrons (SE) and the backscattered electrons (BSE). The microscope used for obtaining the SEM images was FEI Quanta 3D FEG dual beam FIB/SEM system at 10 to 20 kV for both secondary and backscattered electrons micrographs.

The Secondary Electron Micrographs can show the microstructure of the sample including the mineral particle size, boundary, and morphology; The Backscattered Electrons mode helps to further distinguish different minerals by showing the mineral distribution, pores and fractures, because heavier elements appear brighter in the backscattered electron images and black pixels represent void space. The purpose of this analysis was to observe the changes/differences in the material structure and chemical composition. High resolution microscopy offered an insight into the material microstructure at the nano and micrometer scale.

3.2.1.3. Energy Dispersive Spectrometry **(**EDS)

When combined SEM with the EDS, it can be used to determine the chemical composition in areas of interest. EDS uses the characteristic x-rays emitted by the object to determine the elemental composition of the object. Secondary and backscattered electrons signals produced in an SEM/EDS system that is used in the image forming for morphological analysis, while the X-rays signal is used for identification and quantification of chemicals present in the area of interest. For bulk material such as rocks, the EDS can detect both major (concentrations >10 wt%) and minor elements (1 wt% < 10wt%) but not the trace elements (<0. 1 wt%) [Nasrazadani and Hassani, 2016]. The detection limit highly depends on sample surface conditions, which makes proper sample preparation essential.

For SEM imaging coupled with EDS, the samples were dried and vacuumed, then the cement samples sputter coated with 6 nanometers of gold and platinum and shale samples were sputter coated with 10-15 nanometer of carbon. The samples were secured and stuck firmly on the stub by double-sided carbon adhesive tape to avoid any possible movement or vibrations. A thin copper stripe tape was added from the top of the sample to the bottom of the stub to further increase the conductivity and avoid electron charging. The EDS maps help to show the distributions of all elements, by comparing the distributions of key elements, the mineral distribution/ rock microstructure can be mapped. The spot analysis can be also used to identify a certain mineral.

3.2.2. Mechanical Properties Measurements

3.2.2.1. Micro indentation

Conventional mechanical characterization of rock requires retrieving core plugs which can be technically demanding and costly or even impossible [Liu et al., 2016; Xu et al., 2018]; while the micro indentation tests only require a small sample volume and has been used in material characterization of cementitious and metallurgical samples as a routine test. Indentation technique (Oliver and Pharr's method) has been utilized to assess the elastic and plastic properties of metals, thin films, polymers, and biological specimens, following the theoretical framework of Oliver and Pharr [1992, 2004], Vlassak [1993], Delafargue and Ulm [2004] and others, and now this technique has been implemented in characterization of more complicated multiphase composite such as cement [Velez et al., 2001] and rocks [Ulm and Abousleiman., 2006; Pant., 2013; Mighani et al., 2016].

In this study, indentation tests were conducted at both micro and nanometer levels on shale and cement samples to get the mechanical properties of bulk and individual phase of the multiphase materials. For the indentation test, the indenter tip with known geometry (Vickers diamond) is driven into a specific site of the sample to be tested, by applying an increasing normal load. After reaching a pre-set maximum value, the normal load was paused for a few seconds, then reduced until complete relaxation occurs. During the loading-unloading process, the position of the indenter relative to the sample surface is precisely monitored with an optical non-contact depth sensor. For each loading-unloading cycle, the applied load value versus the position of the indenter was plotted [Du et al., 2017b]. Figure 3.3 shows the schematic of the indenter, as well as a typical loading-unloading cycle from a single indentation test. Hardness and elastic modulus are determined through the load-displacement curve using Oliver & Pharr's method [Oliver and Pharr, 1992; 2004]. Both micro and nano tests are based on the same principles. The main difference is that micro indentation gives the average mechanical properties over the large area of different grains while nano-indentation could give the localized mechanical properties of a single grain [Du et al., 2017b].

Hardness is the resistance to the applied compression load from the sharp indenter. It can be determined from the maximum load, P, divided by the indentation area, A:

$$H = \frac{\mathrm{P}}{\mathrm{A}}$$

The Young's modulus, E, can then be obtained from:

$$\frac{1}{Er} = \frac{1 - \mathrm{v}^2}{\mathrm{E}} + \frac{1 - \mathrm{vi}^2}{\mathrm{Ei}}$$

where Ei and νi stand for Young's modulus and Poisson's ratio of the indenter (constant for a given indenter), and ν is the Poisson's ratio of the tested sample.

Er is the reduced modulus, given by:

$$Er = \frac{\sqrt{\pi}}{2} \frac{S}{\sqrt{A}}$$

which can be calculated having derived S and A from the indentation curve using the area function, A is the indentation contact area. The contact Area A is calculated by evaluating the indenter area function.

For the perfect Vickers indenters as used in this experiment (Figure 3.4), the area function is

$$A=24.5\ h^2$$

A power-law fit through the upper 1/3 to1/2 of the unloading data intersects the depth axis at h_t. The stiffness, S, is given by the slope of this line. The contact depth, h_c, is then calculated as [Li and Altstatt, 2014]:

$$hc = \text{hmax} - \frac{3\ \text{Pmax}}{4\ \text{S}}$$

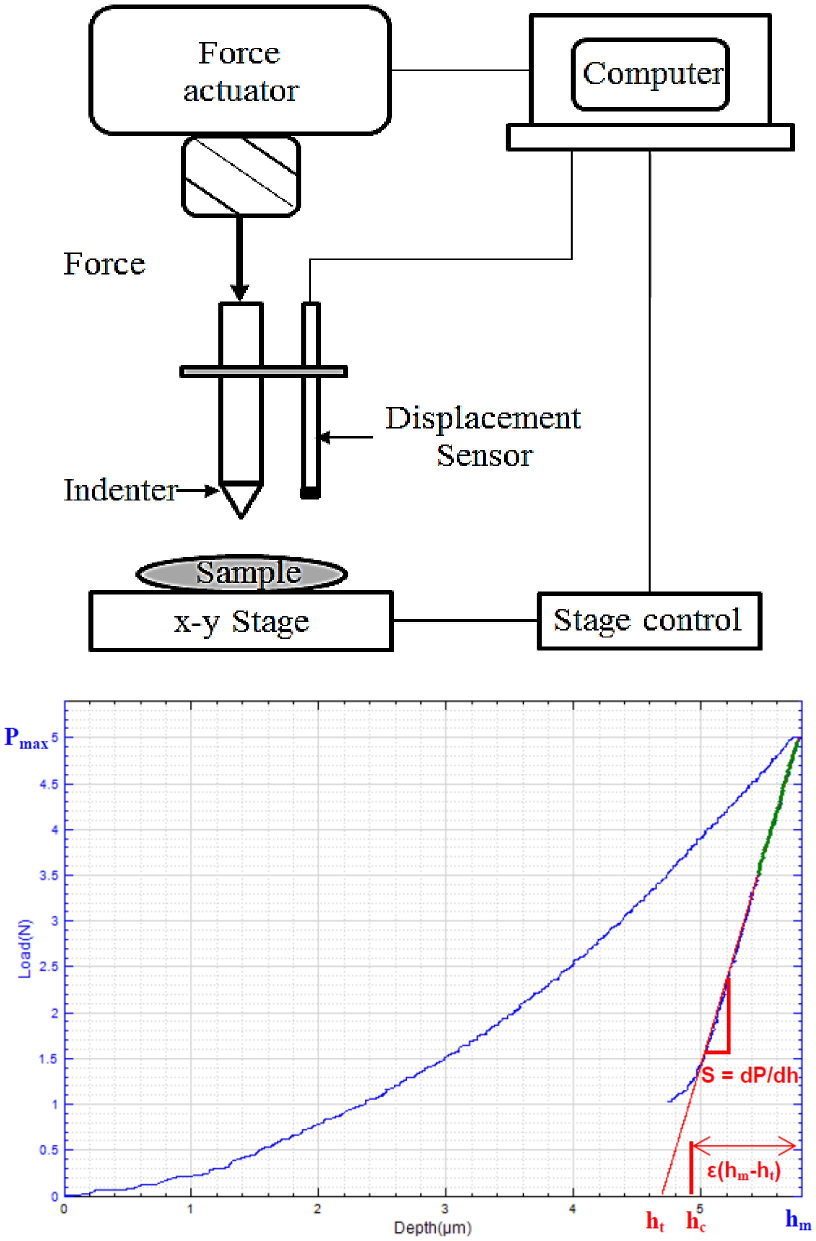

Fig. 3.3. (Top) Schematic of the indenter, and (Bottom) Example of the loading-unloading curve for Hardness and elastic modulus calculation. Hardness (H) and elastic modulus (E) are determined through the load/displacement curve. A power-law fit through the upper third to half of the unloading data line intersects the depth axis at ht. The stiffness S is given by the slope of this line [adapted from Alexis Celestin]

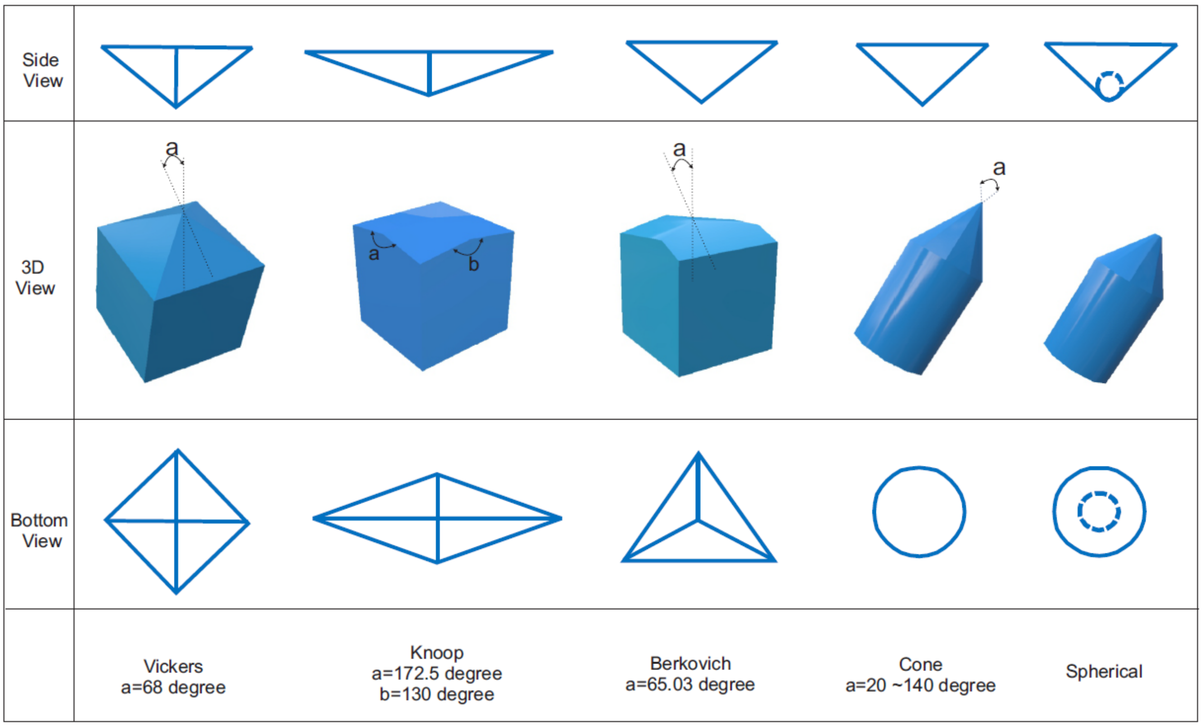

Fig. 3.4. Schematic illustration of several types of standard indenter tips. These tips were selected based on the requirements of the application. [Figure redraw from Gong et al., 2010]. For the study on hard materials such as rock and ceramic, the Vickers and Berkovich tips are the most commonly used. As for this study, both micro and nano indentation used a Vickers indenter tip.

3.2.2.2. Nano indentation

The micro indentation gives the average mechanical properties over the large area of different grains, often clays and non-clays; the nano-indentation can give the localized mechanical properties of a single grain [Du et al., 2017b], therefore provides separation between clays and carbonates, quartz, feldspars, and iron/zinc sulfides. Both micro and nano indentation are based on the same principles and the main difference during the experiments is the measurement of displacement. For micro, displacement sensor shots a light beam to the sample and reflected by a mirror placed on top of samples, the distance is calculated by the time of the light travel back. For nano, the displacement sensor was built–in with the indenter tip, so that the indenter tip and sensor moved at exactly the same speed, this way the measurement was more accurate and precise, it also reduced other errors may be associated with the mirror, such as a tilted surface or a signal out of range problem.

The experimental operating conditions for micro and nano indentation are listed in Table 3.4 below. The Poisson's ratio of the material (ν) in this study was assumed as a constant equal to 0.2, based on large-scale measurements on shales from the literature [Mavko et al., 2009; Wang et al., 2001]. The experiment was conducted at ambient conditions, on dry rock /cement samples, so the water content, P and T conditions were kept the same, while each of the two rock sample sets was tested at different orientations to the bedding, parallel and perpendicular. In addition, it is relevant to state that microstructural and mechanical properties widely vary in geo-materials, there was an attempt to compare samples at the same spatial scales.

Table 3.4. Operational Settings for Micro and Nano Indentation during data acquisition on Nanovea PB1000 [Du et al., 2017b]

	Micro	Nano
Maximum force	10 (N)	35 (mN)
Loading rate	20 (N/min)	70 (mN/min)
Unloading rate	20 (N/min)	70 (mN/min)
Pause at maximum load (s)	30	15
Contact load (mN)	15	0.08
Poisson's ratio*	0.2	0.2
Indenter type	Vickers	Vickers

* Poisson's ratio was assumed as a constant equal to 0.2, based on large-scale measurements

Mechanical maps were generated using MATLAB based on the nano-indentation data. Each map was generated based on at least a hundred nano-indentation test results (10 x10 grid), as shown in Figure 3.5. The idea of making mechanical maps to show the properties' difference was inspired from the contour maps. Contour maps were first used in 1791 by

French engineer J.L. Dupain-Triel to show the difference of elevations, later, other types contour maps were generated such as isopach (thickness), isobar (pressure), isotherm(temperature), etc.[Wilford, 1998]. More recently, Randall et al. started to use indentation data to generate micro mechanical maps in the multiphase composites [Randall et al., 2009]. The color bar was used for this study in these maps to represent different values of the measurement. As the color on the map changed from yellow to green, then blue, and finally deep blue, the value of E and H decreased. The brighter (yellow) spots represent grains with higher mechanical properties. The map gives the distribution of mechanical properties of the materials in a selected area. Since the minerals within shale have distinguished properties, the current approach is correlating the measured properties with properties of each mineral from literature, thus, the mineralogy/morphology and the mechanical properties in multiphase materials were correlated.

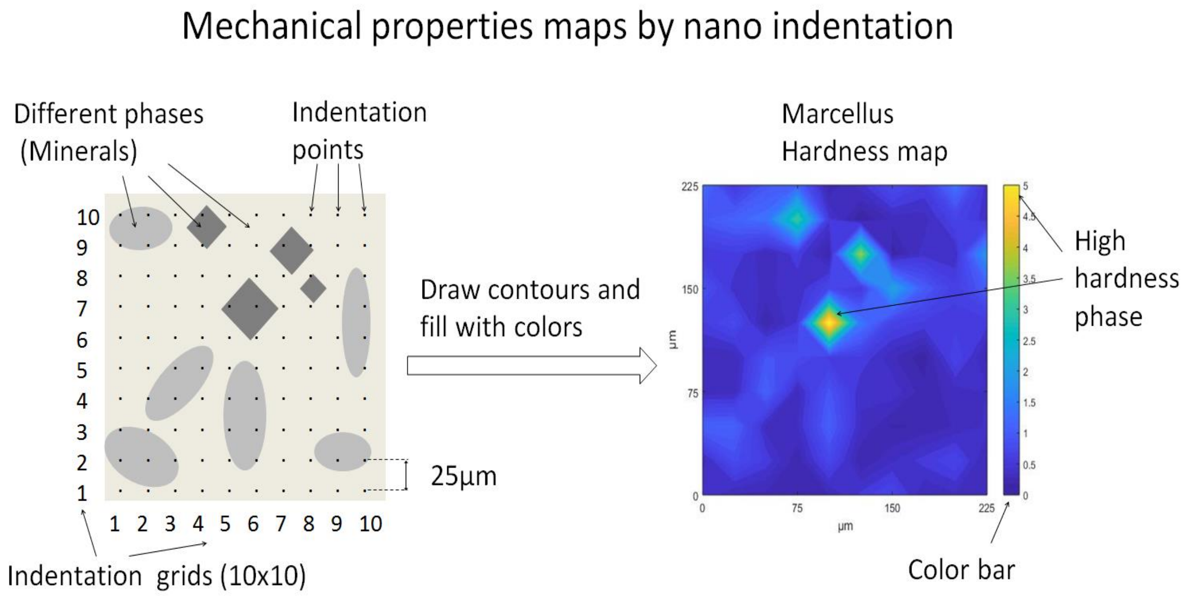

Fig. 3.5. (left) Schematic of the grid indentations performed on a multi-phase material and (right) an example of color-fill contour map of the hardness of Marcellus shale

3.2.2.3. Validation of the indentation techniques (cement data)

Triaxial compressive strength test was used to validate the results from indentation techniques, the results were shown in Figure 3.6. All of seven samples are cement from the same batch. The sample 1, 2, 3, and 4 (shown in purple) were measured with indentation, each sample was tested with at least 10 points and results were averaged and showed here with a standard deviation. Sample A, B, and C (shown in gold) were measured with the triaxial compressive strength test by the lab of a major oil company. The results indicated that Young’s modulus measured by indentation were in good agreement with the conventional mechanical characterization method.

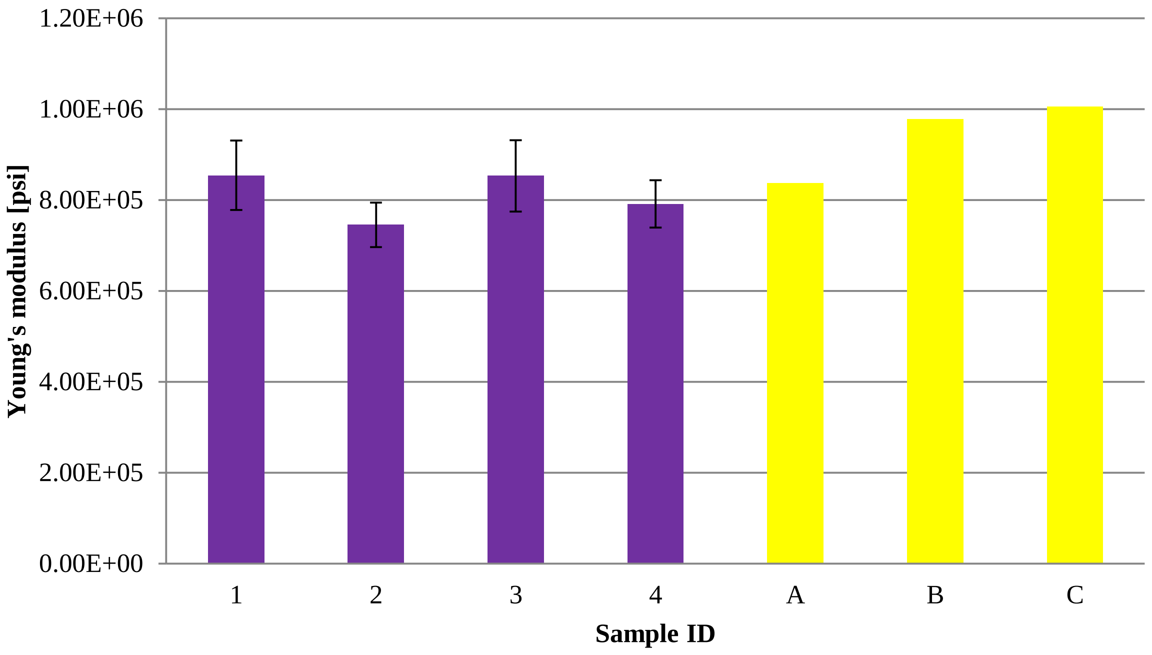

Fig. 3.6. Validation of the indentation techniques with the triaxial compressive strength test. All seven samples are cement from the same batch. Sample 1, 2, 3, and 4 (left) were measured with indentation and sample A, B, and C (Right) were measured with the triaxial compressive strength test.

Besides the accuracy, the indentation test also has several advantages over the conventional mechanical property test: 1) it can be done on the same sample multiple times while conventional test breaks the sample every time; 2) it only requires a small piece of sample while the conventional test has more restrictions over the sample size. These advantages make a dynamic study of shale from drilled cuttings possible.

3.2.2.4. Indentation fracture toughness

The Vickers Indentation Fracture (VIF) test was first proposed in the late 1970s to estimate the fracture toughness of ceramic materials through the measurement of induced crack lengths by a Vickers indenter [Lawn et al., 1980; Anstis et al., 1981]. More recently, this technique was also adapted and applied to biomaterials such as tooth and bones for fracture toughness measurements [Khor et al., 2003; Denry and Holloway, 2004; Şakar-Deliormanli and Güden, 2005]. As same as the indentation process, this method used a Vickers indenter to make a hardness impression on a polished specimen surface. The normal force was applied to the indenter to create a plastically-deformed imprint on the specimen surface. Cracks were also induced at the same time emanating radially outward from the four corners of the imprint. Combined measurements of the cracks with the indentation results (hardness and Young’s Modulus), the Fracture toughness of the material can be computed. [George D. Quinn, 2006]. More than 40 different equations have been presented in the literature for the fracture toughness determination based on observed crack length on the sample surface, because most of them are arrived at by curve fitting to data [Quinn and Bradt, 2007; Kruzic et al., 2009]. Only the most cited and applied in practice and were mentioned in this discussion.

Anstis et al. (1981) derived the formula of fracture toughness (Kc) under the assumption that the indentation induced a radial-median crack system:

$$\mathrm{Kc} = \xi_V \left(\frac{E}{H}\right)^{1/2} \frac{P}{c^{3/2}}$$

where P is the applied load, E is Young's modulus, H is the hardness, c is the length of radial crack measured from the center, and ξ_V is a constant depending on the indenter geometry (0.016 ± 0.004 for Vickers diamond) [Anstis et al., 1981]. Laugier [1985] derived a similar expression where (E/H) had the power of 2/3 instead of 1/2.

Later, Laugier [1987] also added the formula under the assumption that the indentation induced a Palmqvist crack system:

$$\mathrm{Kc} = \xi_V \left(\frac{a}{l}\right)^{1/2} \left(\frac{E}{H}\right)^{2/3} \frac{P}{c^{3/2}}$$

where a is the indentation impression length, and l is the average length of a Palmqvist crack [Laugier, 1985; Laugier, 1987].

Comparing with conventional fracture toughness measurement, the Vickers indentation fracture test only requires only a small volume of material, simple sample preparation, and low costs. All of which makes the method attractive, but the traditional fracture mechanics community has been skeptical of this method because it frequently produces inaccurate results [Quinn, 2006; Quinn and Bradt, 2007]. All the equations have some weak points in common: 1) the uncertainty of empirical calibration constant (ξ_V); 2) the measurement of the crack lengths on the surface (c, a, and l); and 3) the assumption on the crack system. These problems will be further discussed later.

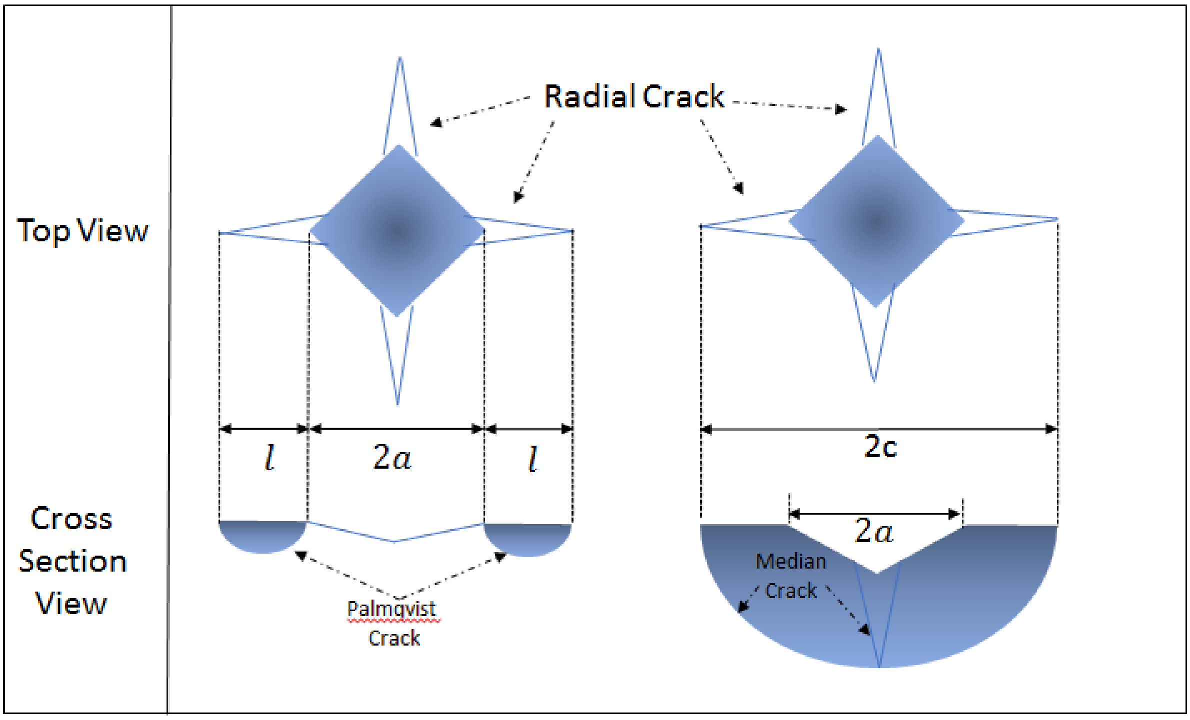

Fig.3.7: Palmqvist (left) and median crack (right) geometries around a Vickers indentation. [Figure redraws from Sakar and Guden, 2006]

Although the results calculated by this method are frequently inaccurate with a lot of uncertainties, the term E/H* were appeared in various fracture toughness equations. The ratio of hardness to Young's Modulus (H/E) describes the material deformation relative to yielding [Finkin, 1974], when multiplied by a geometric factor, it is defined as "plasticity index" which describes the deformation properties of a rough surface in contact with a smooth surface [McColm, 2013]. During the indentation test, materials with lower H/E ratios show less pile-up effect than materials with higher H/E ratios [Pintaude, 2013]. Therefore, this study adapted the ratio concept and used it as an indicator of the fracture initiation.

3.2.2.5. Image-based correlation of microstructures and micromechanics maps

As a natural multiphase composite, shale contains varies of minerals with different sizes, chemical composition, petrophysical and mechanical properties. The high resolution electron microscopy offered an insight into the material microstructure at the nano and micrometer scale so that every single phase, as well as its distribution within the composite can be identified. The nano-indentation offered mechanical properties measurement of particles at micrometer to sub-micrometer scale, which means the properties of every single mineral can be measured. With grid indentation, the mechanical maps could be generated to better characterize the rock, such as where the fracture is initiated, how the fracture propagates. The maps could be also useful as input data for modeling rock behavior. When combined mechanical maps with SEM/EDS/BSE microstructural characterization, geochemical and geomechanical changes can be monitored in an interdependent manner during a dynamic study (rock-fluid interaction)

4. RESULTS

4.1. FRACTURES IN SHALE: FUNDAMENTALS AND MECHANISMS

4.1.1. Shale Mineralogy and Microstructure

Shales consist of broad-scale quartz, feldspar, plagioclase, calcite, dolomite, pyrite chlorite, kaolinite, illite, and smectite. The chemical composition of each mineral was shown in Table 2.1 before. Based on the structures of them, they can be divided into three main Categories: Clay (tectosilicates), quartz & feldspar (phyllosilicates), and carbonate (other minerals). Table 4.3 below shows the summary of core-scale experimental data on the properties of well-characterized shales and mudstones compiled from multiple studies [Bourg, 2015; Amann et al., 2013; Bai et al., 2013; Busch et al., 2008; Chalmers et al., 2012; Josh et al., 2012; Swift et al., 2014; Nelson, 2009]. The top section is sealing shales for CO2 and waste storage while the bottom section is the brittle shales for hydrocarbon extraction. The table includes the average mineralogical composition as a percentage of total mineral mass, total organic carbon as a percentage of solid mass, porosity as a percentage of the rock volume. The database used to calculate average porosity values was restricted to studies that quantified. The total porosity neglected data obtained with water immersion and mercury intrusion as these techniques significantly underestimate the porosity of clay rich rocks. The comparison shows sealing shale has a much higher clay content, lower quarts/feldspar, and carbonate content. The porosity of sealing shale is much higher than the brittle shale which is not fully understood and needs further investigation.

As indicated by the Table 4.1, Shale formations with higher clay content are more likely utilized as seals for carbon capture and storage (CCS) and nuclear waste storage, while formations with lower clay content and higher TOC are the potential targets for hydrocarbon extraction. Therefore, clay mineral content was identified as a very important variable that controls key material properties of these formations [Du et al., 2017a].

Table 4.1. Sealing shales vs. brittle shales. Average mineralogical composition, total organic carbon and porosity of core-scale experimental data on the properties of well-characterized shales and mudstones compiled from multiple studies (Detail data in appendix) [Bourg, 2015; Amann et al., 2013; Bai et al., 2013; Busch et al., 2008; Chalmers et al., 2012; Josh et al., 2012; Swift et al., 2014; Nelson, 2009].

Formation	Clay (%)	Quartz & feldspar (%)	Carbonate (%)	TOC (%)	Porosity (%)
Sealing shales average	52.6	33.6	12.1	1.6	18.5
Brittle shales average	25.4	43.7	25.7	4.7	5.7

The mineralogical composition determines the sensitivity of the shale formation to particular fracture fluids. It also has an important part in determining the mechanical properties. Miro indentation tests were conducted on different types of shales in this study. The results are shown in Figure 4.1 below. Eagle Ford, Marcellus, Woodford, and Bakken are been known as major source rocks, while Pottsville, Mancos, Wilcox, and Wolfcamp are potential caprocks for CO_2 storage (Woodford and Wolfcamp data from Shukla et al., 2013) [Shukla et al., 2013]. The plot was made with clay content increase from left to right from 10% to over 60%, but the mechanical properties of E and H are not a proportional to its clay content. Another observation is that the E and H have a similar trend, in another words, samples with higher E also have higher H. This can be explained from the typical stress and strain curve as shown in Figure 4.2 below. During the indentation test, both elastic and plastic deformation happened as the indenter penetrating the material, but E only describes the slope of the elastic zone while H is correlated with the total strain including both elastic and plastic zones. The relation of E, H and the deformation type (plastic Vs. elastic) is further discussed in the later section.

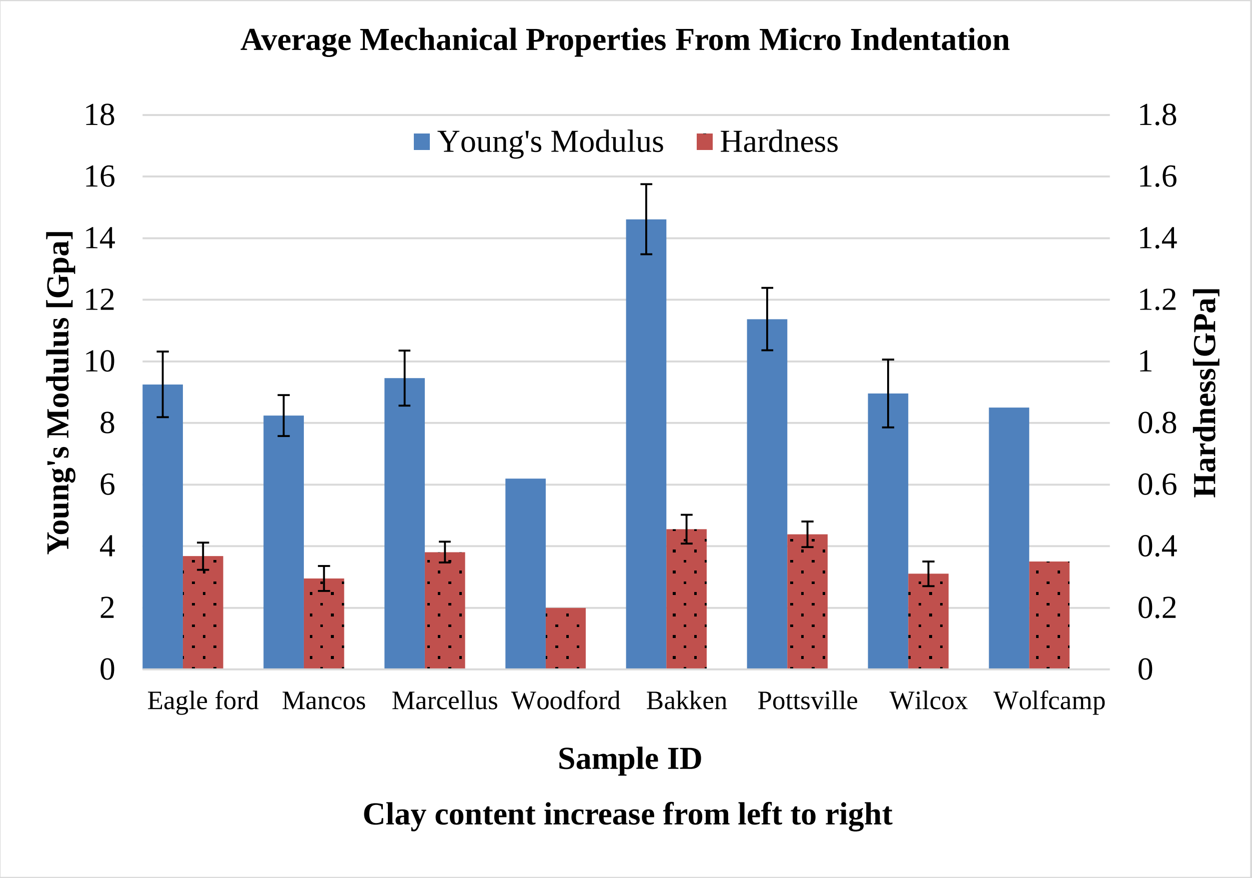

Fig. 4.1. Indentation results on different shale samples, The clay content increase from left to right, but the mechanical properties do follow the same trend. (Woodford and Wolfcamp data from Shukla et al., 2013)

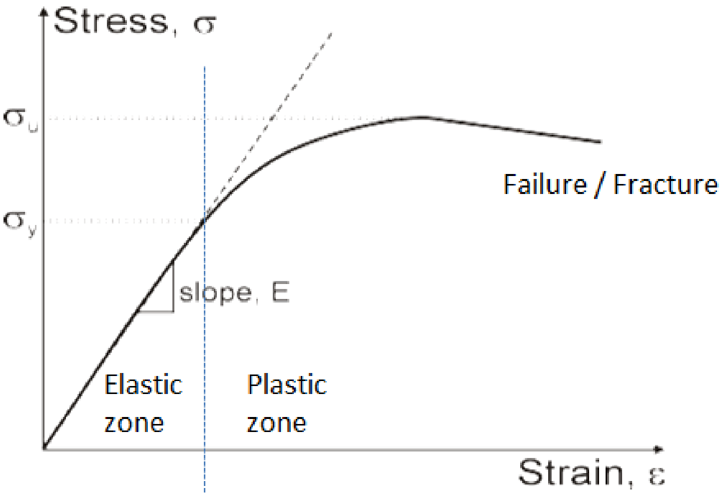

Fig. 4.2. Schematic of stress and strain curve showing the elastic and plastic zone

Few BSE micrographs (Fig 4.3) of the rock samples were shown here as an example to see the difference in mineral contents and microstructures. With some experiences on the BSE micrographs, even some of the mineral types can be identified. For example, the large, flat and relatively dark particles in Pottsville and Wilcox were quartz, and the small, amorphous particles were clay minerals. To be more accurate on the mineral identification, EDS with element maps were used as it determines chemical distribution and concentration in areas of interest, results from EDS is shown later in the property anisotropy section.

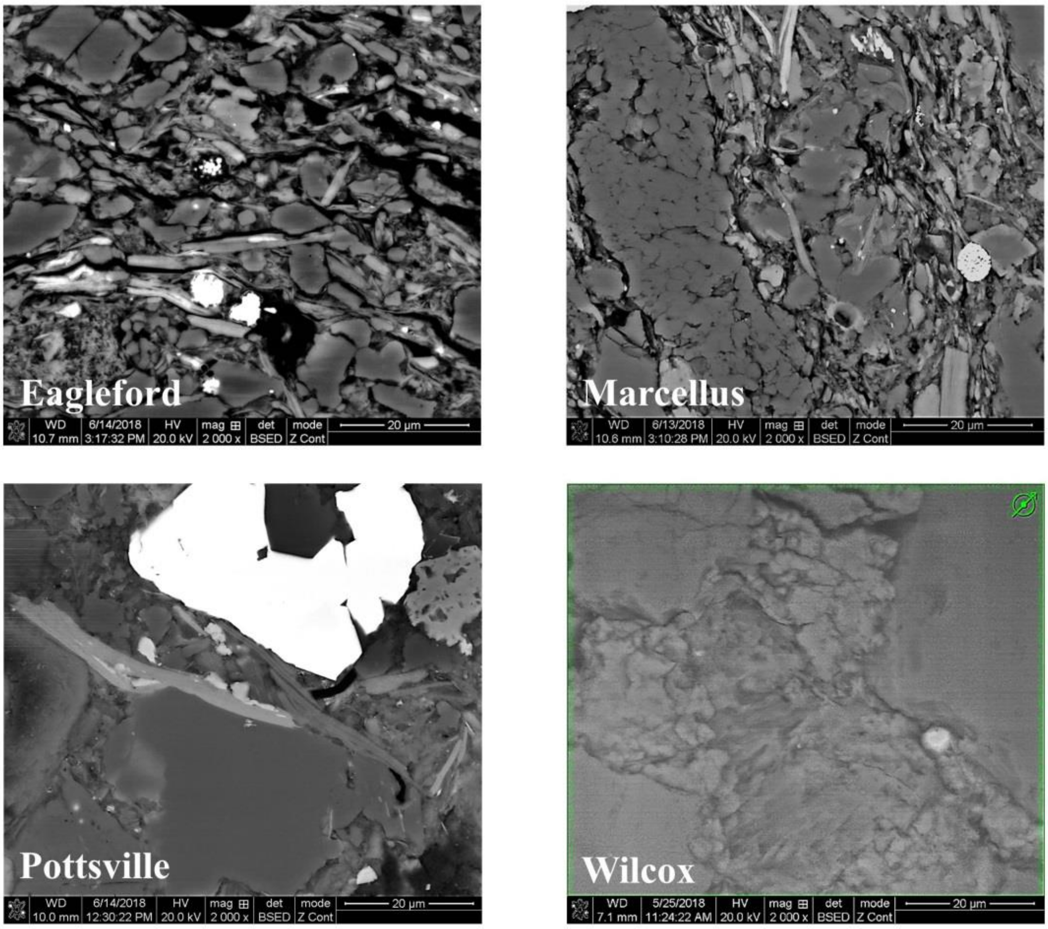

Fig. 4.3. Backscattered Electrons (BSE) Microscopy micrographs of rock samples from different formations with a 20μm scale obtained on FEI Quanta 3D FEG dual beam FIB/SEM system at 20 kV. Heavier elements appear brighter in the backscattered electron images, and black pixels present in all maps could be porosity/fractures or kerogen

From Figure 4.3, Eagleford had more uniform size grains, most of them were below 5 μm while all other three rocks have relatively larger grains distributed (> 20 μm). Also, Eagleford had the highest amount of dark/black area which could be kerogen or void because heavier elements appear brighter in the backscattered electron images. Comparing the other samples, the larger size grains are quartz, carbonate, and metal oxide, which have relatively larger sizes and higher mechanical properties than clay minerals. The Pottsville sample had a large amount of quartz (~50%) which shown as large, plain and smooth surfaces in the micrographs, these large grains are the main load-bearing phase and the clay matrix partially filled the space between these grains. While for the Wilcox sample, these large grains are separated apart and the clay matrix itself becomes the main loadbearing phase. Therefore, the Pottsville sample had higher mechanical properties than the Wilcox sample. In another word, the manner of how the clay matrix fills the space between larger grains controls the mechanical properties of shales [Rybacki et al., 2015].

Out of all these shale samples, Marcellus and Pottsville were taken to be further compared as representatives of unconventional reservoir rock and shale cap rock respectfully. Because the 1) the Eagleford shale consists majorly fine-grained carbonate and much less clay mineral than other shales [Elston, 2014] and the sample available is an outcrop instead of drilled cores like other samples; 2) Although the Wilcox shale samples were also drilled cores, the cores from same well and different depths showed huge difference in all aspects including the mineralogy, grains size, petrophysical and mechanical properties, the Wilcox samples from top and bottom of the formation can be seen as two totally different types rocks; 3) the Mancos sample was obtained from a former colleague of the lab without some key information such as the location and depth of core; 4) the Bakken samples were embedded within epoxy resin, although the epoxy resin could be a good background contrast for imaging, the fact that it fills the pores of material is still an alteration of the microstructure and mechanical properties as it provides additional confinement to the mineral grains. Therefore, Marcellus and Pottsville samples were mainly focused for the rest of this study.

4. 1.2. Variations on Mechanical Properties

4.1.2.1. Depth (outcrop and drilled cores of marcellus shale)

Shales are complicate multiphase natural composites, the composition and microstructure can vary even in the same formation. To study the effect of depth, seven Marcellus shale samples are tested in this study, including one outcrop and six core samples from an active production well. The schematic of the well profile and the core samples ID and their corresponding depths are shown in Figure 4.4 below, and the average mechanical properties (Young's Modulus and Hardness) were measured by micro indentation and shown in Figure 4.5.[Du et al., 2017b].

Results from micro indentation tests (Figure. 4.5) showed that the outcrop had overall better mechanical properties (i.e., higher Young modulus and greater hardness) than the drilled core samples. It was also important to note that mechanical properties had a decreasing tendency with depth increased. Optical images of the samples were taken before indentation was performed. These images were shown in Figure 4.6. It was easy to see the differences in fracture widths and basic compositional lamination differences. Optical microscopy images of the outcrop sample showed the least amount of fractures of all samples, while both the amount and the width of fractures in the deep core samples increased with an increase in depth. Based on the micro indentation results, it can be concluded that the bottom portion of the formation was more likely to initiate fractures as it was less mechanically stable. However, the softer grains of the bottom portion also suggested that the fractures were likely to heal faster at the subsurface condition. Higher stress was required to initiate fractures in the top portion, but their greater hardness makes them behave more rigid, which will help to support the open fractures [Du et al., 2017b].

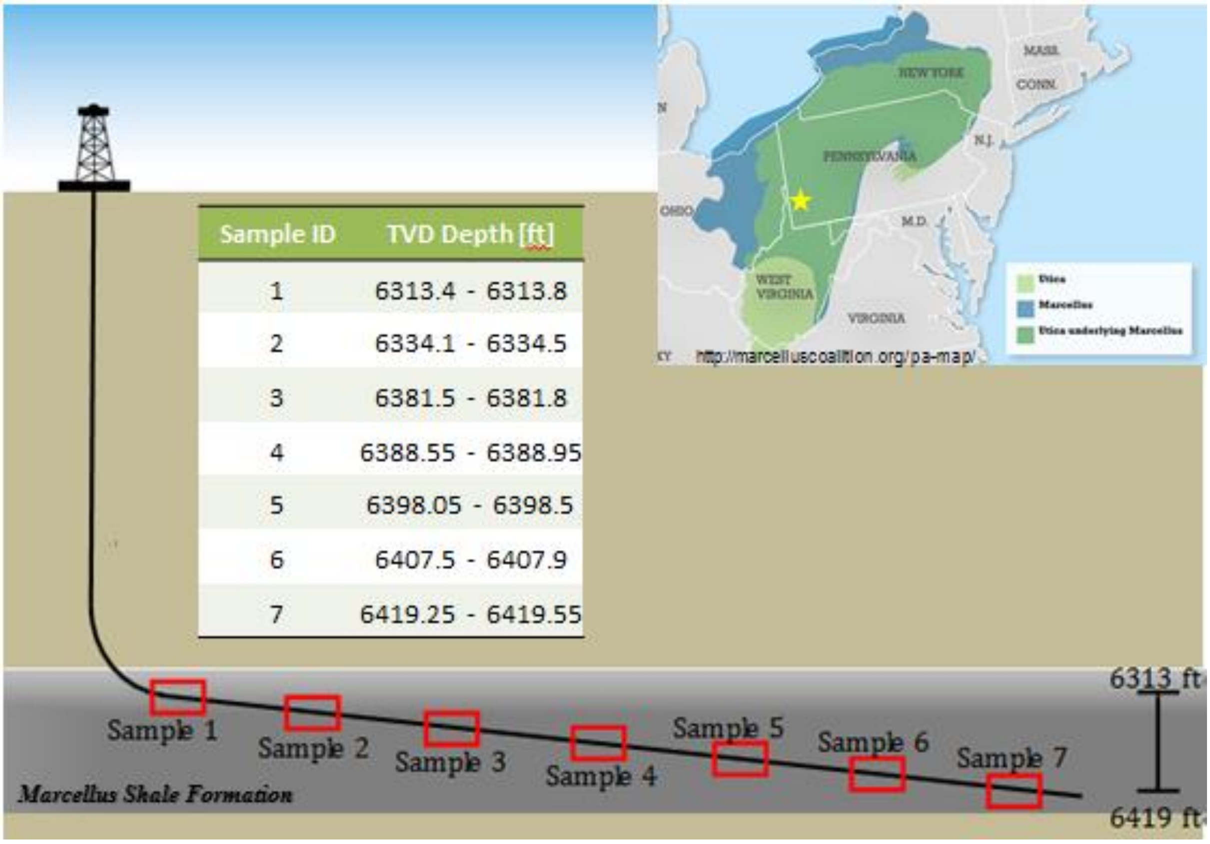

Sample ID	TVD Depth [ft]
1	6313.4 - 6313.8
2	6334.1 - 6334.5
3	6381.5 - 6381.8
4	6388.55 - 6388.95
5	6398.05 - 6398.5
6	6407.5 - 6407.9
7	6419.25 - 6419.55

Fig. 4.4. Schematic of the well profile and the core samples ID and their corresponding depths. The bulk size of each core was about four inches in diameter and one inch thick. [Du et al., 2017b]

The SEM analysis of the samples highlights major differences in texture, composition, and fracture size. Figure 4.7 showed a micrograph of the outcrop and core 2 at a 200 µm scale. Figure 4.8 showed a comparison of the outcrop and core Sample 7 at 100 µm. SEM micrographs suggest that the outcrop sample had a lot more iron sulfide pockets than both core samples and the average fracture width increased (from 7 to 15µm) as the depth increases. The larger fractures in the deeper samples indicate that they most likely have lower mechanical properties as the depth increases, which is also verified in the indentation experiment [Du et al., 2017b].

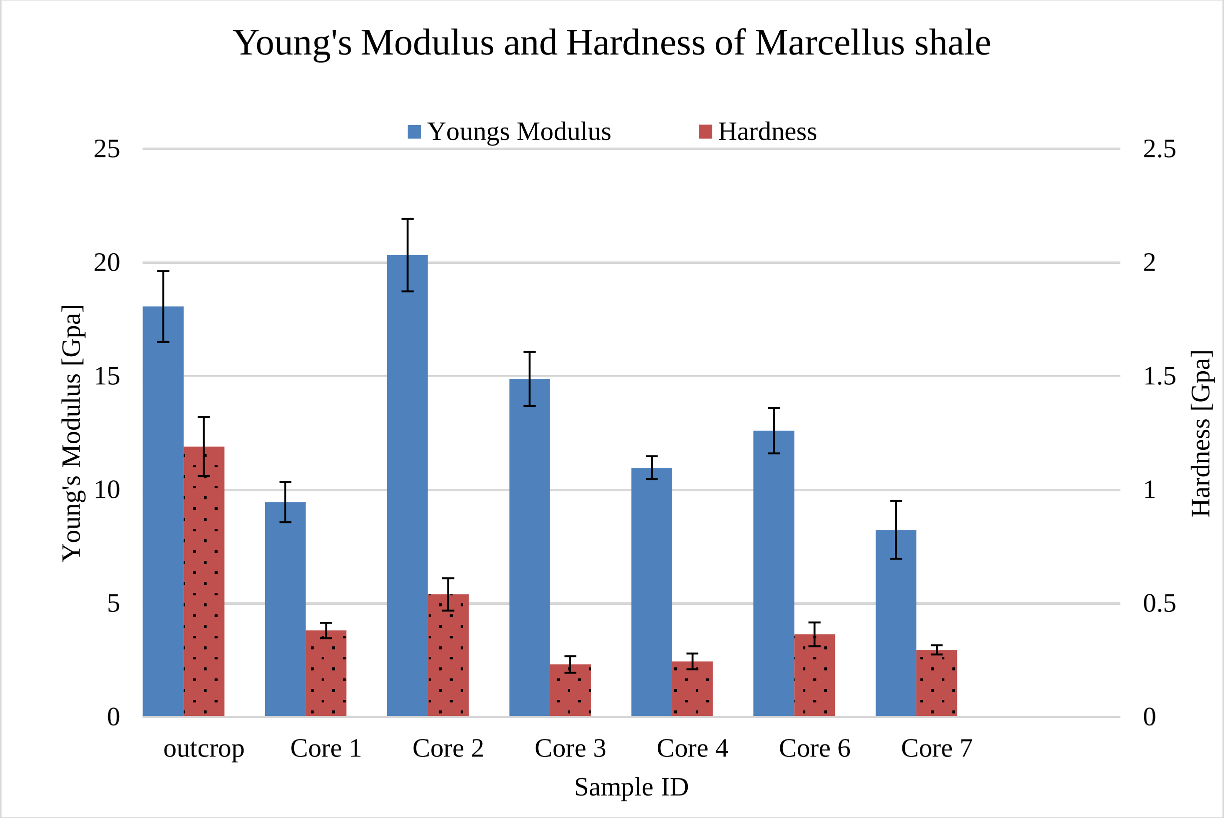

Fig. 4.5. Mechanical properties of Marcellus shale outcrop and drilled cores measured by micro-indentation. Core 5 was not listed here for comparison because it was a layer of coal instead of shale. [figure reproduced from Du et al., 2017b]

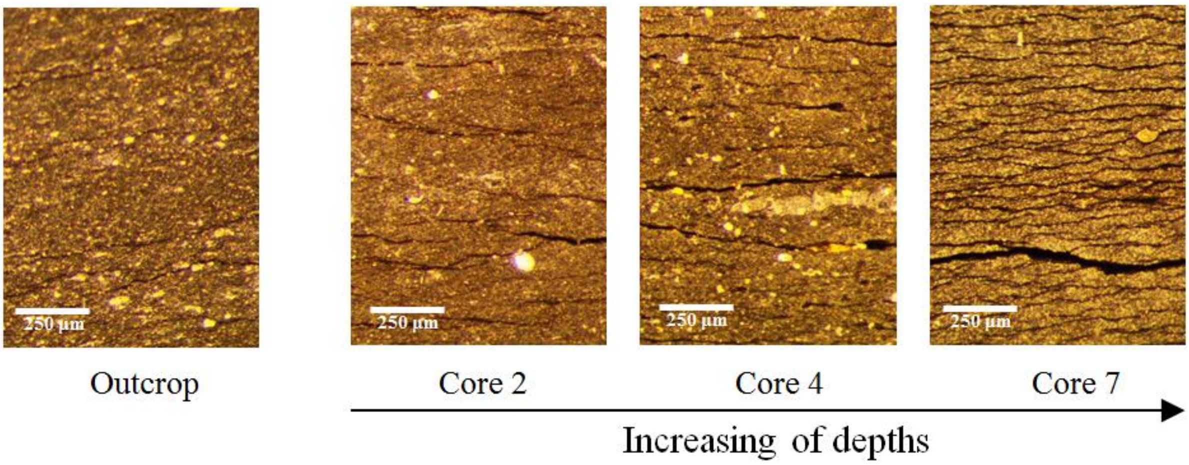

Fig. 4.6. Optical microscopy images of samples cross-sections showing the fractures along the bedding. Outcrop sample has a minimum amount of fractures, as the depths increase both the number and width of fractures increases [Du et al., 2017b]

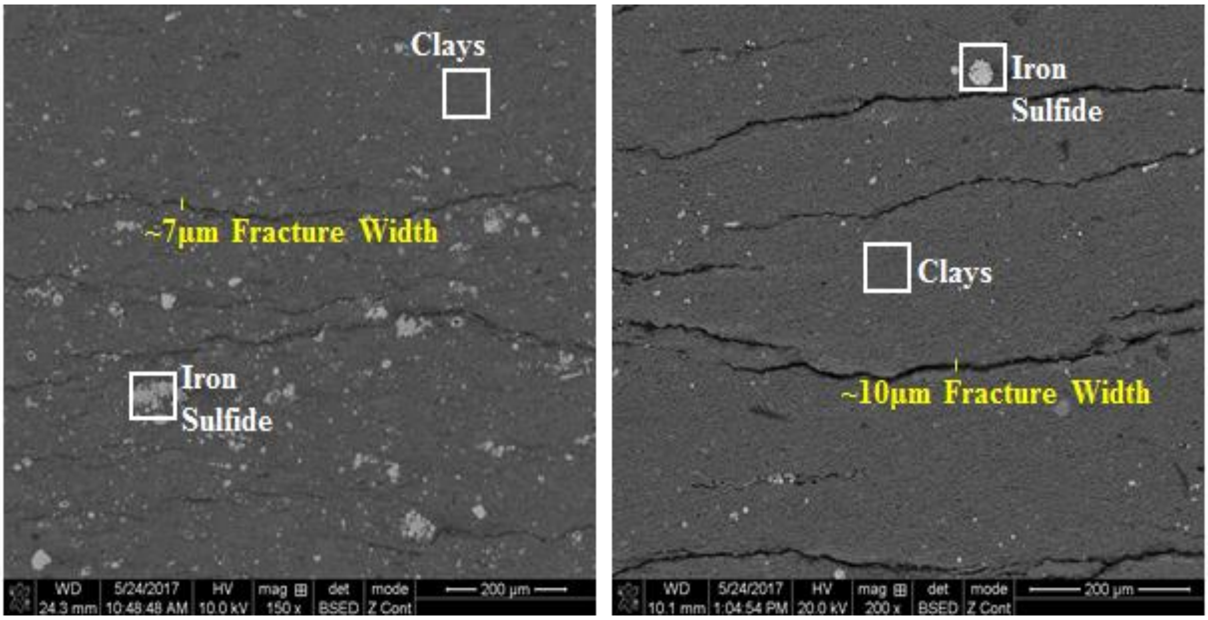

Fig. 4.7. Backscattered Electrons (BSE) micrographs of outcrop and core 2 (depth 6334.1-6334.5ft) with 200μm scale; Fracture width on the outcrop is slightly smaller than on the core sample 2; outcrop fracture width averages around 7μm, while sample 2 fracture width averages around 10μm. [Du et al., 2017b]

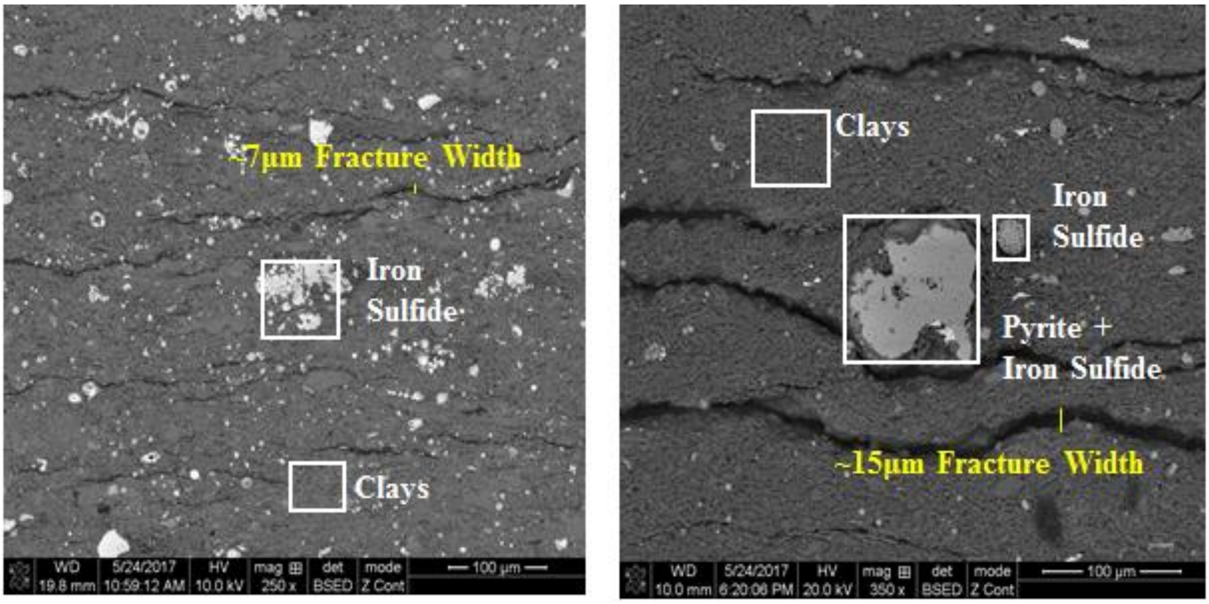

Fig. 4.8. BSE micrographs of outcrop and core 7 (depth of 6419.25-6419.55ft) with 100μm Scale; The number of fractures on core 7 is significantly higher than the outcrop, also the average fracture width is much larger (15μm compared with 7μm) [Du et al., 2017b]

Nano indentation tests were performed on both outcrop and core 3, and the results were depicted in Figure 4.9, both samples had a large portion of data points in the range of clay minerals of kaolinite, smectite, and illite while the outcrop may had higher quartz and mica content. The outcrop sample also had some high E grains, which could be chlorite or metal oxide. The properties of clay mineral from the literature have much wider ranges due to the properties anisotropy caused by its platy and layered microstructure. Clay minerals have layered structure which often carry negative surface charges and can adsorb and hold cations by electrostatic force forming a double layer. The cation exchange capacity (CEC) of shale is proportional to its clay content, and has been shown to be related with its geomechanical properties [Dewhurst, 2008]. The existence of this double layer can also reduce effective porosity, resulting in a decrease in permeability. The thickness of the double layer is dominated by the clay mineralogy, increasing from chlorite to kaolinite to illite to smectite and is influenced by the salt concentration in the pore fluid [Mesri, 1971]. Therefore, the type and amount of clay content are the key factors affecting shale sealing capacity, as both of them control the CEC, which determines the mechanical and petrophysical properties of the rock [Du et al., 2017b].

After showing the effect of depth on Marcellus shale, rock samples from Pottsville and Wilcox formation were also compared here in Figure 4.10 below. Samples shown here marked as top and bottom were from the same well at different depth (M-top and M-bottom are core 1 and core 7 mentioned before). The top sign did not mean the top of the given formation, it meant from all the samples available to this study, the top sample had the shallowest bury depth, and similarly, bottom meant the deepest bury depth. As shown in the

Figure 4.10, Wilcox had the largest difference between the top sample and the bottom, the top Wilcox sample had the highest E and H and lowest E/H value among all samples, which means it was the most mechanically strong and least likely for fractures to be initiated when under pressure. The bottom Wilcox had very similar values compare to bottom Marcellus, it showed low E and H and high E/H value, meaning it was mechanically weak and more likely to initiate fractures. Pottsville samples were overall stronger than the Marcellus shale as they had higher E and H and lower E/H value.

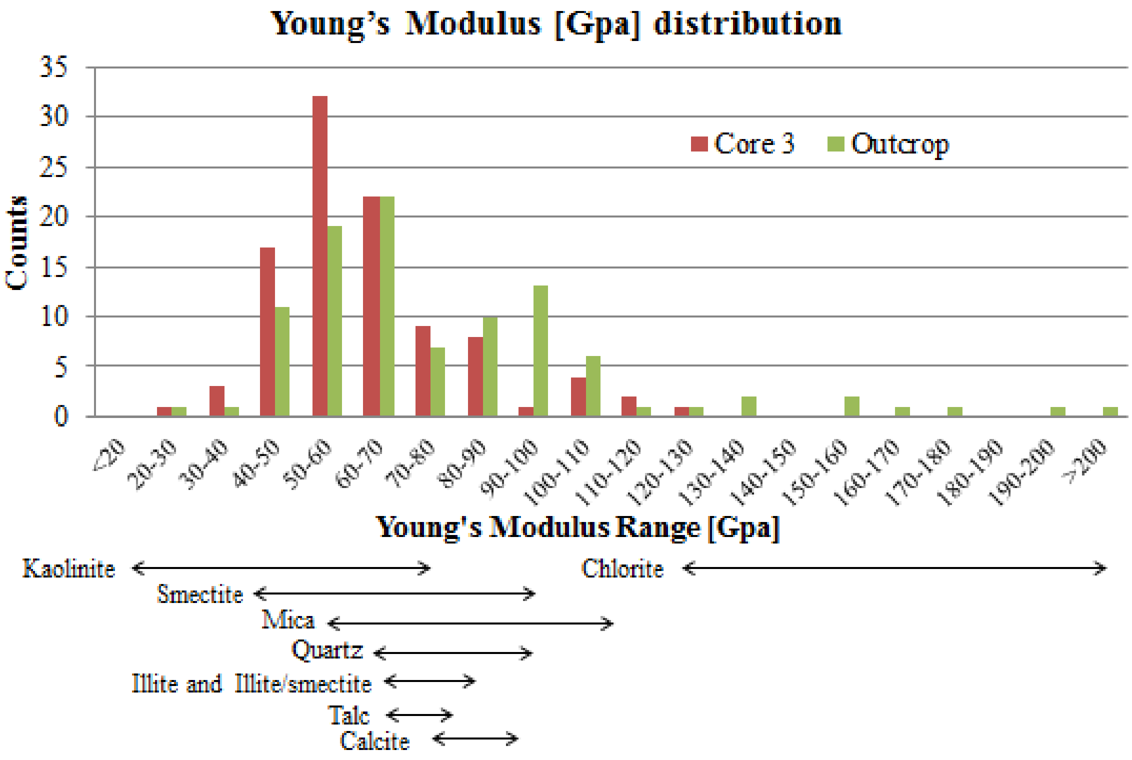

Fig. 4.9. Young’s Modulus (E) data distribution of outcrop and core3 measured by nano-indentation compared with literature E data [Wang et al., 2001; Mondol et al., 2008; Pawley et al.,2002] of common minerals found in shales. Both samples have a large portion of data points lay in the range of clay minerals of kaolinite, smectite, and illite while the outcrop may have higher quartz and mica content. The outcrop sample also has some high E values which could be chlorite or metal oxide [Du et al., 2017b]

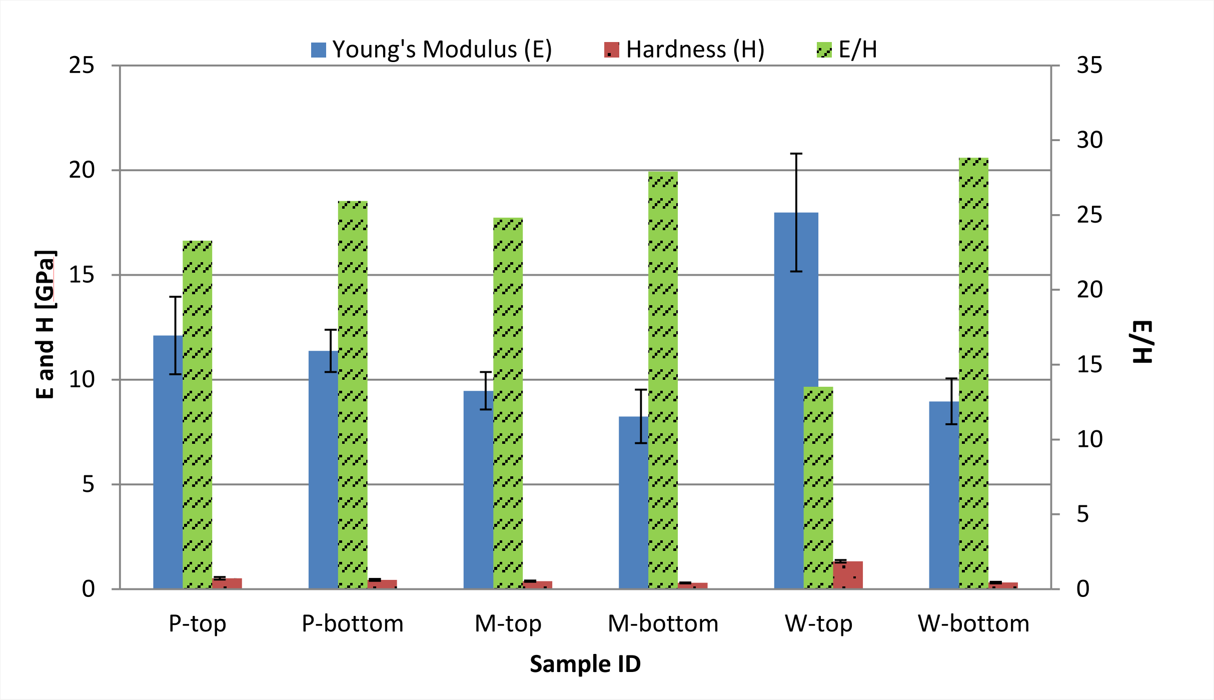

Fig. 4.10. Mechanical properties of Shales from different depths. P-Pottsville, M-Marcellus, and W-Wilcox. The blue bar is Young's Modulus (E), Red is the Hardness (H), Green is the Ratio of E to H.

When compared the differences between the top and bottom samples in all three sets of rocks, the top samples have higher mechanical properties and lower E/H value. Although this observation suggested rock cores from shallower depth had higher mechanical properties than the deeper cores, it can be only used as a general guide for mechanical properties prediction for shale cores from the same formation. For a specific set of cores, it may not be true depending on the sample selection, for example, if Marcellus core 1 was compared to core 2, the result would be different.

4.1.2.2. Properties anisotropy

Micro indentation tests were conducted on Marcellus and Pottsville shales at 0 degrees and 90 degrees to the bedding direction. Each of the directions was measured with at least 25 micro indentation points, each point is around 250 x 250μm (as shown in Figure 4.12 and

4.13), which is the same size of nano maps. The results were shown in Table 4.2. Pottsville showed overall higher average values for E and H, lower E/H values than Marcellus shale in both directions. Although both the E and H results from parallel direction were lower than the perpendicular direction for both samples, the E/H suggested that Pottsville was easier to be fractured perpendicular to the bedding while Marcellus was easier to be fractured parallel to the bedding. The Young's Modulus for all samples were quite close when considered the standard deviations, but the hardness showed a bigger difference, which may be caused by the visible fractures in the Marcellus shale as shown in Figure 4.11. Hardness was directly related to the penetration depth, when loaded with the same force, the one with more fractures/void (Marcellus) was easier to be penetrated deeper. The standard deviations of all measurements from Marcellus were much lower than Pottsville, which may because the distribution of grains' mechanical properties was more concentrated.

Table 4.2. Average data of mechanical properties measured from the micro indentation tests on Pottsville and Marcellus samples from two different directions, show larger error for Pottsville comparing to Marcellus [Du, and Radonjic, 2019]

Shale	Indentation Grid Direction	E [Gpa]	H [Gpa]	E/H [dimensionless]
Pottsville	Parallel (0 degree)	9.55 ± 1.7	0.50 ± 0.12	19.91
	Perpendicular (90 degree)	11.03 ± 2.4	0.53 ± 0.17	21.78
Marcellus	Parallel (0 degree)	7.48 ± 1.4	0.24 ± 0.08	33.11
	Perpendicular (90 degree)	8.96 ± 1.9	0.31 ± 0.05	29.04

The Figure 4.11 shown before indicated Marcellus shale had higher anisotropy and visible fractures along the bedding while Pottsville shale had dense, well-compacted texture and relatively more isotropic, when visually inspected and observed under an optical microscope. Therefore, Marcellus shale samples were ideal to show the difference a shale-rock can manifest as a result of bedding orientations. Progressive burial of the sediments caused mechanical compaction during the deposition; clay platelets are forced towards a parallel bedding alignment with a rapid reduction of porosity and permeability created by layered structured shale [Dewhurst et al, 1998; Dewhurst et al, 1999; Yang and Aplin, 2007]. From the micrometer size platy grains to meso-/ marco- scale layered rock, the significant anisotropy of properties were inherited [Du et al., 2017b].

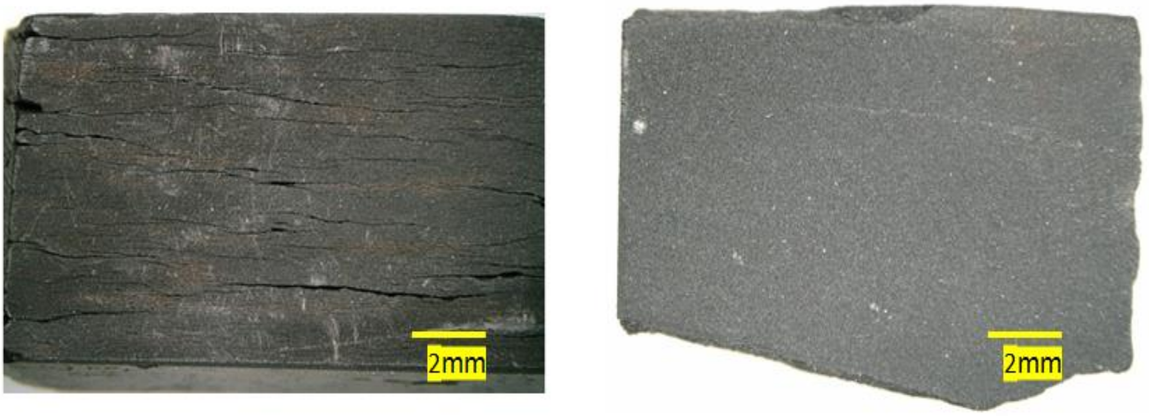

Fig. 4.11. Large filed view optical microscopy (OM) images obtained from Keyence VHX-6000 digital microscope, showing the different textures of shale samples: Left: Marcellus shale showing high anisotropy and visible fractures along the bedding; Right: Pottsville shale is dense compacted and more isotropic. [Du, and Radonjic, 2019]

When grid micro indentation was done parallel to the rock bedding (Figure 4.12): the imprints showed a pyramid shape due to the Vickers diamond tip. The material at the contacted area also pile-up on all four edges because of the shear failure and plastic upward flow along the indenter tip. When indentation was done perpendicular to the rock bedding (Figure 4.13): the material was compressed and densified under the same amount of force with no visible pile-up at edges, also, the bottom of the imprint has already shown signs of a rebound after the force released.

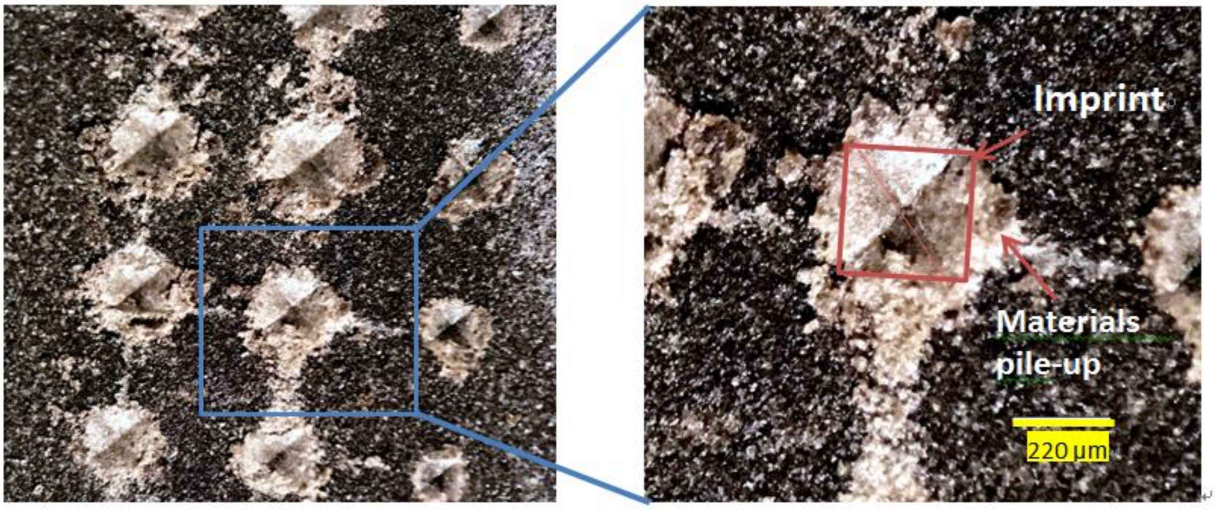

Fig. 4.12. Optical images of the Marcellus shale taken by the Echo Revolve optical microscope, indentation grid is parallel to the bedding direction. Left: the grid of the indentation imprints grid, right: zoom in to a single imprint [Du, and Radonjic, 2019].

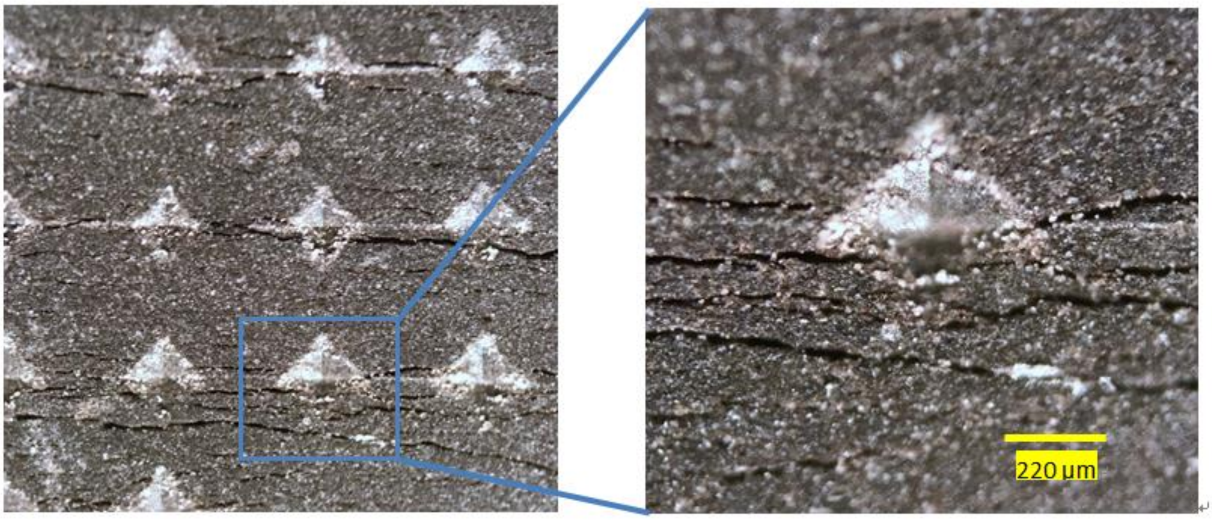

Fig. 4.13. Optical images of the Marcellus shale, indentation grid is perpendicular to the bedding direction. Left: the grid of the indentation imprints grid, right: zoom in to a single imprint [Du, and Radonjic, 2019].

Both indentation results and the optical images had clearly shown a higher degree of anisotropy in the Marcellus over Pottsville shale. As for the reasons for that, it can be concluded in two parts. The first one was the amount of the anisotropic minerals, shale is a mixture of large grains and a fine-grained clay matrix, and the clay mineral itself is anisotropic as introduced before. Therefore, a higher amount of clay content gives a higher degree of anisotropy. But this one can't explain the observation in this study. The Pottsville had a much higher clay content than Marcellus (43% vs 22%) but a lower degree of anisotropy. The other reason for the anisotropy is the distribution of the anisotropic minerals. As shown in Figure 4.14 below, the distribution of anisotropic minerals can be classified into two types, lenses network and scatter patches, of which the lenses network distribution of the minerals will end with a higher degree of anisotropy. The lithology of the shale samples (Table 3.1) also suggested all the producing shales including Marcellus were described as "fissile". In geology, fissility is the tendency of a rock to split along the bedding [Hise, 1896]. This is also because the lenses network distribution gives a higher degree of anisotropy.

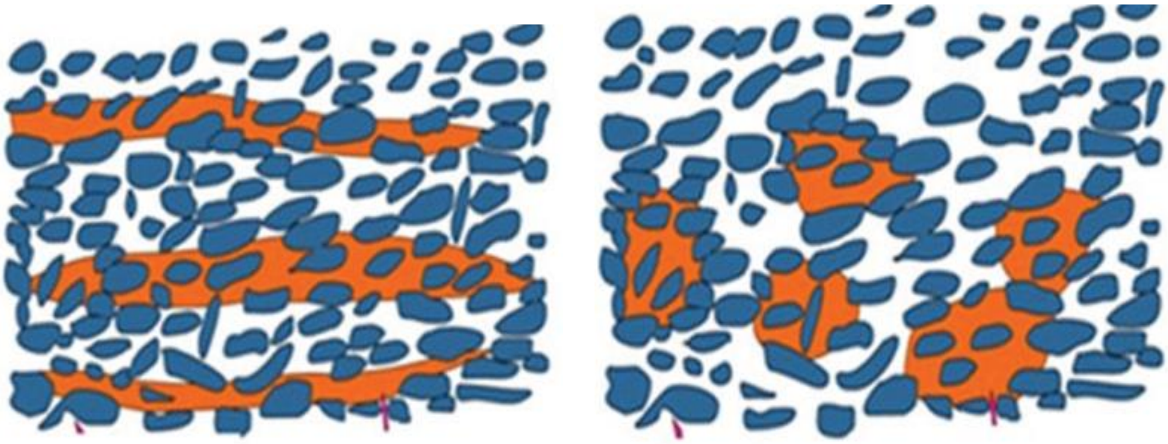

Fig. 4.14. Conceptual model of lenses network (left) and scatter patches (right), the orange color represents the small anisotropic minerals (clays), the blue color represents the large mineral particles [Zhao et al., 2016]

To confirm the different distributions of the minerals, BSE and element maps were used. Comparing Figure 4.3 and 4.4, the BSE micrographs and the element overlay maps shown Marcellus shale had lamination from top left to bottom right indicated by the large and elongated grains, which clearly showed the "lenses network" distribution; while for Pottsville, the grains were evenly distributed with no visible lamination, same as the scatter patches distributions.

Besides the distribution pattern, the element maps also gave useful information. The Si map showed the distribution of quartz as large, clean, and bright (high concentration) spots, both samples had a large amount of quartz and grains size of quartz in Pottsville was slightly bigger. The Ca maps indicated that the elongated grains in Marcellus are mainly calcite, while Pottsville only had a small amount of Ca. The S and O maps can be combined to show the porosity of the samples because the majority of the minerals in sedimentary (shale) rock contains O with some exception such as Pyrite (FeS) and Halite (NaCl). Since both Na and Cl were negligible (< 1%) in both samples, combining S and O maps covered most areas of the map, and the black pixels left could be porosity/fractures or kerogen. From which can be seen, the Marcellus had higher porosity due to more black pixels and Pottsville was more dense compacted. Combined S and Fe maps also showed that the majority of the bright spots in Marcellus shale BSE map were Pyrite, including the large grain in the middle-left and small round grains evenly distributed all over the map. The Fe map in Pottsville showed the large bright area in the middle of the BSE map is Fe-rich minerals, which were identified as Siderite and Hematite with spot analysis. The Al, Mg and K maps in both samples showed very similar distributions because they were commonly seen elements in clay minerals, which filled in the gaps between large particles such as quartz and iron oxide/sulfide. The brighter color in all Al, Mg and K maps in Pottsville also indicated higher clay content in the Pottsville sample over Marcellus sample.

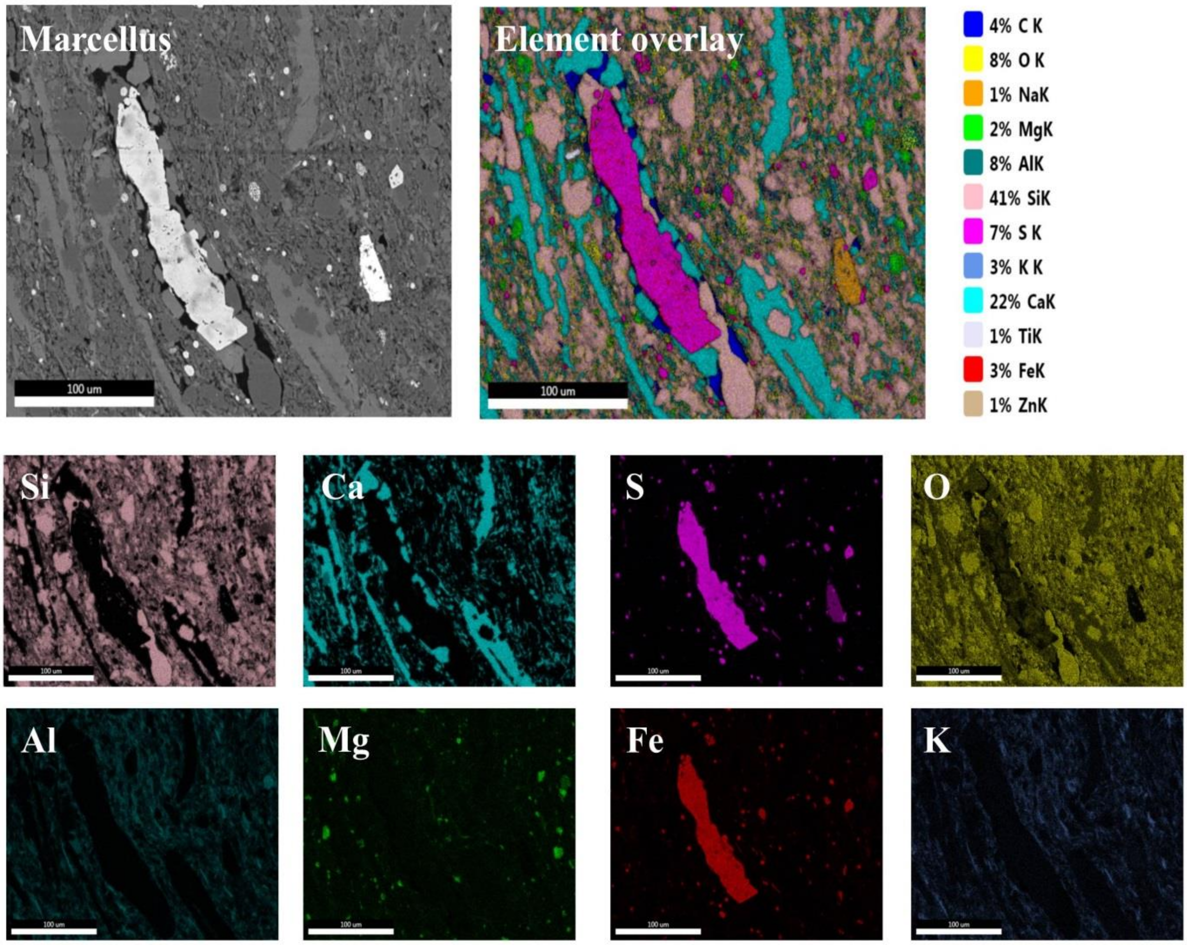

Fig. 4.15. Backscattered Electrons (BSE) micrographs of Marcellus (top left) rock and overlaid EDS elemental map (top right) with a 100 µm scale. The bottom part is the key elements distribution maps, brighter color on the micrograph means the higher the concentration of the corresponding element. The top two micrographs clearly showed the “lenses network” distribution of mineral like the conceptual model in Figure 4.14; while the bottom elements distribution maps help to identify the minerals within the area of interest.

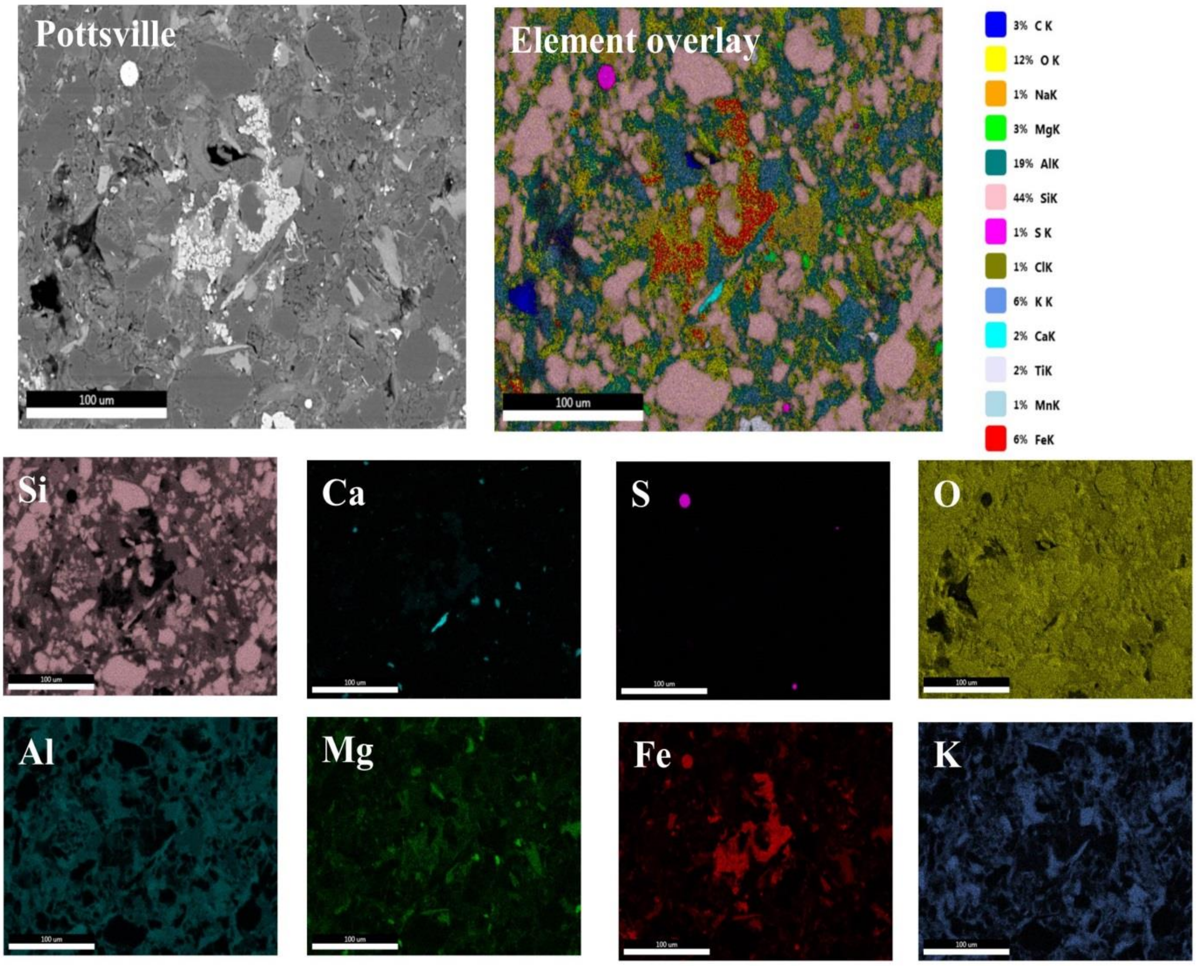

Fig. 4.16. Backscattered Electrons (BSE) micrographs of Pottsville (top left) rock and overlaid EDS elemental map (top right) with a 100 μm scale. The bottom part is the key elements distribution maps The top two micrographs clearly showed the "scatter patches" distribution of mineral like the conceptual model in Figure 4.14.

4.1.2.3. Change under mechanical stress

The failures of material were usually classified into brittle or ductile, which are related to the plastic and elastic deformation correspondingly. Due to the heterogeneity of shale, when subjected to a load, both types of deformations manifest simultaneously at different degrees, leading to a difference in failure/fracture response. Shales can be utilized as unconventional reservoir rocks for hydrocarbon extraction; caprocks in conventional oil and gas reservoirs; as well as hydraulic barriers in subsurface gas/ waste storage. In all above mentioned scenarios, the successful performance of shale directly depends on rigorous petrophysical and geomechanical characterization, which makes the understanding of the rock deformation behavior essential.

Six samples from three different formations were tested here (Pottsville, Marcellus, and Wilcox) with the same amount of force (10N), each formation contains two samples from different depths represented as top and bottom respectively. First round all of the six samples were indented on the polished surface to get their mechanical properties; Second round, each sample was indented at the exact same spots (on the imprints) to see how much the properties changed after they exposed to mechanical stress from the first round. The results were shown in the following Figures (4.17, 4.18, and 4.19). Examples of Loading-unloading curves on six different samples were shown in the appendix as well.

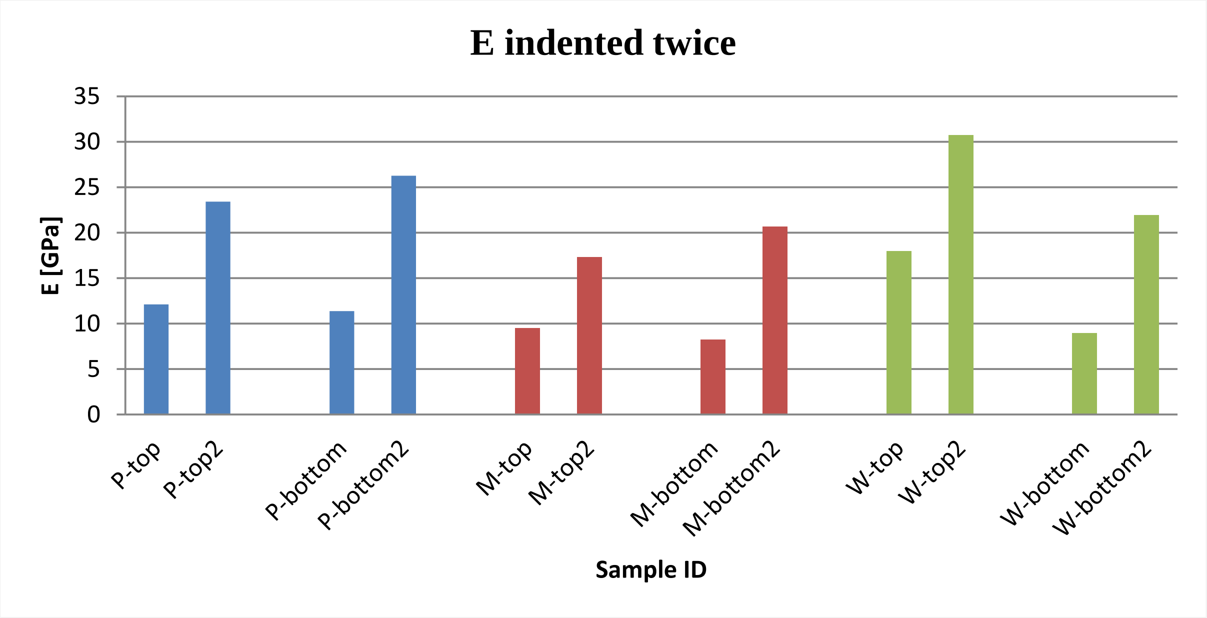

Fig. 4.17. Young’s Modulus (E) of six shale samples from three different formations. Each sample was tested twice with two 3x3 grids, the second test grid was on top of the first one at the same spots. Marcellus showed overall lowest E both before and after the first round indentation.

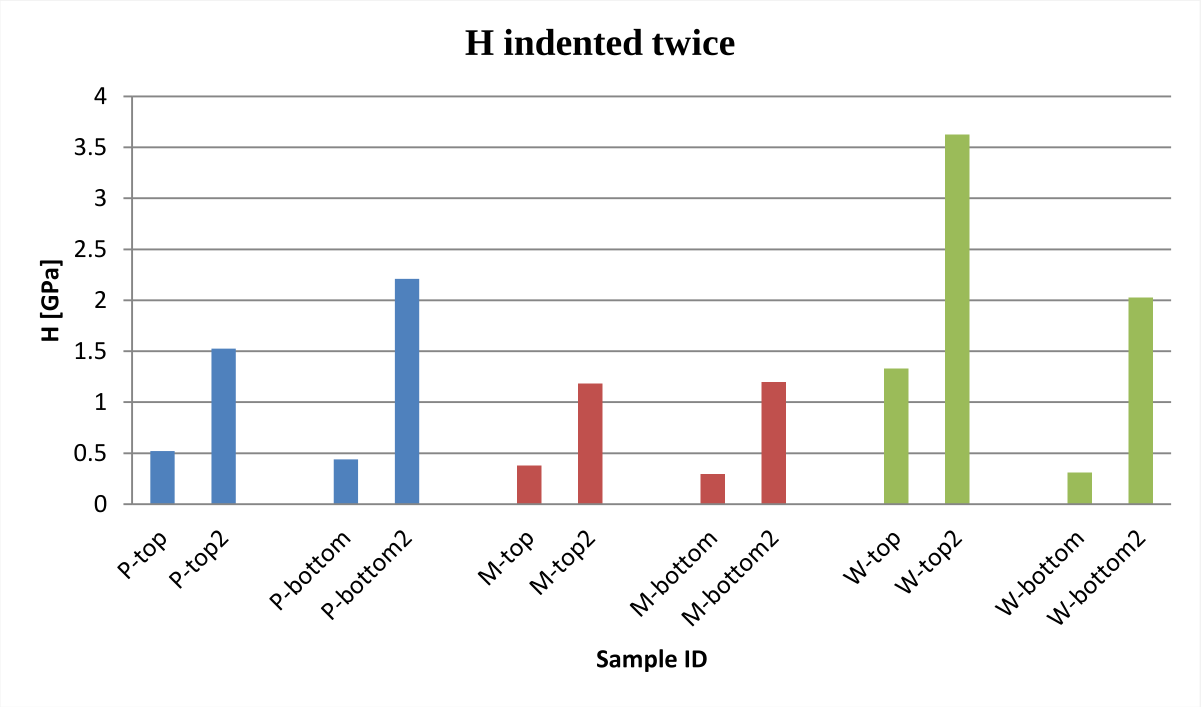

Fig. 4.18. Hardness (H) of six shale samples from three different formations. Marcellus still showed overall lowest H both before and after the first round indentation. Wilcox showed a much higher increase in H than the other two after indentation

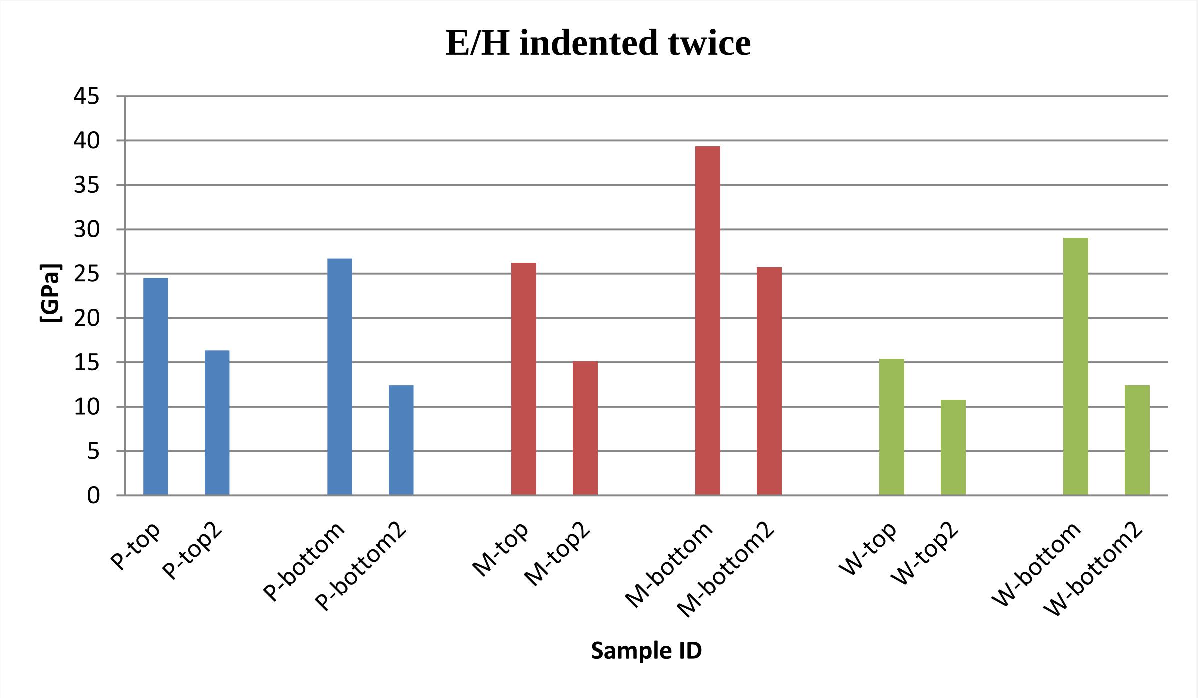

Fig. 4.19. Young's Modulus over Hardness value (E/H) of six shale samples from three different formations. All samples showed a decrease after indentation compress which means became mechanically stronger, with Wilcox being the strongest and Marcellus being the weakest.

As shown in the three figures above, for all samples, the second tests had significant higher E and H, while much lower E/H, meaning for all samples, the material at the contacted area were compressed and solidified at different degree and becoming strong with higher mechanical properties, and less likely to initiate fracture after compression.

Table 4.3. The change rate of Hardness, Young's Modulus, E/H value of six shale samples after indentation

Change rate	**H**	**E**	**E/H**
P-top	193.13%	93.33%	-33.34%
P-bottom	403.86%	130.91%	-53.55%
M-top	210.26%	82.70%	-42.33%
M-bottom	304.39%	150.44%	-34.61%
W-top	172.74%	70.72%	-30.09%
W-bottom	551.32%	144.37%	-57.19%

The same amount of force was applied through this part of the experiment, but the changes in different samples showed a significant difference. The change rates of each property of each sample were listed in Table 4.3. As shown in the table, Hardness increased from 172% to 551%, Young's Modulus increased from 70% to 150%, and E/H decreased from 30% to 57%. For each formation, the bottom section always showed a higher change rate under the same amount of compression force. Pottsville and Marcellus shale samples showed a very similar trend: in the first round at a flat surface, the top samples have overall higher E and H than the bottom; after compression, the bottom samples experienced higher change rates become stronger than the top samples (Figure 4.15 and 4.16). As for the Wilcox shale, the top and bottom samples showed the most significant differences, the W-top was the strongest rock among all six samples and showed the least amount of change in all three categories while W-bottom was the weakest rock and shown the most amount of changes.

4.1.2.4. Micro/nano mechanics maps

Nano indentation tests were performed on both Marcellus outcrop and core 3 to show the difference between outcrop and drilled cores, and the results are depicted in Figure 4.20. The yellow spots represent grains with higher mechanical properties, which are clearly more prominent in the outcrop. These rigid grains were evenly distributed in the outcrop sample which ends up an overall higher bulk hardness as shown in the result from micro indentation before (Figure 4.5).

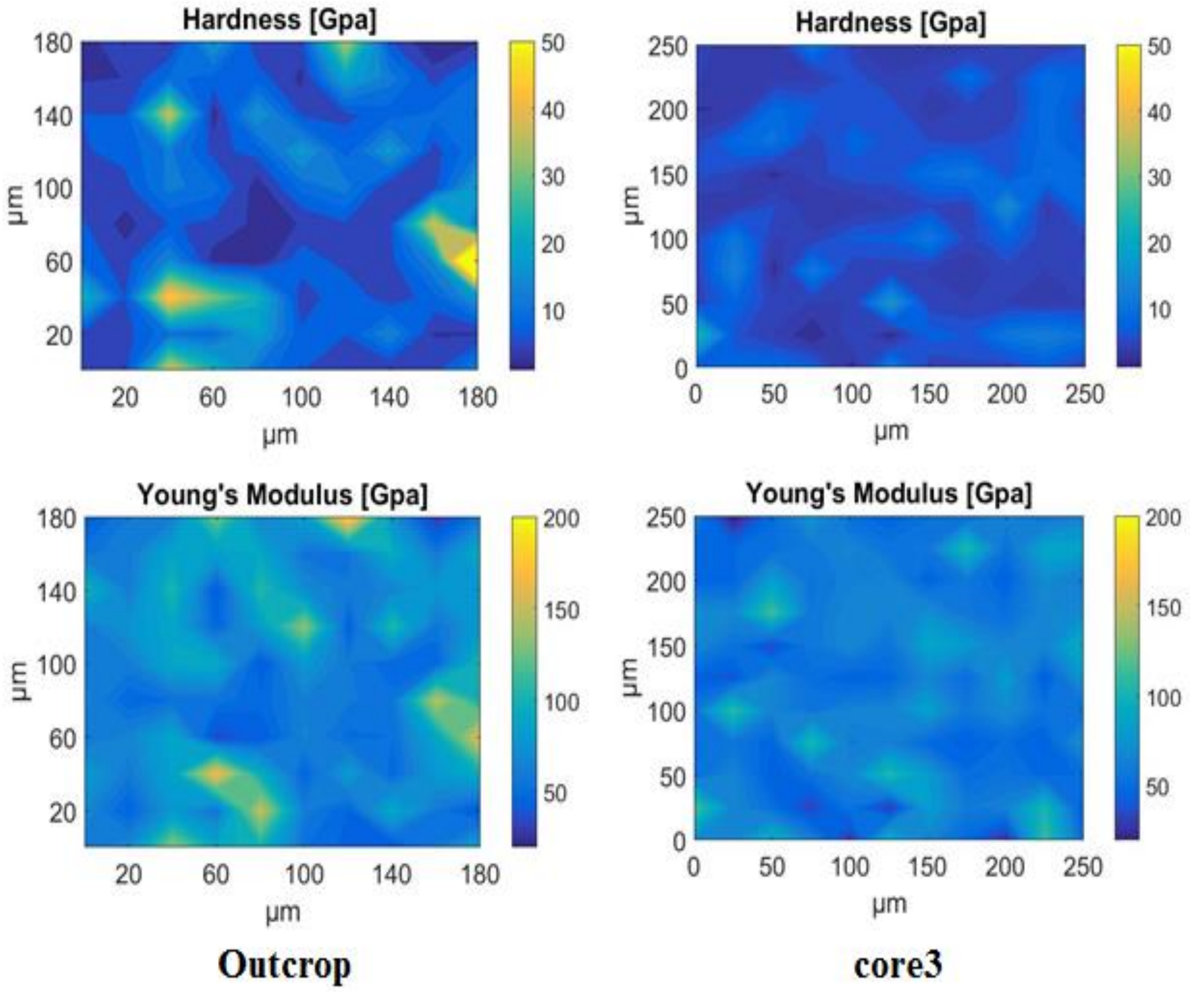

Fig. 4.20. Mechanical properties maps of Marcellus shale outcrop (left) and core 3 (right) based on 100 nano-indentation test results (10x10 grid) Yellow spot represent grains with higher mechanical properties which shows more on the outcrop sample, resulting in a higher bulk mechanical properties. [Du et al., 2017b]

Comparing the maps from the same sample, both maps showed a similar pattern because grains with higher hardness often had higher Young's modulus. When comparing between different samples, grains in the Young's Modulus maps were relatively close compared with the hardness maps, this might because the calculation of hardness is based on plastic deformation of single grain, while Young's modulus is always a composite response from all surrounding phases [Du et al., 2017b]. Since hardness maps showed better contrast between grains with different mechanical properties, they were used later to show the area/grains for fracture initiation (Figure 4.21).

Nano indentation tests were also performed on both Pottsville and Marcellus core samples perpendicular to the bedding direction, and the results are depicted in Figure 4.21 below. As the color on the map changes from yellow to deep blue, the value of Hardness (H) and the ratio of Young's Modulus over hardness (E/H) decrease. Since shale contains a variety of minerals in different shapes/sizes. To simply it, the minerals were divided into three groups depending on their mechanical properties [Du et al., 2017b], so the shale can be represented by a composite of the soft, medium, and rigid mineral gains (Gs, Gm, and Gr, respectively). For hardness map, the yellow/green spots represented Gr (as marked by rectangular boxes), light blue represented Gm and deep blue represented Gs. Pottsville shale had overall higher hardness as the map was brighter and had more yellow spots (Gr) than the one for Marcellus. The E/H value is a dimensionless number related to the deformation type: higher E/H indicated more plastic deformation, which usually precedes fracture and enhances the porosity and permeability. The E/H map showed the weak spots in which the fracture mostly likely to be initiated under the same amount of load (as marked by ellipses). Marcellus

E/H values are brighter meaning easier to deform plastically (fracture), and the ellipses were continuous making it easier for the fractures to propagate and even connect to each other. Finally, on the right were the overlaps of the rectangular boxes ellipses from the H and E/H maps. For both rocks, the weak spot was always at the boundaries between two different groups of minerals (Gr/Gs, Gm/Gs, and Gr/Gm) [Du, and Radonjic, 2019].

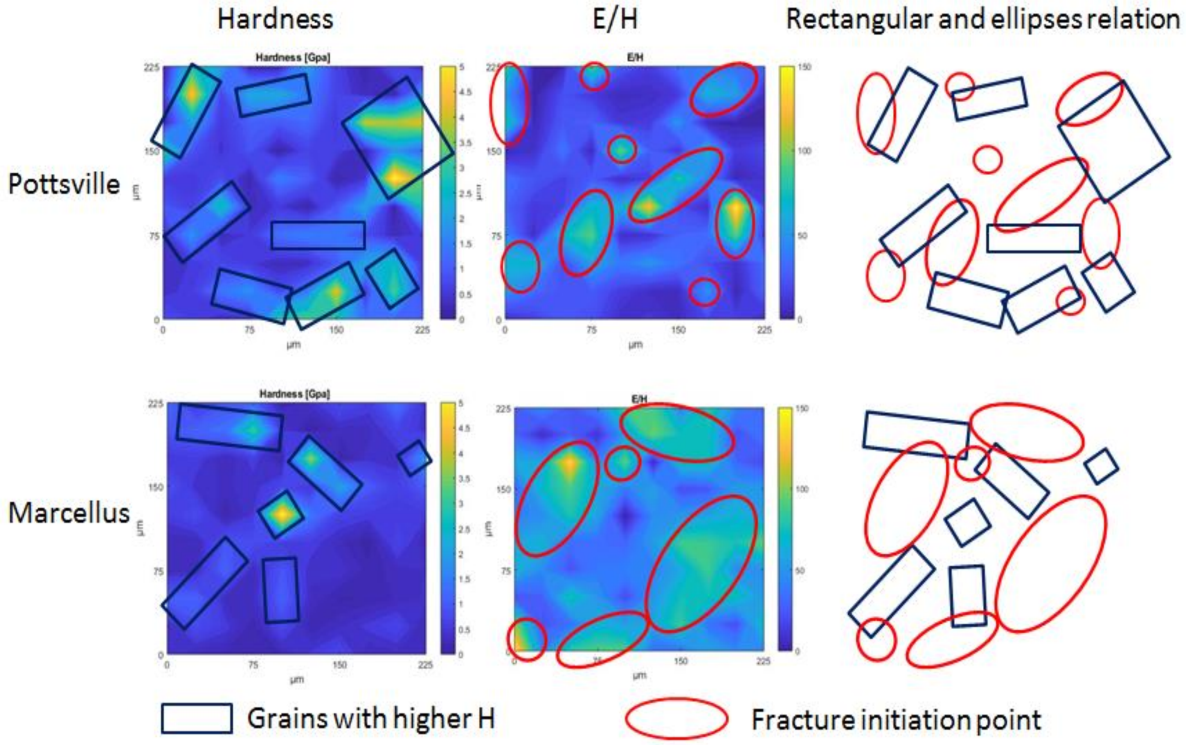

Fig. 4.21. Left: harness maps of two shales, the rigid grains were marked with blue rectangular boxes; middle: E/H value maps, higher values were shown in yellow/green, and marked with red ellipses; Right: combined blue rectangular boxes and red ellipses, showing the weak points/area where fracture may initiate [Du and Radonjic, 2019].

The Micro/Nano mechanics maps results presented above used Marcellus samples to show the difference between outcrop and drilled core. Then the drilled cores from Marcellus and Pottsville formation were compared to see the difference of mineralogy and grain distribution, and its impact on fracture initiation. More data were shown in the appendix, including the mechanical properties maps of Marcellus, Pottsville and Wilcox shale from the top and bottom of the formation, maps of Eagleford outcrops, as well as the comparison of the Young’s Modulus distributions between the top and bottom samples.

4.2. ENGINEERING APPLICATIONS OF SHALE FRACTURES

4.2.1. Hydraulic Fracturing of Shale

The primary objective of hydraulic fracturing is to stimulate the low-permeability reservoirs (usually shale) to create a conductive pathway for the fluid to flow into the wellbore. A specifically designed fluid was pumped downhole at high pressures to initiate fractures in the rock, and a propping material was then pumped into the created fractures to prevent them from closing. Although hydraulic fracturing has been used to produce hydrocarbons from shales for more than a decade, the fundamental mechanism to initiate and propagate these fractures remains unclear.

With the costs of fracture treatments climb up to millions of dollars per well, optimizing the fracture treatment design becomes extremely important. A hydraulic fracturing treatment involves two steps, initiate the fractures and prevent them from closing. This study used the indentation technique as a primary tool to detect fractures initiation and predict fracture closure due to proppant embedment in shale to get a better understanding of both treatment steps.

4.2.2.. Fracture Initiation under Stress

The failures of material were usually classified into brittle or ductile, which are related to the plastic and elastic deformation correspondingly. Due to the heterogeneity of shale, when subjected to a load, both types of deformations manifest simultaneously at different degrees, leading to a difference in failure/fracture response. The indentation experiments directly showed this response difference.

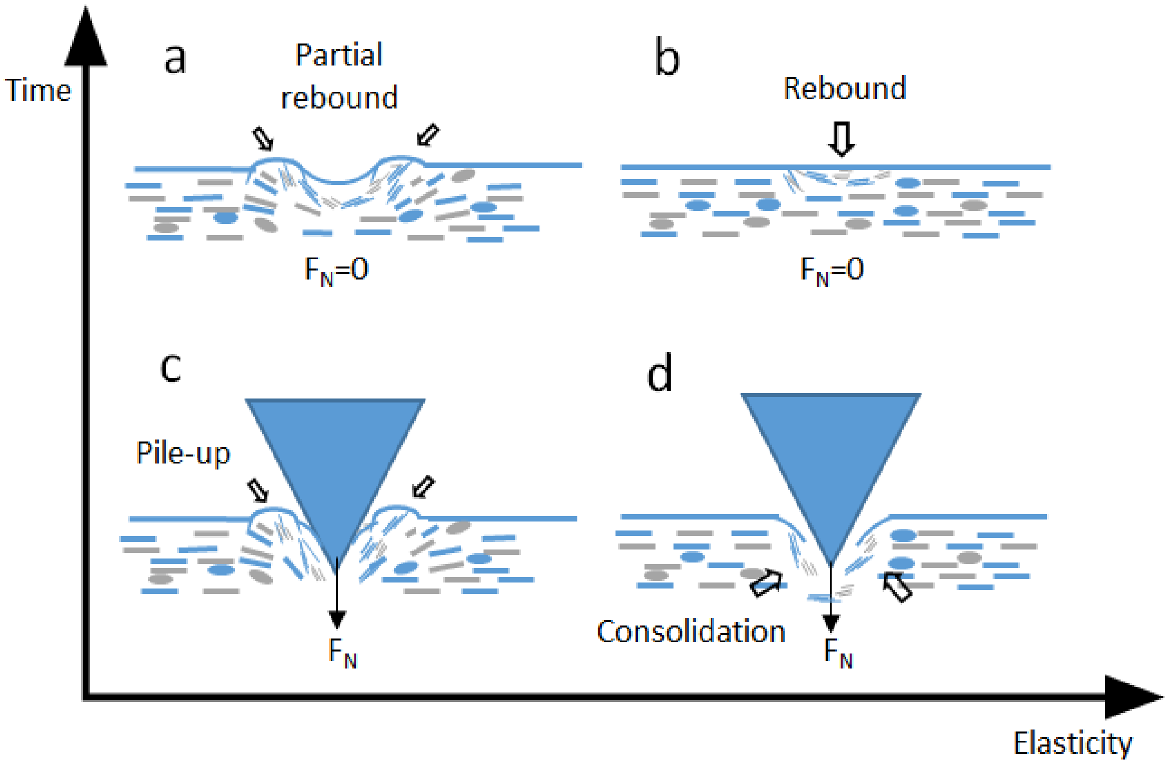

Fig. 4.22. Schematic of the indentation process on materials with different elasticity, explaining the pile-up formation during indentation. The Marcellus rock is close to the case shown on the left (a&c); Pottsville rock is close to the case on the right (b&d). [Du and Radonjic, 2019]

Figure 4.22 illustrated two cases of fracture responses of rocks under stress. On the left (a&c) were the rocks with a lower elasticity. During the indentation process, the material at the contacted area was first compressed and densified, when geometrically necessary dislocation (GND) density exceeds the maximum density that can be stored, a shear failure formed and the material was pushed out along the indenter tip wall which is marked as “pile-up”. After the force released, some compressed material in the center rebounded, but the pile-up remained. On the right (b&d) were the rocks with higher elasticity. The elastic limit was not reached during the indentation/compression, therefore, after the force released, the material rebounds back in time. For the rock used in this study, the rebounding took months [Du and Radonjic, 2019].

Figure 4.23 below was taken four months after the indentation tests, the imprint on Marcellus sample was about 16μm in depth and the pile-up is up to 4μm in height; while the imprint on Pottsville sample had completely recovered after indentation with no visible depth or pile-ups (<2 μm), only the cubic shape scars were left because of the sharp edges of the Vickers diamond tip. Table 4.4 listed the history of the imprint on both rocks. At maximum force, the Marcellus shale had a depth of 37.68 μm; after the unloading process, the imprint rebounded to 23.23 μm, which is about 62% of its max value; four months after the indentation, the imprint had a measured depth of 16.16 μm, which is 43% of its max value. As for the Pottsville shale, these numbers changed from 31.48 μm to 17.73 μm then <2 μm, corresponding to the percentage of 100% to 56% then <6%, respectively.

Table 4.4. Indentation imprint depth is a time-dependent factor and shows a significant difference between two types of shale [Du and Radonjic, 2019].

	Max depth at maximum load	Right after unloading	Four months after indentation (Figure 4.23)
Sealing shale (Pottsville)	31.48 μm	17.73 μm (56%)	<2 μm (<6%)
Brittle shale (Marcellus)	37.68 μm	23.23 μm (62%)	16.16 μm (43%)

Material with lower values of E/H experiences lower residual driving forces means the material at the indented area tends to be compressed and densified, and once the load is removed, the material rebound back as seen in the Pottsville shale; while for higher E/H value, material tends to pile-up around the indenter, as seen in Marcellus shale [Anstis et al., 1981; Du and Radonjic, 2019].

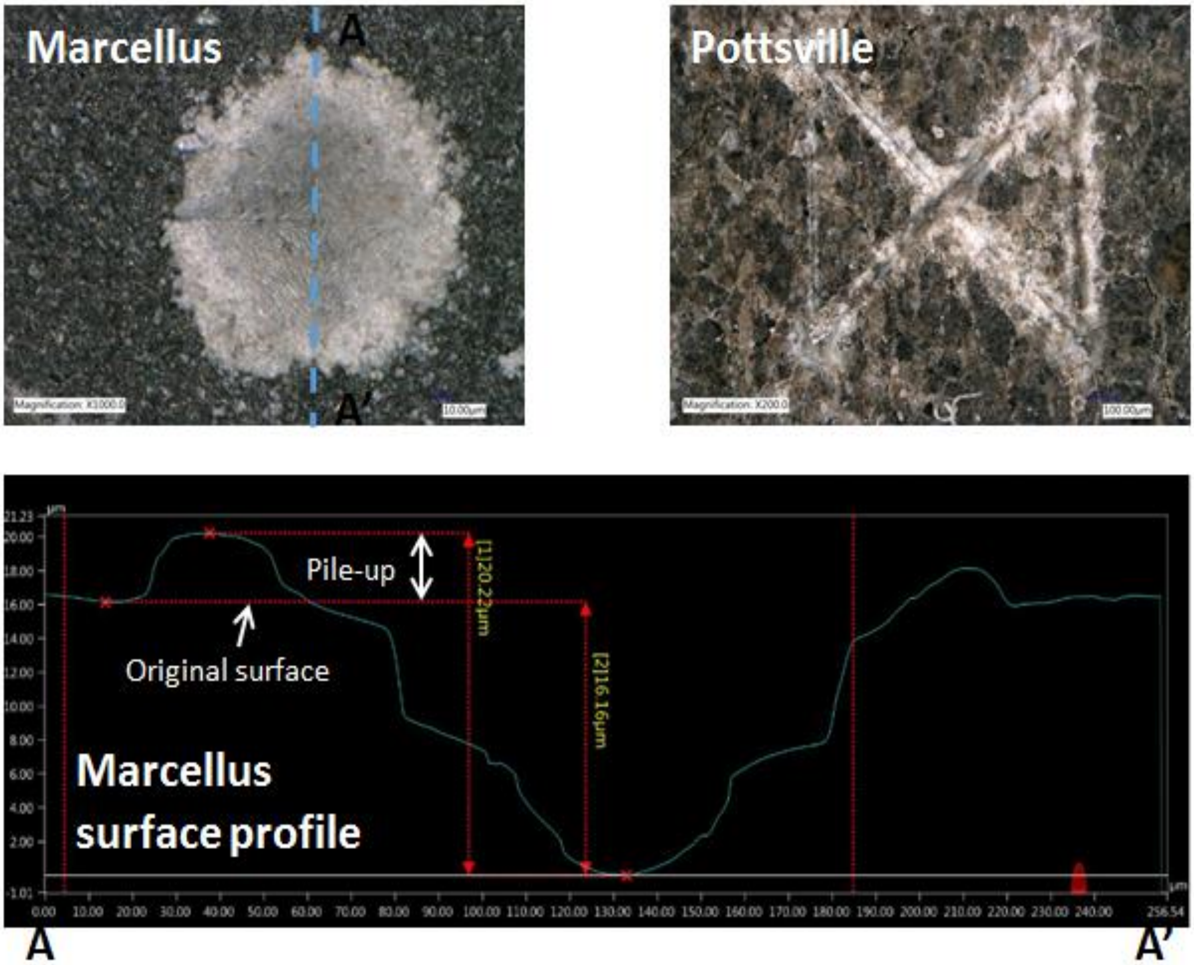

Fig. 4.23. Optical Microscopy images of Marcellus and Pottsville shale took four months after the indentation tests (Top) and the surface profile of the imprint on Marcellus shale (Bottom). The imprint on Marcellus sample was about 16μm in depth and the pile-up is up to 4μm in height, which is the case in Figure 6(a); while the imprint on Pottsville sample had completely recovered after indentation with no visible depth or pile-ups (<2 μm), which is the case shown in Figure 6 (b). Keyence VHX-6000 digital microscope was used for both images and surface profile [Du, and Radonjic, 2019].

Since the ratio of Young's Modulus to Hardness (E/H) value was a good indicator for plastic deformation /fracture initiation, combining this information with the nano indentation maps gave the area where fractures most likely to be initiated under stress (Figure 4.24). The mechanical properties maps shown here were the same ones from the previous section (Figure 4.21) with 100% enhanced contrast. For the hardness maps, lighter color meant grains with higher hardness; For E/H maps, brighter color meant higher value, decreased from yellow to green, then light blue, finally dark blue; For the overlapped maps on the right, both of them indicated that the boundaries of the grains with different mechanical properties were the weak point, which is the area for plastic deformation, as well as the area where fracture mostly likely to be initiated under the same amount of load.

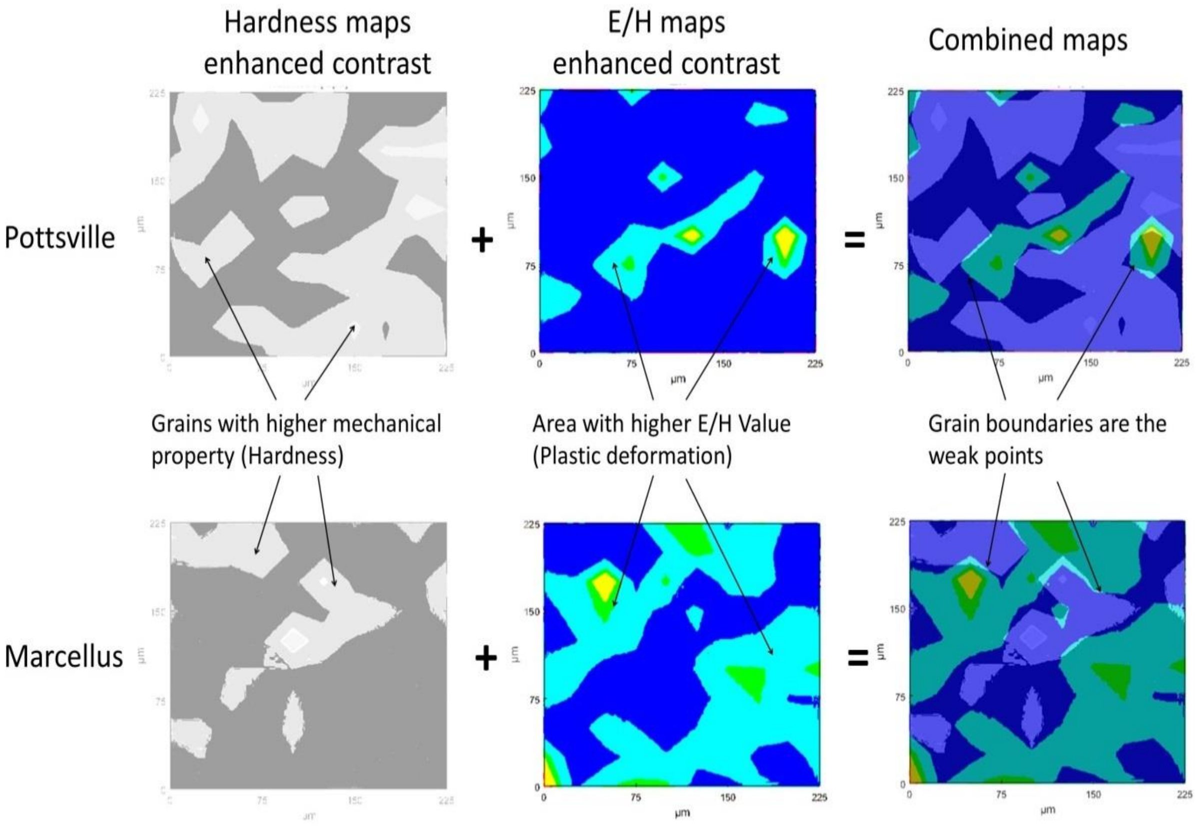

Fig. 4.24. Mechanical properties maps of shales, brighter color means higher value. The contrast of original maps was enhanced by 100% then shown here. The hardness maps (left) were overlapped on E/H maps (middle) to get the combined maps (right), showing the boundaries of the grains with different mechanical properties are the areas for plastic deformation. It is also the area where fracture most likely to be initiated under the same amount of load

The grain boundaries are well known as the defect for cracks to initiate and propagate [Coffman, 2007], while in this study for a complicated multi-phase composite such as shales, grain boundaries between different grains are different, in another word, not all grain boundaries act same way when under pressure depending on the mechanical properties of the neighbor grains. The maps shown in Figure 4.24 indicated that the boundaries between two mechanically different grains are more likely to be fractured.

4.2.3. Fracture Closure due to Proppants Embedment

The fracture conductivity is a major focus for hydraulic fracture treatment design as it is directly related to the well performance. Fracture conductivity is defined as the product of the fracture width and fracture permeability. It is affected by both proppant and rock characteristics. Since the main focus of this study is on shales, the proppant was assumed to be a rigid body and other aspects on the proppant will not be discussed here such as concentration, sensitivity, shape, and size.

Alramahi and Sundberg [2012] studied the relationship between shale mineralogical composition and mechanical properties. They claimed that shale with lower clay content yields a higher Young’s Modulus, which can significantly reduce proppant embedment [Alramahi and Sundberg, 2012]. The proppant embedment is a major factor in conductivity loss as it leads to decreased fracture width, especially at a low proppant concentration (at high proppant concentrations, the conductivity is dominated by proppant characteristics instead of rock properties) [Jansen, 2014].

When the proppant was seen as a rigid body, the proppant embedment was similar to the loading process of indentation. Pottsville shale has higher clay content was more ductile and able to take more dislocation of the material and showing a higher degree of embedment, meaning even after hydraulic fracturing, the fracture width can be significantly reduced. Marcellus as brittle shale has a lower clay content, the material at the contact area can’t accommodate much deformation, means less proppant embedment and the fractures can remain open longer. Therefore, the indentation technique can be used to descript how hydraulic fractures produced in certain shales behave over time to reduce their permeability, which will help to understand and predict the time-dependent conductivity loss of hydraulic fractures in shales.

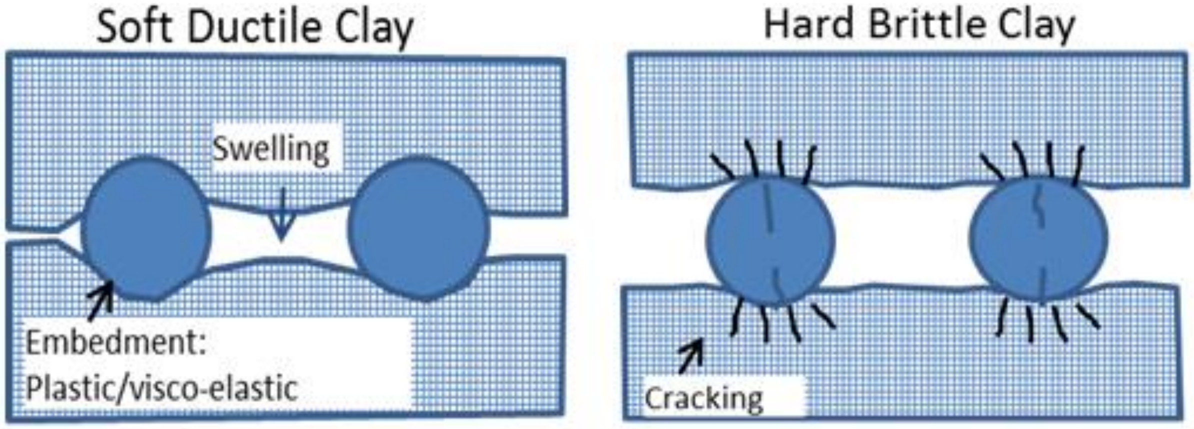

Fig. 4.25. Schematic of grain-scale modeling of proppant embedment for shales of high clay content (left) and shale of lower clay content (right) [Nakagawa et al., 2017]

4.2.4. Characteristics of Perfect Shale Caprocks

4.2.4.1. Ductile vs brittle mineral phases

As mentioned before, shale contains a variety of minerals in different shape/size, and these minerals were divided into three groups depending on their mechanical properties [Du and Radonjic, 2019], so the shale can be represented by a composite of soft, medium, and rigid mineral gains (Gs, Gm, and Gr, respectively). Gs are majorly clay minerals with small particle size (< 2 μm); Gm are quartz/feldspars, calcite, and some illite, the particle size range from 10 μm up to 200 μm; Gr are Pyrite, Chlorite, and other metal oxides/sulfides, with a size range from a few to about 50 μm.

X-ray Diffraction data [Olabode and Radonjic, 2017] were combined to get the fraction of each group in both shales as shown in Table 4.5 below. For Marcellus, the soft, medium, and rigid mineral gains were about 22%, 73%, and 4%, while the numbers for Pottsville were 33%, 57%, and 10%. Comparing this two shales, Pottsville had more uniform grain size, the Gm and Gr were around 10 to 50μm and more heterogeneous grain properties; while for Marcellus, the Gm and Gr had a larger size range from 10 to 200 μm, and more uniformed grain properties (less Gs and Gr than Pottsville, majority is Gm) [Du and Radonjic, 2019].

Table 4.5. The distribution of soft (Gs), medium (Gm), and rigid (Gr) mineral grains in Marcellus and Pottsville shales [Du and Radonjic, 2019]

	E range (Gpa)	Size range (μm)	Pottsville (%)	Marcellus (%)	Possible composition
Gs	0-70	<2	33.08	22.46	Clays (e.g. Kaolinite, Smectite), Kerogen/pore
Gm	70-120	10 to 200	56.55	72.74	Quartz/feldspars, calcite, illite
Gr	>120	2 to 50	10.37	4.01	Pyrite, Chlorite, other metal oxide/sulfide

Although clay minerals have drawn great attention and been extensively studied during the last few decades, most publications simply classify clays as small, soft and ductile minerals. In fact, the mechanical properties of clay have a large range that they can even be rigid. For example, the chlorite here is in the Gr group. The chlorite members are still not well known. Chlorite is capable of trapping CO_2 permanently under the solid form as it reacts with CO_2 and forms siderite, dolomite and kaolinite [Gaus, 2010], but so far, they had no known industrial uses. Chlorite is introduced briefly in the previous section: Structurally, chlorite is similar to illite, but between each 2:1 (T-O-T) layer, there is an additional O layer forming a 2:1:1 layer structure with the sequence of (T-O-T) O (T-O-T) O. Mechanically, the properties of chlorite is significantly higher than other commonly seen minerals As for the charge, generally, clays with larger surface area will end with a higher CEC (eg. kaolinite <illite < smectite), but chlorite don’t follow this order either. For these reasons, chlorite was not always considered a part of the clays and sometimes left alone as a separate group within the phyllosilicates

4.2.4.2. Grain boundaries: nature, surface area, and reactivity

Since the fracture initiate at the grain boundaries, Marcellus shale was more likely to have larger fractures as shown in Figure 4.26 and 4.27. Because of the larger and continuous grain boundaries, the relatively clean and smooth grain boundaries may also help the fracture to propagate. As for the properties of the grains, Pottsville has higher Gs and Gr content while Marcellus has relatively uniform grain properties. The Gr in Pottsville are evenly distributed with short and irregular boundaries, which may act as barriers to prevent fracture propagation [Du and Radonjic, 2019].

Furthermore, shales contain grains with distinct mechanical properties, generally, grains with heavier element is also superior in mechanical properties than the grains with lighter elements in shale (e.g. Fe rich hematite > Ca rich calcite > Si/Al rich clays). BSE images might be used bypassing other mechanical characterization technique to see the likelihood for fractures to initiate in certain shale, as it marks the boundaries between the grains with different elements [Du and Radonjic, 2019].

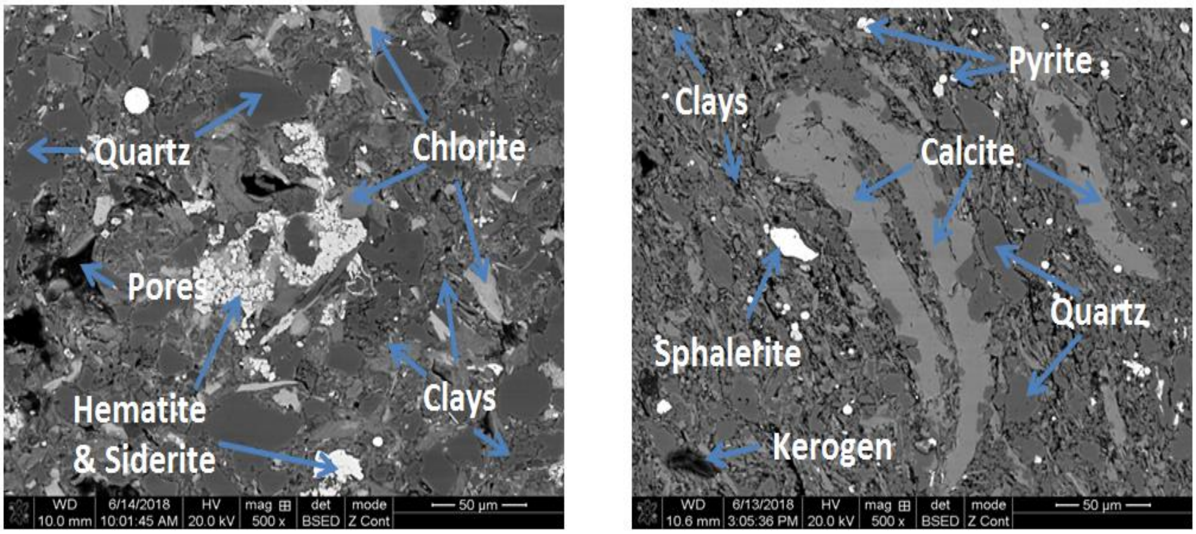

Fig. 4.26. Backscattered Electrons (BSE) micrographs of Pottsville (left) and Marcellus (right) rock, with a 50μm scale obtained on FEI Quanta 3D FEG dual beam FIB/SEM system at 20 KV. Heavier elements appear brighter in the backscattered electron images, Energy Dispersive Spectrometry **(**EDS) elementally maps were done to help identify the minerals [Du and Radonjic, 2019].

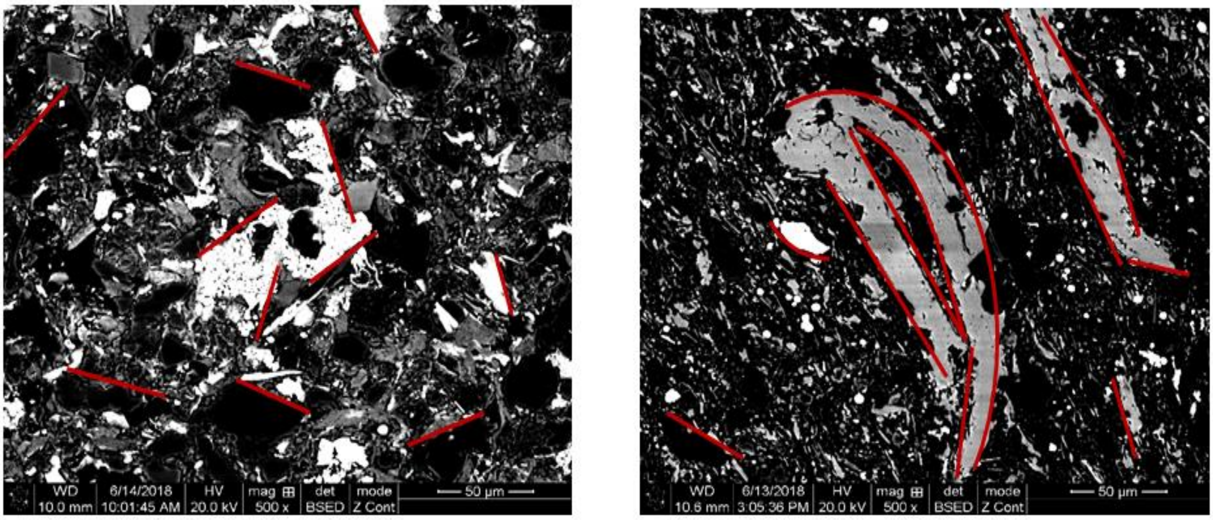

Fig. 4.27. Binary maps from Backscattered Electrons (BSE) micrographs of Pottsville (left) and Marcellus (right) rock showing the grain boundaries (Large ones are marked in red) [Du and Radonjic, 2019]. Comparing these two shales, the Marcellus has larger and continuous grain boundaries, these relatively clean and smooth grain boundaries with same direction may also help the fracture to propagate

4.2.5. Comparison between Shale Caprock and Cement

Shale cap rocks are nature’s best hydraulic barrier geo-materials. They are effective seals over geological time for underground hydrocarbon bearing formations as well as CO2 storage formations in carbon capture and storage (CCS) projects While the main artificial hydraulic barrier in wellbores, cement sheath, can be subjected to many types of failures during the well life. The objective was to investigate the similarities of hydraulic barrier features between shale caprock and wellbore cement, which could help to improve the subsurface application of cement in zonal isolation [Du et al., 2017b].

The shale caprocks, although highly heterogeneous in chemical compositions (being a natural material), have low permeability primarily due to compaction and clay dehydration during the diagenetic evolution of the rock in the subsurface. Clay minerals, the major constituent of shales are composed of expandable smectites, whereas in older rocks, especially in mid to early Paleozoic shales, non-expansive illites predominate. This transformation of smectite to illite is known as illitization, it normally happens at a temperature over 80^0C and produces silica, water, and other sodium, calcium, magnesium, iron based minerals. The minerals formed in this process include authigenic quartz, chert, calcite, dolomite, ankerite, hematite, and albite, all of which can be traced to minor (except quartz) minerals found in shales and other mudrocks. The morphology is such that they are laid down in flat sheaths and cores retrieved from the subsurface show platelet like structures on the SEM image (Figure 4.28 c). [Radonjic et al., 2015]

Cement, on the other hand, consists of hydration reaction products of calcium and silica based compounds. Cement can react with water, form calcium-silicate-hydrate (C-S-H). This semicrystalline, nanoporous composite material has a large surface area, it is also the major phase within the hydrated cement paste, the C-S-H can make up to 70% of the volume and is largely responsible for cement strength. Calcium hydroxide (CH) is the second common mineral in hydrated cement making up to 25% of the volume, it is also referred as portlandite; The CH crystals form hexagonal plates of indeterminate shape that may be intimately inter-grown with C-S-H, [Taylor, 1997]. The third largest mineral group in hydrated cement is the aluminoferrite group. The major mineral of this group is ettringite which can make up to 20% of a hydrated cement paste. The aluminoferrite group is formed in the early stage of hydration and often presenting as hexagonal rods [Radonjic et al., 2015].

The SEM images presented in Figure 4.28 (a-d) showed the microstructural characteristics of cement sheaths compared to shales. The highly organized features in cement micrographs stem from being an engineered material compared to the irregular features in the shale images. Fig 4.28 indicated both cement and shale showing fissure-like characteristics. Shales also have similar sizes of inter-particle pores (around the clay particles) like cement. Since all the cement and shale samples were devoid of water for imaging, these pore sizes might be amplified during the drying process because of the shrinkage of the swelling clays. Even though, it can be still seen that the particle sizes for both cement and shale were within the same range while shales seem denser packed [Radonjic et al., 2015].

Shales have similar mechanical properties range comparing with cement as shown for Pottsville and Wilcox shale in Figure 4.29 and 4.30. Wilcox shale had a distinctively low hardness and Young’s modulus value due to the presence of swelling clay resulting in soft texture on adsorption of water and ultimate weakening of the material. Wilcox shale has a significant percentage of montmorillonite (a well-known swelling clay) which becomes softer in the presence of water resulting from the adsorption of water molecules into the matrix structure of the shale. This difficult-to-reverse adsorption process results in reduced compressive strength and Young’s modulus as observed in the measured hardness values for this shale [Stephens et al., 2009]. The Pottsville shale, which is swelling clay free, did not exhibit this phenomenon when polished with water. For the cement samples, the pipe expansion caused fractures in cement resulting in a reduction of the mechanical properties. The highest decrease immediately after the expansion was from 8% pipe expansion where the hardness decreased by 35%, and Young’s modulus decreased by 33%. One month after the expansion, mechanical properties of the cement recovered. The highest increase of hardness and Young’s modulus after one month of rehydration was also for the same sample where the hardness reached 90% of the initial strength before pipe expansion, and Young’s modulus reached 85% of its original value before expansion [Radonjic et al., 2015]. The same expansion/ compression experiment was also performed on the cement sample with w/c=0.87, results were very similar (both E and H followed the same trend) to the one shown in Figure 4.29 and 4.30 here, detail data of the cement sample with w/c=0.87 can be found in the appendix.

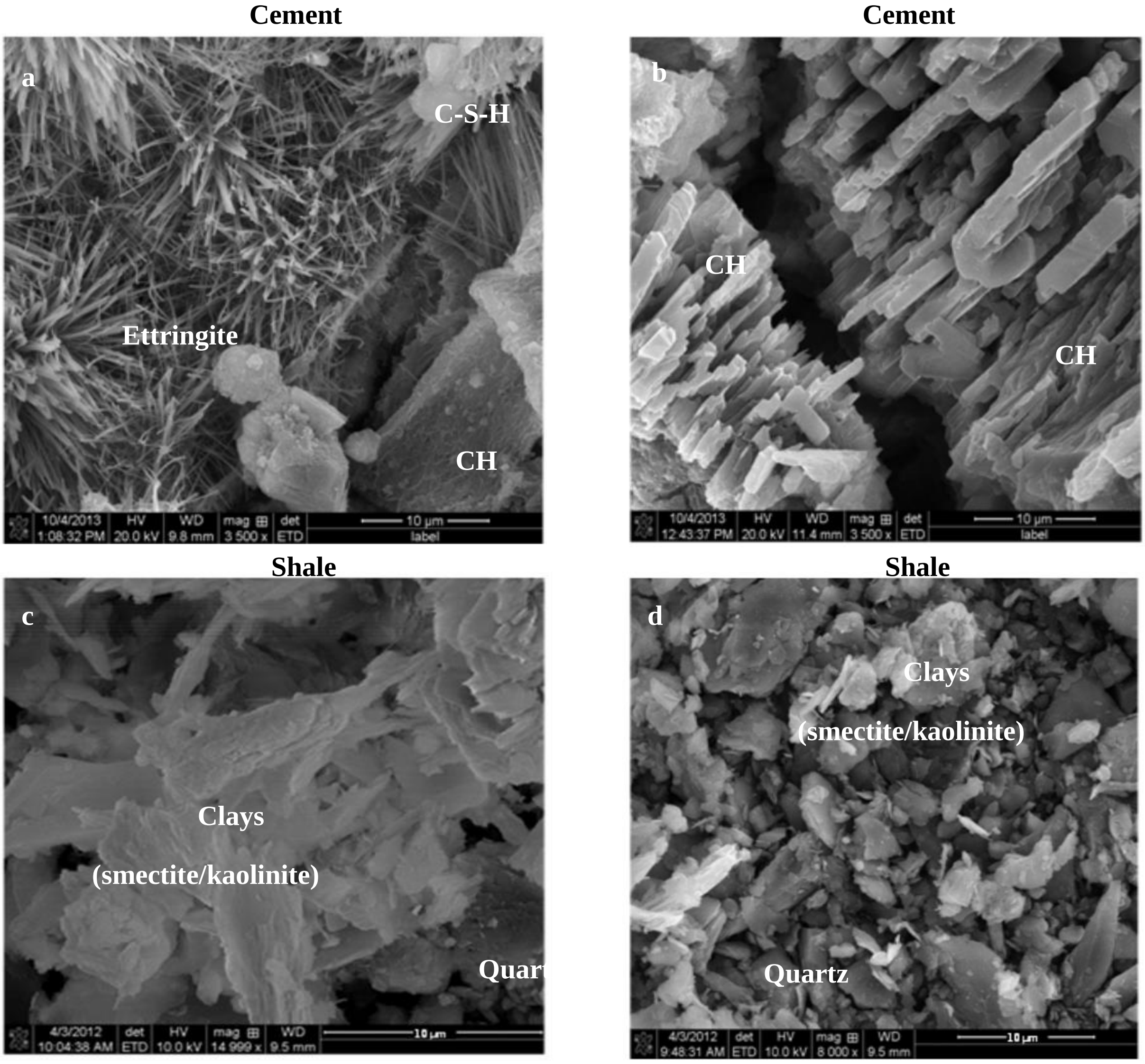

Fig. 4.28. SEM morphological characteristics of cement (a & b) and shale caprock (c & d) with cement showing fissure-like characteristics (b). The shale caprock also showed some pores at the 10 µm resolution (c). The depositional environment and tremendous geologic compaction process tended to affect the morphological and petrophysical characteristics of shale conferring it with tightness features. It should be noted that all the cement and shale samples analyzed with SEM are devoid of water. [Radonjic et al., 2015]

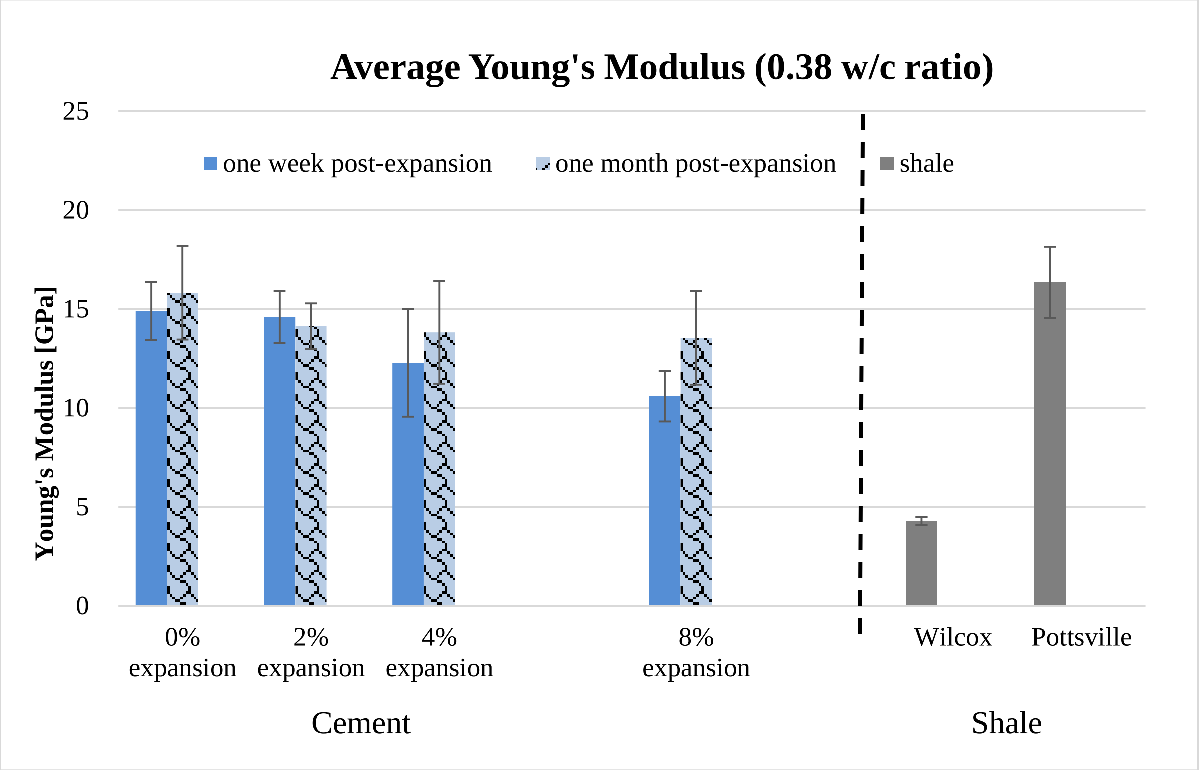

Fig. 4.29. Young’s Modulus of 0.38 w/c ratio cement with different expansion ratios and shale sample (Wilcox) and sample 2 (Pottsville). [Figure redraw from Radonjic et al., 2015]

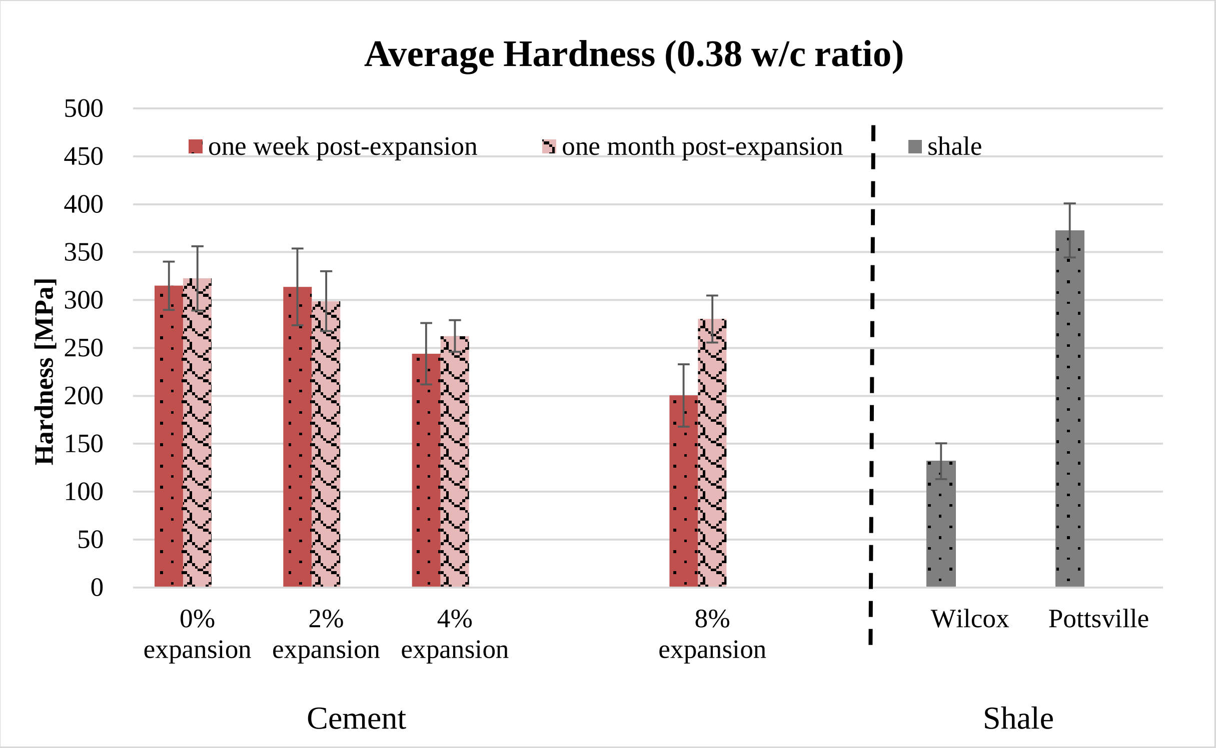

Fig. 4.30. Hardness of 0.38 w/c ratio cement with different expansion ratios and shale sample (Wilcox) and sample 2 (Pottsville). [Figure redraw from Radonjic et al., 2015]

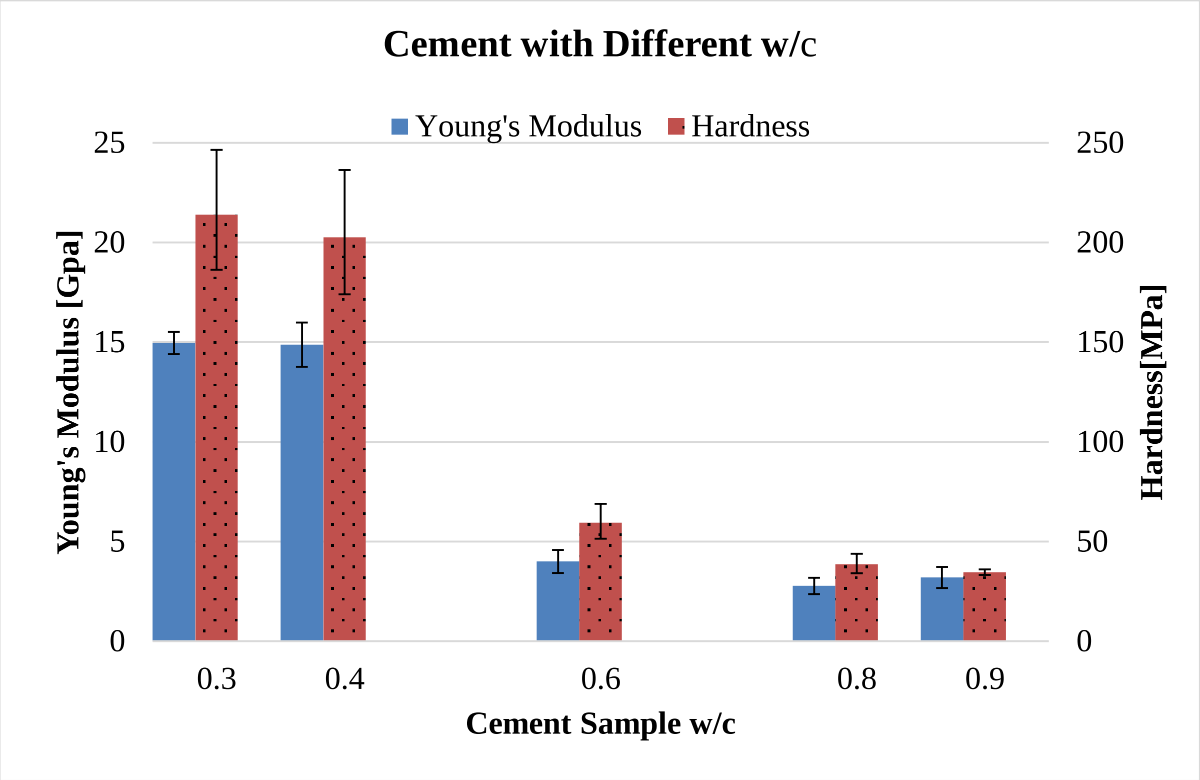

Fig. 4.31. Mechanical properties of cement with different water to cement ratio

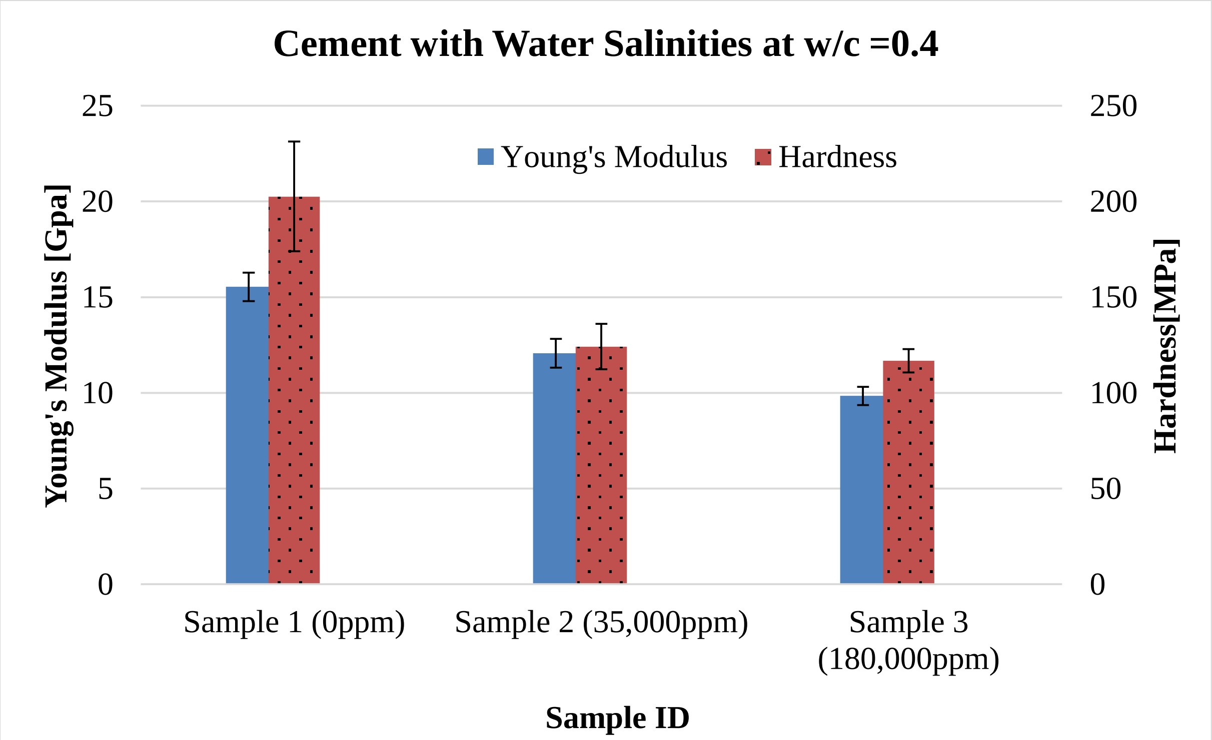

Fig. 4.32. Mechanical properties of cement with different water salinities

For the evaluation of the effect of salinity and water to cement ratio, results are shown in Figures 4.31 and 4.32 below. From Figure 4.31, as water to cement ratio increased, both hardness and Young’s Modulus significantly drops. The reason can be concluded as: 1) The water is not consumed by the hydration reaction may leave the cement microscopic pores. When the water becomes trapped within the cement, it has additional weakening effects on the surface; 2)When cement mixed with too much water, it will experience more shrinkage as the excess water leaves, resulting in internal cracks and visible fractures [Du et al., 2015]; 3). Higher water to cement ratio means more space between the cement particles, more room for the unhydrated cement particles to develop into outer CSH, which has lower mechanical properties than the inner CSH

From Figure 4.32, as water salinity increased, the mechanical properties of cement drop. This may cause by 1) As sample dries, salt becomes crystallized, and the solid form of salt takes more room than it takes in the solution, this creates an internal expansion force making the sample easier to crack; 2) High salinity may trigger the diffusive flow of water from the curing solution/surrounding environment to the cement slurry, additional water might be absorbed during the curing. Higher salinity enhanced the hydration rate, resulting in more outer CSH with lower mechanical properties

4.2.6. Lab-Made Samples

Lab-made samples were used in this study for the mineralogy impact. Because natural shales are heterogeneous and their mineralogical compositions vary even from the same formation; meanwhile, the lab-made samples can have controlled and exact mineralogical composition as well as constant mineral ratios through any given design. Thus, the impact of mineralogical composition variation on mechanical properties and microstructures can be systematically quantified and compared between samples [Du et al., 2017a].

Figures 4.33 shows the platy clay particles overlapping each other in both natural and lab-made samples, this is because during the sedimentation process, as effective stress increases, the porosity reduces, platy clay particles become aligned perpendicular to the direction of major loading [Day- Stirrat et al., 2012]. The lab-made sample also has a relatively large porosity and loose texture compared with the natural rock. The tight packing structure in natural shale occurred as a result of millions of years of tectonic compaction, which the lab-made samples had not experienced [Du et al., 2017a].

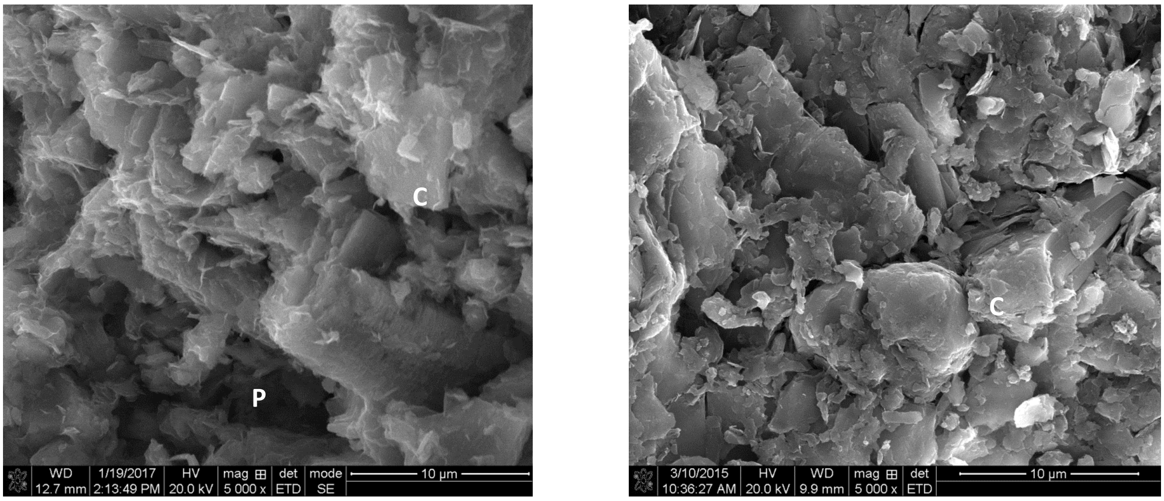

Fig. 4.33. Fracture surface of control sample (fresh/45%clay) (left) and Pottsville shale (similar clay content: 43%) (right). Both images showed layers of clay mineral stack over each other, while the control sample has less dense packing. (C-Clay, P-Pores)[Du et al., 2017a]

Samples with different clay content were compared in Figure 4.34 below in both low and high magnification. These two samples are deposited in the same environment with the same loading. The overviews on the left showed a denser packing for the high clay content sample, also a better lamination as clay content increases. At higher magnification, the sample with lower clay content has visible interconnected pores between particles with the size around 1μm, while sample with higher clay content has no visible porosity, which means the sediments with low clay content will have higher permeability when compared with high clay content sediments under the same deposition environment [Du et al., 2017a]

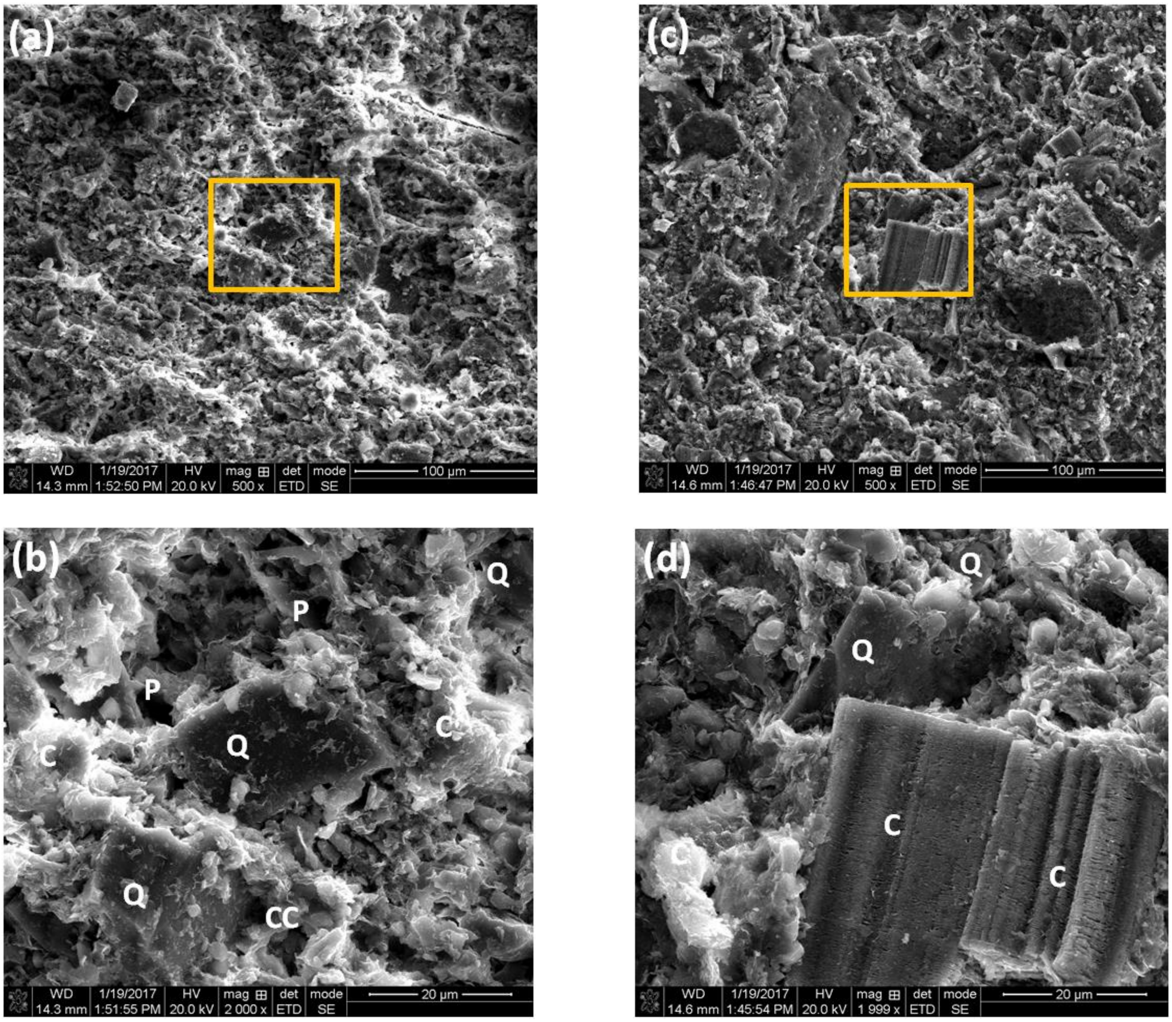

Fig. 4.34. Fracture surface of (a) sample 4 (low salinity/45%clay) overview and (b) higher magnification, (c) Sample 6 (low salinity /75% clay) overview, and (d) higher magnification. The texture of sample 4 exhibiting weakly developed laminae composed of stacked clay with visible pore space and fracture. Sample 6 shows a moderate lamination from top left to bottom right with more dense packing, no visible porosity. (C-Clay, Q-Quartz, CC-Carbonate, P-Pores) [Du et al., 2017a]

The mechanical properties were tested with the micro-indentation technique. As shown in Figure 4.35, hardness and young's modulus increased as clay content increases for both lab-made samples and natural shales. Quartz and calcite as individual phases have a much higher hardness than clay minerals, but the results are showing an increasing trend of hardness as clay content increases, which means the microstructure altered. Because clay acts as a binder in the mixture, with increasing clay content bonding also increases. Comparing samples with different salinities at the same clay content, the mechanical properties decreased as the salt concentration getting higher. Increasing salinity pore fluid can decrease the thickness of double layers, causing an increase in permeability [Mesri and Olson, 1971] because of the increase of effective porosity. The extension of the double-layers is less under high salinity condition, which means the clay mineral expands to a larger volume in low salinity condition [Pusch and Yong, 2006]. Furthermore, the sample tested in this study was oven dried, once samples are dried, salt becomes crystallized, and solid form of salt takes more room than it takes in the solution, this creates an internal expansion force making the sample easier to crack [Du et al., 2017a].

Comparing the sample with the natural shale of similar clay content (Pottsville shale), the mechanical properties are one order of magnitude lower, the Pottsville shale has a hardness of 350 MPa and Young’s modulus of 15 GPa. This is because even with similar composition, both deposition time and pressure of the samples are significantly smaller than the natural. The tight packing structure obtainable in natural shale occurred as a result of millions of years of tectonic compaction. The lab-made samples have much looser packing and higher porosity which can be verified from the scanning electron microscopy micrographs [Du et al., 2017a].

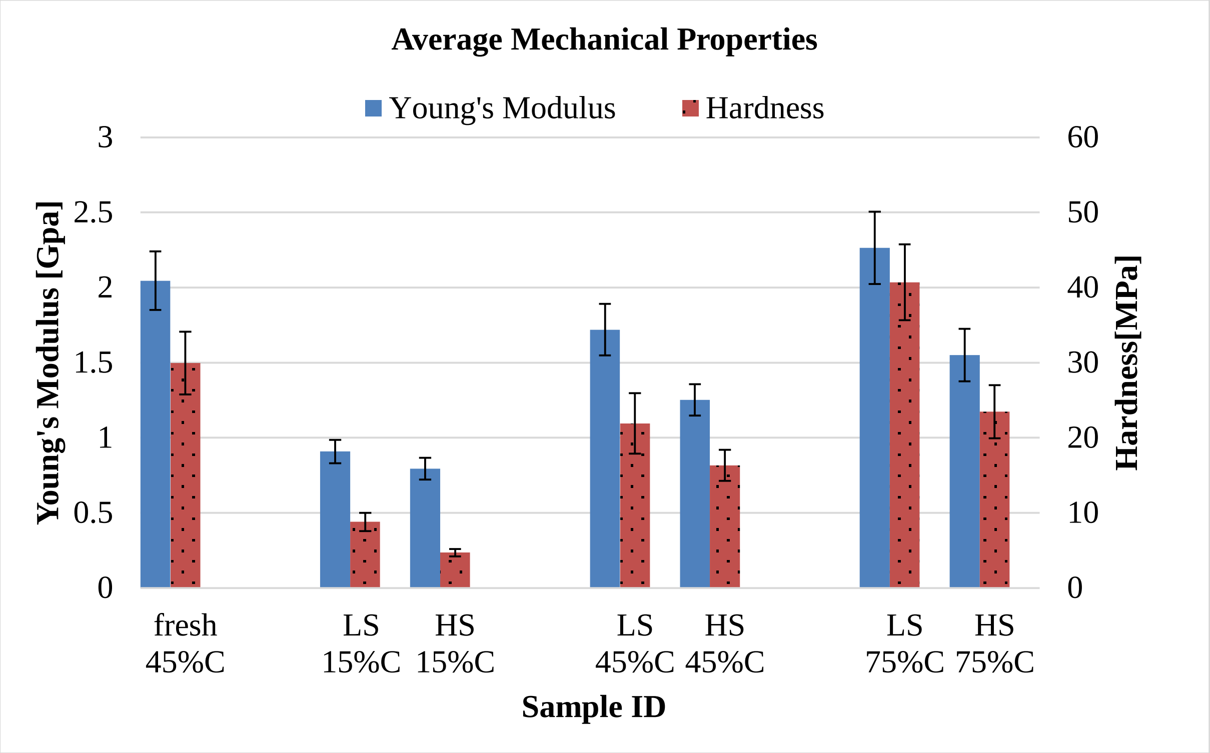

Fig. 4.35. Mechanical properties measurements from the indentation tests on lab-made samples showing the effect of salinity and mineralogy [Figure redraw from Du et al., 2017a].

The deposition of sedimentary rock starts with physical weathering/ failure of the parent materials into smaller sediments, the enlarged overall surface area accelerates the chemical weathering/erosion, after which these sediments are deposited with series of mineral dissolution and participation and finally compacted and cemented into sedimentary rock. While lab-made sample used end member fines to represent the sediments after weathering under the assumption that no chemical reaction happened between different minerals, also, the pressure and the amount of time applied during the deposition process in the lab are significantly smaller than that in nature, these lead to the limitation of showing the natural fabric of minerals as well as lack of intimacy of contact between neighboring particles [Du et al., 2017a].

5: DISCUSSION

5.1. SHALE FRACTURING: THEORY, MECHANISMS, AND EXPERIMENTAL OBSERVATIONS

5.1.1. Samples Selection and Preparation

Shales were the main focus of this study. Rock samples from different formations were tested to see the effect of composition, depth, microstructure on their mechanical properties. Since the natural samples are complicated multiphase composite found in the varied depositional environment, the lab samples were made with a controlled environment and exact mineralogical composition as well as constant mineral ratios through the given design. Thus, the impact of mineralogical composition variation on mechanical properties and microstructures can be systematically quantified and compared. Although the results were not ideal, this could be a possible pathway for future rock study to eliminate the variable factors. Finally the wellbore cement, as an engineered hydraulic barrier material, were compared with the natural rock to find the similarities to help improve the subsurface application of engineered hydraulic barriers in zonal isolation

5.1.1.1. Outcrop and drilled shale cores

The deposition of sedimentary rock starts with physical weathering/ failure of the parent materials into smaller sediments, the enlarged overall surface area accelerates the chemical weathering/erosion, after which these sediments are deposited with series of mineral dissolution and participation and finally compacted and cemented into sedimentary rock. Results from micro indentation tests (Fig. 6) showed that the outcrop has overall better mechanical properties (i.e., higher Young modulus and greater hardness) than core samples. The significant difference in mechanical properties between outcrop and drilled cores can result in different fracture responses because the mechanical properties of the rock are the key factors that determine the likelihood of fracture initiating and propagating [Du et al., 2017a]. Therefore, drilled cores are recommended for rock characterization over the outcrop. The result also indicated that drilled cores from the same formation have distinguished properties as their mineralogical compositions vary, but overall, the mechanical properties have a decreasing tendency with depth increase. Attempts for minimizing the impact of mineralogical composition variation on mechanical properties were made during this study by using lab-made samples with controlled and exact mineralogical composition as well as constant mineral ratios.

Although drilled rock cores were used in this experiment, these core samples are not completely representative of the in-situ condition as they were exposed to the surface conditions and oven dried. The release of overburden pressure amplified the fractures while the shrinkage of the swelling clays could also contribute to the development of fractures, which will result in a reduction in the mechanical properties [Du et al., 2017a]. Another observation is, the drilled core is constantly changing at surface conditions, which made the relocation of the indented area challenging. Most literature deals with similar materials merged the sample into epoxy to prevent further changes. Although the epoxy resin could be a good background contrast for imaging, the fact that it fills the pores of the material is still an alteration of the microstructure.

5.1.1.2. Cement and shale

Wellbore cements are primarily designed to provide zonal isolation during the well completion or for well plugging/abandonment as engineered hydraulic barriers, while shale as caprocks, are utilized for subsurface gas/ waste storage as natural hydraulic barriers. The durability is the key issue when it comes to these applications of the barrier materials. At subsurface conditions, materials have to cope with variations in stress, temperature, and pressure, as well as chemical attack. Clay rich rock, as natural barriers, had been experienced a series of oscillations of stress, temperature, and pressure during its deposition and demonstrated both chemical and mechanical stability over a long time scale as it is resident to the alterations over a broad range of conditions because of its low permeability, high retention properties, and unique swelling properties. Cement, as an engineered barrier, shared two essential properties of clays (electrically charged surface and layered structure), appearing similar microstructure of clays with low permeability and considerable high mechanical properties. But the chemical compatibility of cement at subsurface condition is not as good as clay rocks as it had a relatively high pH (10~13). The interactions of cement with the surrounding formation can cause alterations of mineralogy and microstructure for both cement and rock, the dissolution of the primary and participation of secondary minerals could cause dramatic change in porosity and mechanical properties of the material [Tournassat et al., 2015] leading to a risk of material failure or potential pathway for the isolated fluid [Radonjic et al., 2015; Du et al., 2015]. Therefore, chemical compatibility became the key factor for applications of cement as subsurface barriers and is still a formidable challenge by now.

Cement samples were tested and compared with shales in this study. Based on the presented data it is evident that hydrated wellbore cement, once subjected to forces, can undergo microstructural alterations. The confinement prevented the failure of brittle material and instead rearranged microarchitecture within the cement matrix. Although the major phase in cement and shale (CSH and clays) are similar, the processes are quite different. Shale was deposited over geological time after both chemical and physical weathering, while the cement was hydrated mainly through the chemical interaction between particles and water. The compression process was, in a way, similar to the physical weathering and compaction of shale as it reduced the number of large pores, moreover, it improved the packing of the grains, outcome of which is more dense material (we infer should also be less permeable matrix). Some of the larger unhydrated grains can fracture at higher rates of metal expansion (cement compression). This leads to a detachment of CSH from the grain surfaces and allowing pore water to reach unhydrated particles triggering secondary hydration [Radonjic et al., 2015; Du et al., 2015].

Within the scope of the shale data available for analysis, it can be inferred that shale caprock petrophysical properties are tighter than that of cement. Though it is possible to prepare cement with a low w/c ratio with good petrophysical properties, the placement of such cement slurry in the wellbore would not be feasible. The import of these on poro-mechanical properties of both cement and shale would probably reflect on their elastic behavior under high pressure confining stress. The tight packing structure obtainable in shale occurred resulting from million years of tectonic compaction and this probably results in improved compressional strength of shales when compared to engineered material such as wellbore cement [Thomas and Jennings, 2003;Jennings et al., 2007; Iverson et al., 2008; Jennings et al., 2008; Radonjic et al., 2015].

5.1.1.3. Sample preparation

Sample preparations were essential in this study because both the mechanical properties and images were obtained in micro to sub-micro level. Flawed sample preparations can have a huge impact on the quality of results which may lead to false conclusions [Murtey and Ramasamy, 2016]. The sample preparation for both imaging and indentation in this study followed similar steps: cutting, polishing, drying, mounting, and finally the test. An additional coating step was added after mounting for the samples needed SEM/BSE/EDS because all the samples in this study were not conductive.

Conventionally, rock samples were stabilized by mounting and impregnation within an epoxy resin block, which is achieved by placing the resin-covered sample in a vacuum chamber, then withdrawing air and wait for resin curing [Deirieh et al., 2012; Veytskin et al., 2017]. The resin impregnation is normally done before the cutting and polishing to stabilize the sample. A resin impregnated block may also make the cutting, polishing, even the vacuuming process easier, therefore, getting better micrographs and more accurate results from SEM/EDS. Although the resin impregnation helps in many aspects during the sample preparation, it is not implemented in this study, because it significantly affects the mechanical properties measurements. Resin impregnation perfectly preserved the microstructure of the rock, it is ideal if you only need the micrographs from the rock. As for indentation, when solid resin occupies the void spaces/pores within the rock, it provides additional confinement to the particles which will enhance the overall mechanical properties of the sample, especially during the micro-indentation, where the properties are calculated by averaging the properties of the all the particles in contact. A trial test was performed on the same sample before and after resin impregnation, the results showed the resin impregnated sample had up to 30% higher mechanical properties. Basically, the resin impregnation process brought a new phase into the rock of which is already complicated as a multiphase composite, therefore, it should be avoided. The same reason also can be applied for the coating before indentation. So, all of the indentation results showed in this study are done on the samples without resin impregnation and coating.

Another key step in sample preparation is the drying process. Drying is not only necessary for the coating and imaging of samples, it also reduces the error caused by different moisture contents during the indentation test. The water content within the porous composites can be seen as an additional phase, it is avoided by the drying process for the same reason of avoiding resin impregnation. The drying of the samples can also prevent further chemical reactions during the test such as cement carbonation. Although the drying process helps in imaging and testing of the samples, it also brings other problems. For shales, it prevents chemical reactions, but physical changes can’t be avoided such as the shrinkage of the clay minerals, which might cause new fractures or enlarge the original cracks within the rock resulting in a reduction in the mechanical properties. The assumption made here is that the drying process has the same effect on all rock samples so that the test results are still comparable. For lab-made composites and cement samples, the main effect of the drying process is the salt crystallization, as some of the samples are made with high salinity water (2,000 ppm, 35,000 ppm, and 180,000 ppm). The salt crystallization is explained as the reason for the mechanical properties reduction for the samples made with saline water in this study. But it is a subjective interpretation based on the results and is not confirmed by other evidence (such as images). Future investigation is recommended regarding the mechanical properties reduction and the salt crystallization.

5.1.2. Micro/Nano Indentation Data Insights

5.1.2.1. Young s Modulus from indentation

For the mechanical properties measurements, Young’s Modulus was calculated using Oliver & Pharr’s method based on indentation results. The original equation correlated the Young’s Modulus and Poisson ratio of the indenter tip (Ei, νi) and tested material (E, ν), which means the measured Young’s Modulus (E) is valid only if a representative Poisson’s ratio (ν) is implemented at the same scale, but during the calculation, Poisson ratio of the material (ν) were assumed as constant equals 0.2 in this study based on large-scale measurements on shales from the literature. This is because 1) there is no reliable value for the Poisson’s ratio of pure minerals at the nanoscale, 2) changes in the Poisson’s ratio of the tested material do not alter the results significantly when the diamond tip is used (Ei>>E, νi<<1).

5.1.2.2. Pile-ups and material rebound from indentation

During the loading process of the indentation test, excess dislocations align themselves forming dislocation walls and consequently develop into IKBs (incipient kink bank) and KBs. (IKBs are reversible i.e, plastic flow due to formation of IKBs would reverse once the load is removed.) Formation of IKBs and KBs can be developed into pile-ups around the indenter walls, when geometrically necessary dislocation (GND) density exceeds the maximum density that can be stored, whereby the repulsive force acting on the contacted/ compressed area forced the material to spread out [Mares and Kronenberg, 1993; Pant, 2013; Du and Radonjic, 2019].

This study used the E/H value as an indicator for plastic deformation/pile-up, and this was inspired by the indentation fracture toughness method. The results indicated the E/H value can be correlated with the material pile-up, therefore predict the fracture initiation point, but this is still a qualitative method. To go further on this path and make it quantitative, the amount of the pile-up needs to be measured. The measurement of the pile-up may also help to improve the accuracy of the indentation fracture toughness, because as now, the indentation fracture toughness is still skeptical and not well accepted by the traditional fracture mechanics community due to frequently produced inaccurate results [Quinn, 2006; Quinn and Bradt, 2007].

5.1.2.3. Indentation fracture toughness

As mentioned in the methodology section before, there are many different equations have been developed for the indentation fracture toughness test with different powers for the E, H, P and c terms [Li et al., 1989; Ponton et al., 1989; Quinn and Salem, 2002], but none of which have been successful for a variety of materials. All the equations have some weak points in common:

1) The empirical calibration constant (ξ_V). The empirical calibration constant is one of the key components for calculating the fracture toughness. Anstis et al. [1981] estimated this constant was 0.016 ±0.004. This 25% standard deviation is a substantial variability. Other equations from the literature used curve fitting methods to calculate this constant gave an even wider range from 0.0095 to 0.0248 [Laugier, 1985; Ma et al., 2018]. The large

uncertainty (over 150%) made the calculated results questionable.

2) The measurement of the crack lengths on the surface (c, a, and *l*). A practical problem is that it is difficult to measure the crack lengths on the sample surface. The measurement of the crack tip can be very subjective. For example, in this study, when the crack tip reached a boundary line between two large particles, it was impossible to determine where the crack stopped as shown in Figure 5.1. Quinn, [2006] stated that:

> "Between-laboratory consistency is poor due to variations arising from microscopy limitations as well as operator experience or subjectivity…All laboratories said there was considerable interpretation as to where the exact crack tip was and there was difficulty measuring this point….. as much as 20 μm can be added to an optical crack length measurement if the crack is measured with an SEM". [Quinn, G., 2006]

3) The assumption on the crack system. Depending on your assumption whether the crack is Palmqvist or median, equations are different. While during the test, the inducted cracks often are not idealized as Palmqvist or median as assumed, for example, the cracks may form as Palmqvist cracks at first then later extend to median cracks. [Quinn and Bradt, 2007]. Theoretically, the crack type can be visualized directly by modern technology such as Computed Tomography (CT). The micro CT was also attempted in this study, but the resolution was too low to capture these fractures because most of them were in the micro and sub-micro scale.

Because of these weak points, the traditional fracture mechanics community has been skeptical about this method [Quinn, 2006; Quinn and Bradt, 2007], as it frequently produces inaccurate results even on relatively homogenous materials such as metals and tooth. The application of this method on heterogeneous multiphase composite such as cement and rock becomes more complicate and questionable. Therefore, an important assumption is made in this study that the fracture toughness of a material is mainly controlled by the E/H value. Instead of choosing a specific equation developed from different studies, the key components can be summarized and concluded as: empirical calibration constant (ξ_V), crack lengths on the surface (c, a, and *l*), E/H and Indentation load (P). In this study, same load were applied on the same indenter tip (Vickers diamond) to test different samples, the P and ξ_V are constant (ξ_V is defined as constant depending on the indenter geometry). Comparing the crack lengths and E/H, crack lengths are more subjective as discussed and shown (Figure 5.1) before, while both E and H value measured from the indentation tests are more reliable and comparable with other studies. Therefore, the E/H value is used instead of the fracture toughness to show the fracture initiation point/area of the material. Observation in this study also confirmed that E/H value can be correlated with the material pile-up around the indenter tip, and the pile-up can been seen as a micro fracture/ failure of the material.

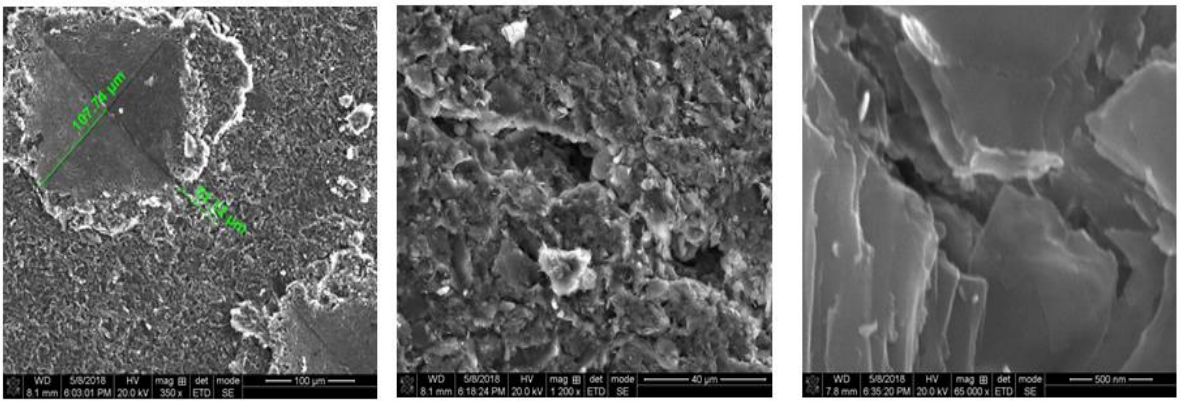

Fig. 5.1. Left: Fracture Toughness measurement by the indentation on Marcellus top sample; Middle: zoom in to the fracture tip; Right: further zoom in, induced fracture or grain boundary.

5.1.3. Anisotropic Shale Properties as Key Factor for Fracturing

5.1.3.1. Properties anisotropy in shale

Macro and Microstructure of shales are dominated by distinct laminated layering characteristics which caused the anisotropy in petrophysical and mechanical properties. Elastic anisotropy of shales is understood to be the result of 1) the anisotropic fabric created by the preferred orientation of platy clay minerals, 2) the anisotropic properties of the clay minerals itself, and 3) the amount of organic content [Vernik and Nur, 1992; Vernik and Liu, 1997].

Isotropic shales are relatively easy to test or interpret, but when it comes to predicting or modeling the strength of anisotropic rocks, it is one of the most important unsolved problems in rock mechanics [Hudson, 2008]. Because isotropic criteria do not work for predicting the strength of anisotropic shales, the strength of highly anisotropic shales may be much lower than its maximum strength, depending on the direction of the maximum principal stress and the angle between the stress and the bedding. Therefore, anisotropic shales need to be analyzed down to finer micrometer scales [Ambrose, 2014].

This study used a dimensionless number E/H measured at the micrometer scale to quantify the fracture potential at different directions to show the anisotropy of the rocks. For the two shale samples in this study, although the number of clay particles with preferred orientation was not quantified for both samples, the Marcellus shale has much higher clay and organic content than the Pottsville shale, which leads to a higher degree of anisotropy. Results showed in Table 4.2 also agreed that Marcellus had a higher degree of anisotropy.

5.1.3.2. Grain Size, Boundaries, and Properties

Compare the Pottsville and Marcellus shales, Pottsville has a more uniform grain size, the Gm and Gr are around 10 to 50μm, while for Marcellus, the Gm and Gr have a size range from 10 to 200μm. Since the fracture initiate at the grain boundaries, Marcellus shale is more likely to have larger fractures as shown in the figure, furthermore, the relatively clean and smooth grain boundaries may also help the fracture to propagate. As for the properties of the grains, Pottsville has higher Gs and Gr content while Marcellus has relatively uniform grain properties. The Gr in Pottsville are evenly distributed with short and irregular boundaries, which may act as barriers to prevent fracture propagation [Du and Radonjic, 2019].

Table 5.1. Summary of differences between brittle shale and sealing shale [Du and Radonjic, 2019]

	Brittle Shale (Marcellus)	**Sealing Shale (Pottsville)**
Microstructures	anisotropic (more oriented grains)	relative isotropic
	wider range of grain size	more uniform grain size
	long clear grain boundaries (defect)	short irregular grain boundaries
Mineralogical composition	lower clay content	higher clay content
	homogeneous	heterogeneous
	(relatively uniform grain properties)	(higher rigid grain content)
Mechanical properties	lower bulk mechanical properties	higher bulk mechanical properties
	higher E/H,	lower E/H,
	more pile-up/plastic deformation	imprint recovered in 4 months

5.2. APPLICATION OF SHALE FRACTURING IN SUBSURFACE ENGINEERING

5.2.1. Shale Characterization

5.2.1.1. Image-based correlation for prediction of fracture initiation in shales

Shales contain grains with distinct mechanical properties, generally, grains with heavier element is also superior in mechanical properties than the grains with lighter elements in shale (e.g. Fe rich hematite > Ca rich calcite > Si/Al rich clays). BSE images might be used alone bypassing other mechanical characterization techniques to see the likelihood for fractures to initiate in certain shale, as it marks the boundaries between the grains with different elements [Du and Radonjic, 2019]. For example, in Figure 4.27, the binary BSE maps of Pottsville and Marcellus rock clearly the grain boundaries. The large, elongated calcite particle in Marcellus had long, continuous and clear grain boundaries between calcite and clays (two mechanically different particles), therefore, these areas were most likely for the fracture to be initiated when under stress. Utilize this information can help to identify the optimal position for perforation. Furthermore, when large cores are hard or expensive to get such as in the deep-water well, the same procedure can be done on the drill cuttings to make the predictions with less time and cost.

5.2.1.2. Proppant embedment in fracture walls

Hydraulic fracturing was used in low permeability shale reservoirs to generate and maintain a conductive pathway for the fluid to flow from the reservoir to the wellbore. The success of these treatments is highly reliant on the fracture conductivity. One of the major mechanisms for conductivity loss is because of the proppant embedment which led to decreased fracture width. The process of proppant embedment is similar to the loading process of the indentation where a rigid body was forced into the rock surface, therefore, the indentation test can be used to calculate and predict the embedment depth.

The surface hardness of the fracture wall was identified as the controlling fact for the proppant embedment depth [Mueller and Amro, 2015], which can be measured by the indentation. However, this hardness may not be the same as shown in all previous indentation tests, especially in the formations where interaction between the fracturing fluid and fracture wall can lead to a change in the mechanical properties of the fracture wall [Weaver et al., 2009; Raysoni and Weaver, 2013]. The interaction with fracturing fluid may cause a reduction in hardness due to the swelling of the clays or dissolving of other minerals, resulting in an increased embedment depth and decreased conductivity. In this situation, the indentation can be used to decide which fracturing fluid or treatment to use on a specific rock to minimize the hardness reduction or even to enhance the mechanical properties of the fracture wall so that generated fractures can remain open for a longer time.

5.2.2. Cement Compression

Based on the presented data it is evident that hydrated wellbore cement, once subjected to forces caused by the expansion of metal casing, can undergo microstructural alterations. Because of the confinement between the two metal pipes, the confinement prevented the failure of brittle material and instead rearranged microarchitecture within the cement matrix. The effect that the metal casing expansion has on the cement is overall positive. It reduced the number of large pores by compaction, moreover, it improved the packing of the grains, the outcome of which is more dense material as shown in Figure 5.2 below. Some of the larger unhydrated grains can fracture at higher rates of metal expansion (cement compression). This leads to a detachment of CSH from the grain surfaces and allowing pore water to reach unhydrated particles triggering secondary hydration. The comparison showed that the poro-mechanical characteristics of wellbore cement appear to be improved when inherent pore sizes are shifted to the predominantly nano-scale range as characteristic of pore-size distribution typical for shales [Radonjic et al., 2015].

The deposition and formation of caprocks as an impermeable subsurface barrier material are based on the squeezing of excess water and mineralogical transformations at different temperatures and pressures. These processes proceed over geologic times. It is expected that, in a similar mechanism, the wellbore cement material when compressed towards the formation, can also experience pore water propagation and secondary mineral precipitation resulting in improved mechanical and hydraulic properties [Radonjic et al., 2015].

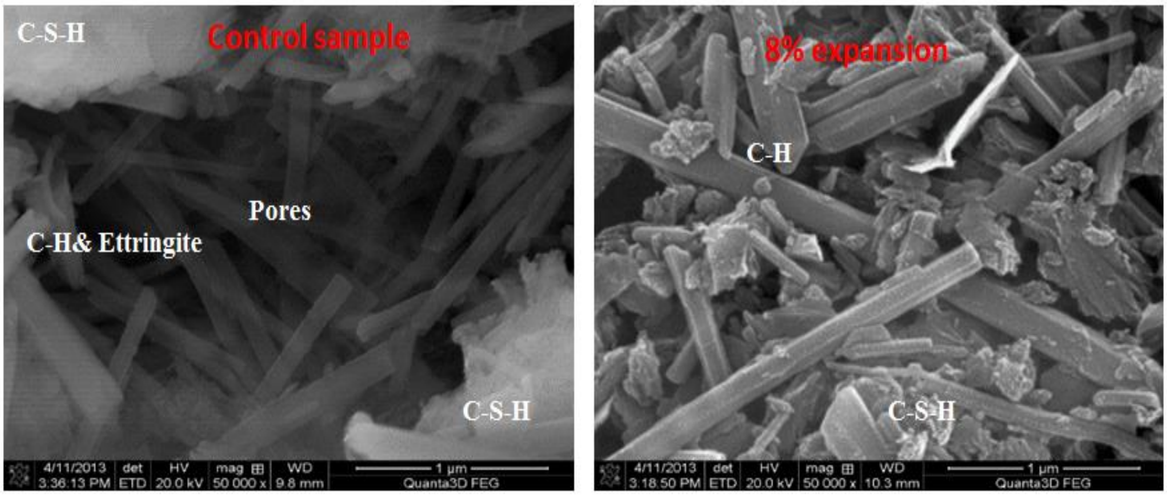

Fig 5.2: Secondary electron micrographs cement samples. Left: control sample; Right one month after 8% expansion. Sample after compression shows the tight compaction and rearrangement of original hydration products

The results from this study show that the metal casing expansion has on the cement is positive overall. Cement regained its mechanical properties and became stronger than the control sample after a certain period of rehydration [Du et al., 2015], which is a piece of important information for field application and long-term wellbore integrity.

6. CONCLUSIONS AND RECOMMENDATIONS

The conclusions and observations of this work are:

1. The grain boundaries are the defect for cracks to initiate and propagate, while in a complicated multi-phase composite like shale, fractures are more likely initiated at the boundary of two mechanically different mineral grains. When other tools are not available, BSE images might be used alone bypassing other mechanical characterization techniques to make a reasonable estimation on where the fractures are likely to be initiated in certain shale, as it marks the boundaries between the grains with different elements.

2. Sediments with higher clay content have a denser packing, resulting in higher mechanical properties and lower porosity. Pottsville shale, as a caprock, has an overall higher mechanical properties over Marcellus shale due to more uniform grain size and higher rigid grain content; these rigid grains were evenly distributed with irregular boundaries that can act as barriers to prevent the fracture propagation; once deformed, the rock was able to rebound to its original state due to the lower E/H value (more elastic deformation). Marcellus shale has a higher degree of anisotropy than the Pottsville shale due to the higher clay/organic content and lenses network distribution; larger fractures are more likely to develop along clear grain boundaries; once fractured, the fracture can stay open for a longer period time due to higher E/H (more plastic deformation)

3. Shale petrophysical properties are tighter than that of cement. The import of these on mechanical properties of both cement and shale would probably reflect on their elastic behavior under high pressure confining stress. The effect of metal casing expansion has

on the cement is overall positive. The confinement prevented the failure of brittle material and instead rearranged microarchitecture within the cement matrix. It reduced the number of large pores by compaction, moreover, it improved the packing of the grains, the outcome of which is a more dense material. Some of the larger unhydrated grains can fracture at higher rates of metal expansion which leads to a detachment of CSH from the grain surfaces and allowing pore water to reach unhydrated particles triggering secondary hydration.

4. Within the same formation, the top portion has a higher mechanical property, which suggests better structural integrity. The bottom portion of the formation is more likely to initiate fractures as it is less mechanically stable. However, this can be only used as a general guide for mechanical properties prediction for shale cores from the same formation, which may not be true for all scenarios due to the complexity of natural materials.

5. Nano indentation could be an excellent two-dimensional mapping tool for examining the properties of the constituent phases independent of each other in composite material microstructures. The indentation can be also used to measure the proppant embedment depth to make a more accurate prediction. After treating the rock with different fracturing fluids, the indentation test can help to decide which treatment or fracturing fluid to use for a given formation. Mechanical property maps could be used for correlating individual phase properties with bulk response measured by micro indentation. Combing the mechanical properties map with high resolution microscopy, the mineralogy/morphology

can be also correlated. The mechanical property map can be also done on other multiphase composites such as cement to study the intrinsic properties of each component, as well as the interaction and properties of the bond and interfacial regions of different phases. It might also be useful for modeling the rock/cement behavior to predict the fracture occurrence potential, as it links the microstructural features with their mechanical properties.

6. This study is focused on establishing how indentation data can be used in evaluating the mechanical properties of shale and their susceptibility to fracturing. The value of this approach is a reduction of time and cost in geomechanical evaluation, as indentation could be done on drill cuttings instead of core samples. Also, the non-destructive nature of testing makes it possible for the dynamic study in contact with different fluids and dry/wet cycling conditions. In addition, when combined with SEM/EDS/BSE microstructural characterization, geochemical and geomechanical changes can be monitored in an interdependent manner.

APPENDIX A. AVERAGE MINERALOGICAL COMPOSITION OF DIFFERENT SHALES

Table A.1. Sealing shales (top) Vs. brittle shales (bottom). Average mineralogical composition, total organic carbon and porosity of core-scale experimental data on the properties of well characterized shales and mudstones compiled from multiple studies [Bourg, 2015; Amann et al., 2013; Bai et al., 2013; Busch et al., 2008; Chalmers et al., 2012; Josh et al., 2012; Swift et al., 2014; Nelson, 2009].

Formation	**Clay (%)**	**Quartz& feldspar (%)**	**Carbonate (%)**	**TOC (%)**	**Porosity (%)**
Keuper claystone	49.2	19.8	19.2		13.3
Kirtland formation	63.5	39.0	1.5	0.2	8.1
Nordland shale	55.3	39.3	9.2	1.0	34.8
Eau Claire shale	34.6	44.5	13.6		8.6
Janusfjellet shale	52.5	26.5	20.5		
Draupne shale	51.1	32.5	14.6	3.5	28.0
Fjerritslev formation shale	51.0	42.0	5.0		23.5
Norweglan shelf Jurassic mudrocks	65.5	26.7	4.2	0.5	36.4
Chimney rock and Gothic shales	39.0	27.4	34.0	2.7	6.8
ZeroGen shale	56.0	38.0	9.0	2.7	
Anahuac shale	71.7	28.3	0.0		
Tuscaloosa mudstone and shale	41.6	39.1	14.1	0.8	6.9
AVERAGE (Sealing shales)	**52.6**	**33.6**	**12.1**	**1.6**	**18.5**
New Albany shale	38.0	49.5	2.4	9.4	
Barnett shale	23.0	53.9	14.6	4.3	5.8
Shahejie formation shale	25.0	15.0	60.0		
Haynesville shale	36.0	25.5	32.9	3.0	8.0
Doig siltstone	5.5	73.7	19.1	0.7	6.6
Doig phosphate	10.5	38.7	45.0	6.8	2.5
Marcellus shale	35.7	36.5	26.3	3.5	5.7
Woodford shale	28.2	56.0	5.7	8.8	6.3
Eagle ford shale	12.6	9.5	72.5	2.6	6.0
Fort St.John shale	36.0	57.0	4.0		
Fayetteville shale	25.0	47.5	15.0	2.6	5.8
Bakken shale	39.8	47.5	8.5	11.2	
Duvernay shale	23.8	46.0	24.3	3.8	5.2
Muskwa shale	10.3	72.3	13.3	4.2	5.5
Conasauga shale	31.6	26.2	41.5	0.5	
AVERAGE (brittle shales)	**25.4**	**43.7**	**25.7**	**4.7**	**5.7**

APPENDIX B. CEMENT AVERAGE MECHANICAL PROPERTIES WITH DIFFERENT EXPANSION RATIOS

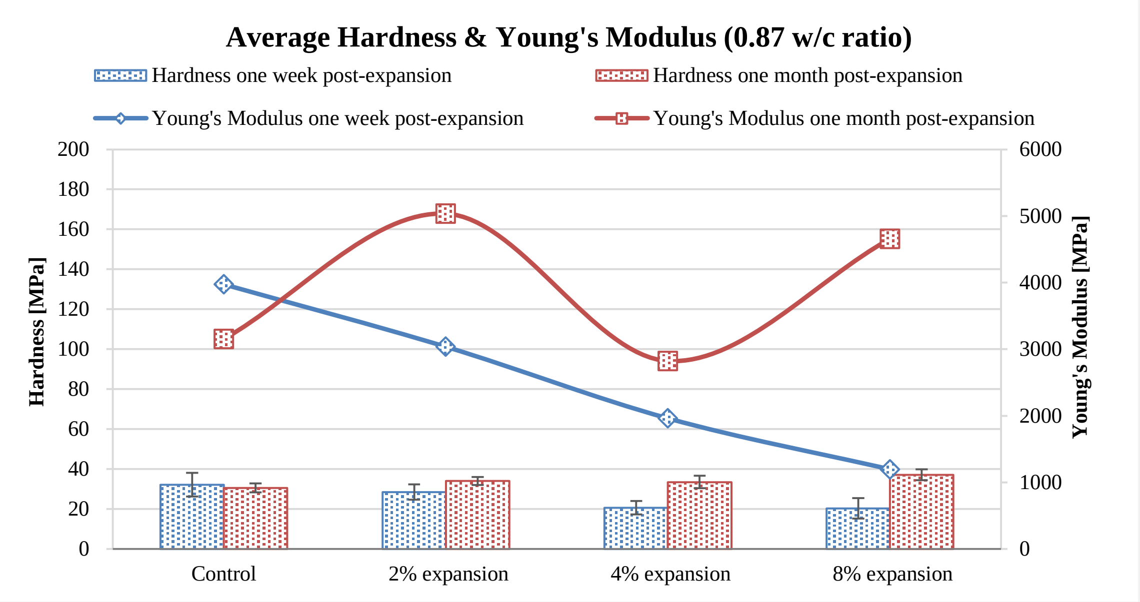

Fig. B.1. Average mechanical properties of 0.87 w/c ratio cement with different expansion ratios

The indentation results of the 0.87 w/c ratio samples one week post-expansion show decrease in both hardness and Young's modulus for all samples, where the highest hardness decrease of 30% was recorded in the samples which underwent 4% and 8% expansion (Figure B), and Young's modulus decrease linearly as the expansion ratio increase. The indentation results of the samples one month post-expansion showed an average increase in the cement's hardness and Young's modulus after pipe expansion. Both hardness and Young's modulus increased the most in the sample 8% post-expansion (20% increase in hardness, 40% in Young's modulus).

APPENDIX C. YOUNG'S MODULUS DISTRIBUTION OF TOP AND BOTTOM SAMPLES

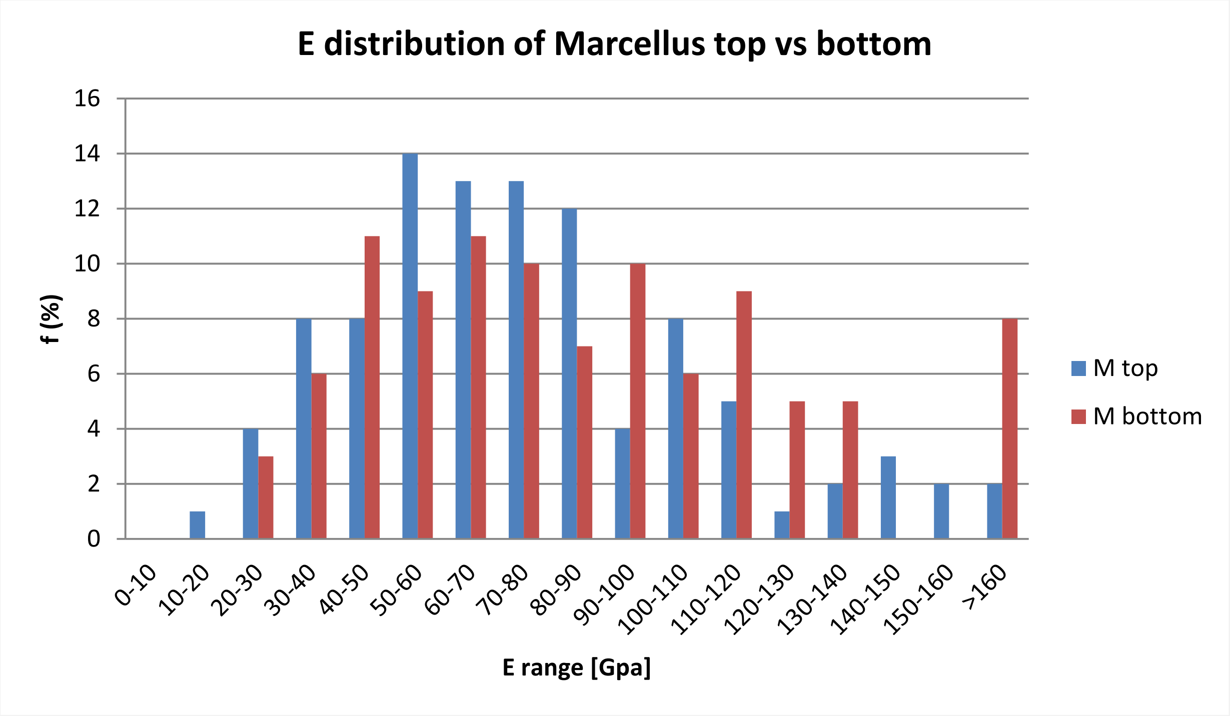

Fig. C.1. Comparison of Young's Modulus distribution of Marcellus shale top and bottom samples

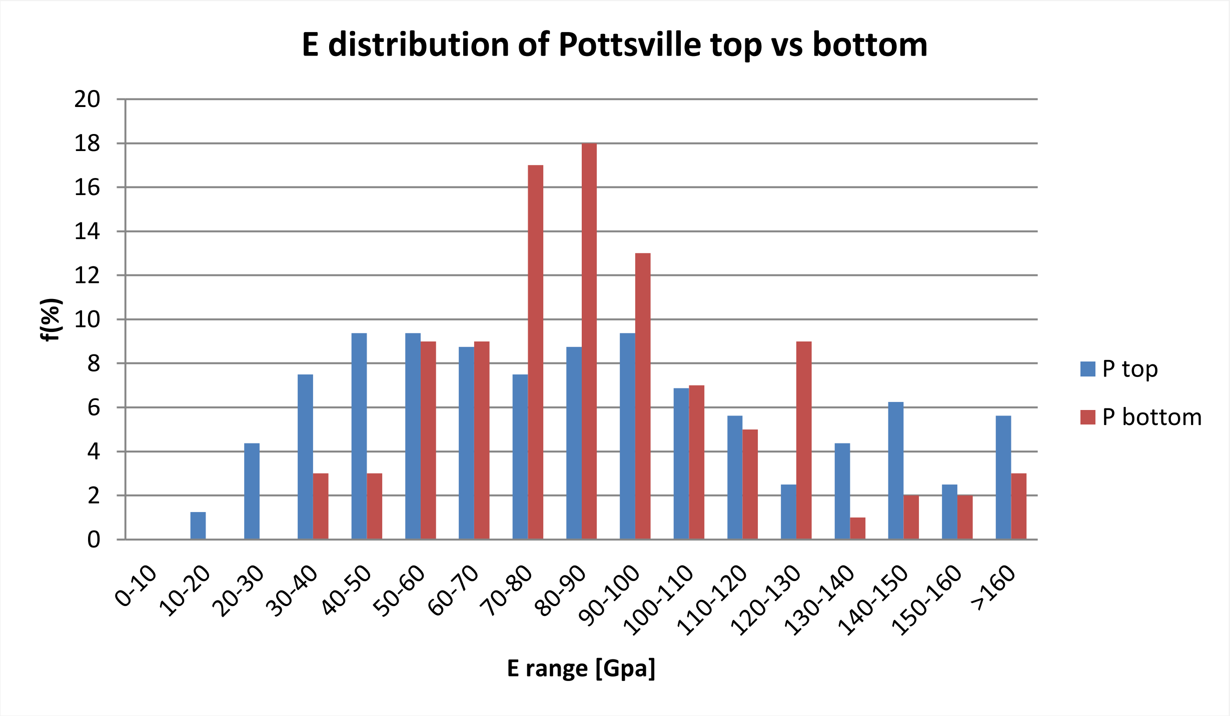

Fig. C.2. Comparison of Young's Modulus distribution of Pottsville shale top and bottom samples

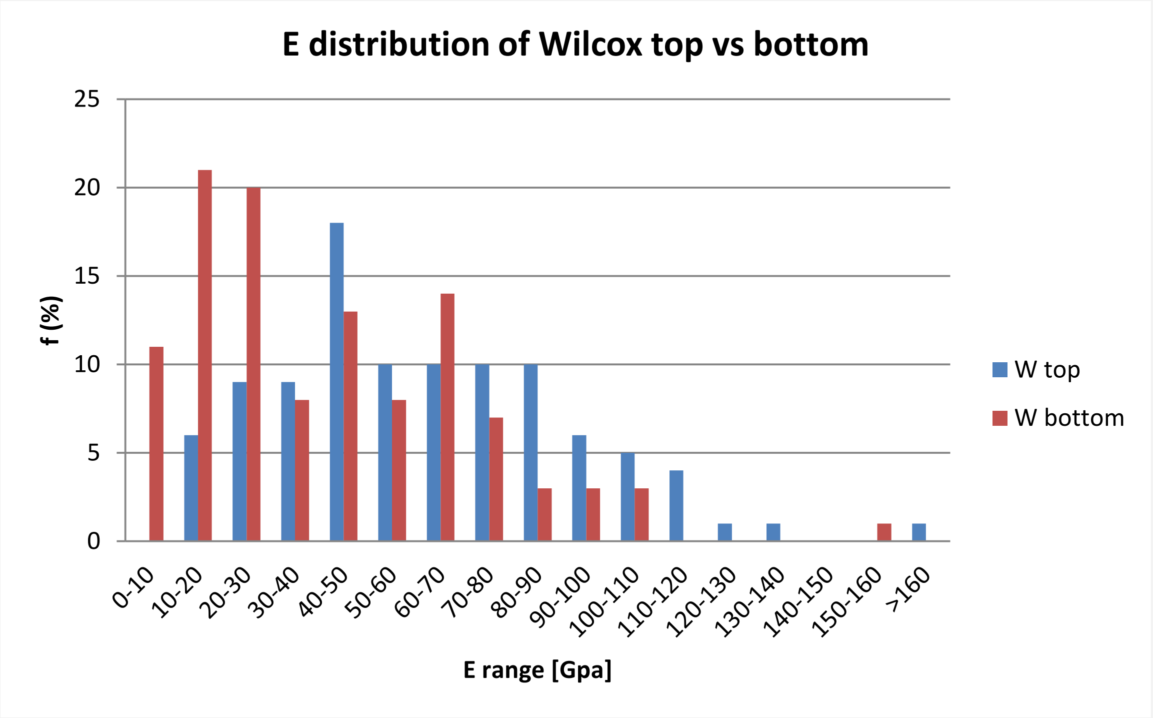

Fig. C.3. Comparison of Young's Modulus distribution of Wilcox shale top and bottom samples

APPENDIX D. MECHANICAL PROPERTIES MAPS OF DIFFERENT SHALES

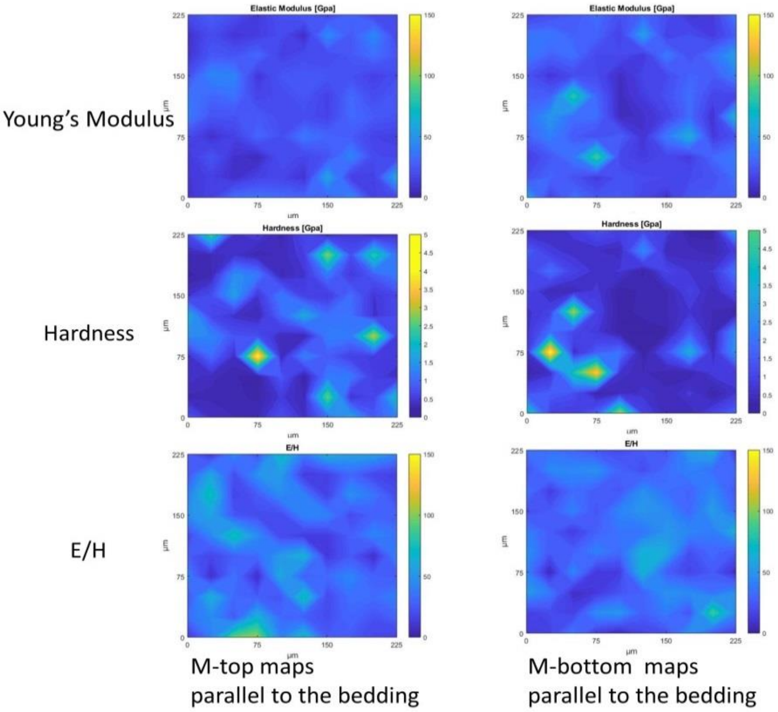

Fig. D.1. Mechanical properties maps of Marcellus shale from the top and bottom of the formation

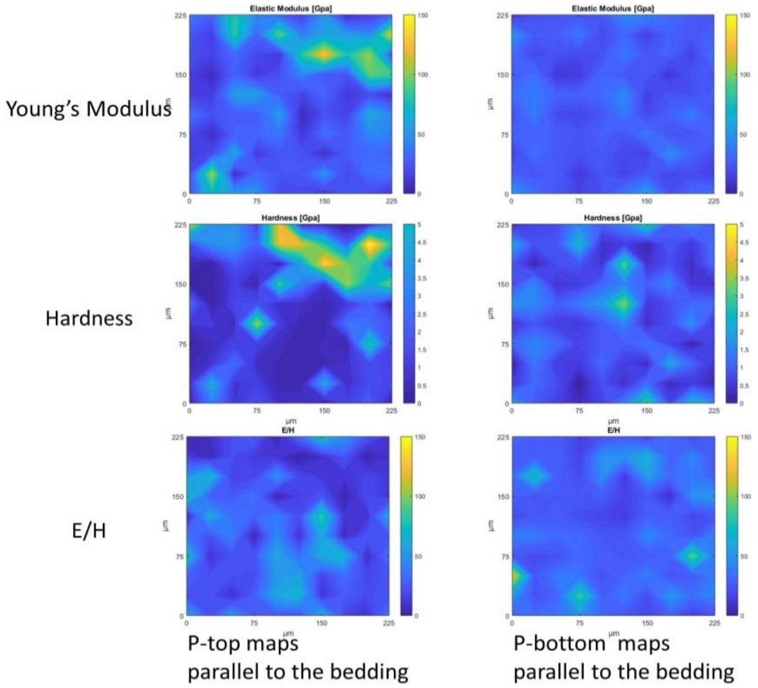

Fig. D.2. Mechanical properties maps of Pottsville shale from the top and bottom of the formation

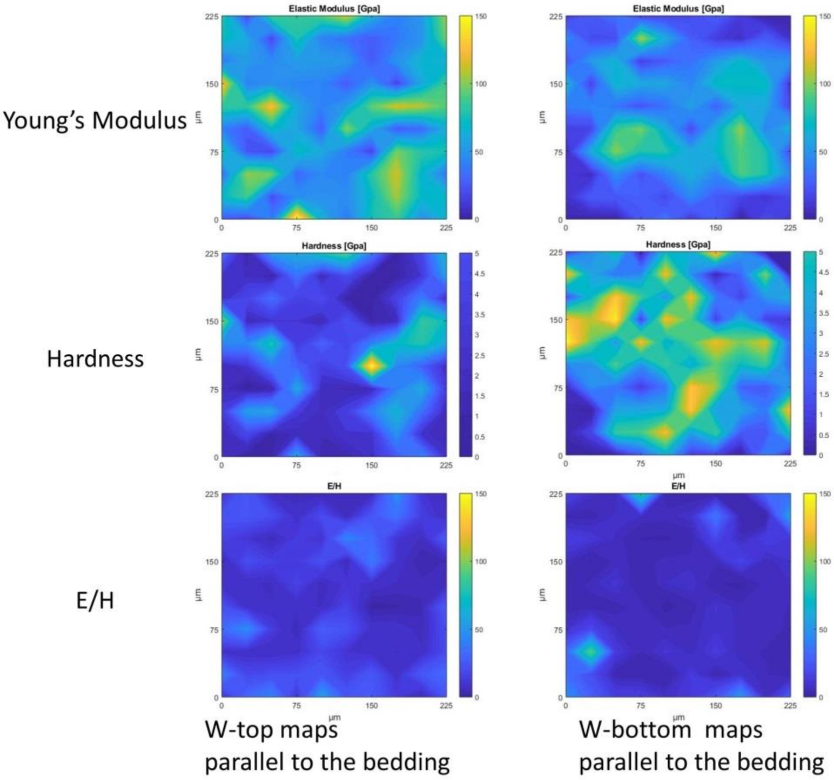

Fig. D.3. Mechanical properties maps of Wilcox shale from the top and bottom of the formation

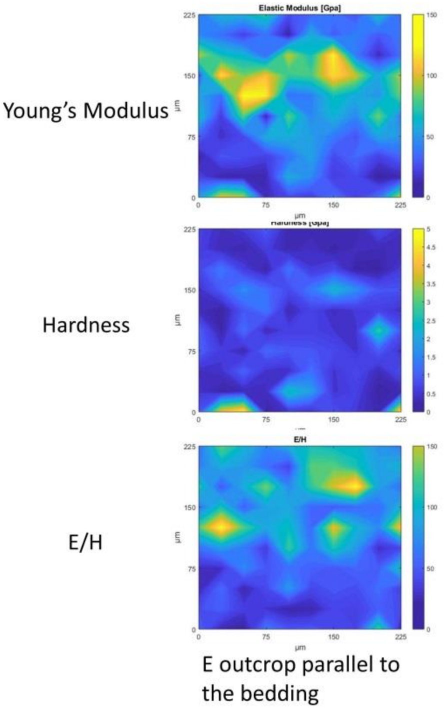

Fig. D.4. Mechanical properties maps of Eagleford shale outcrop

APPENDIX E. LOADING-UNLOADING CURVES EXAMPLES

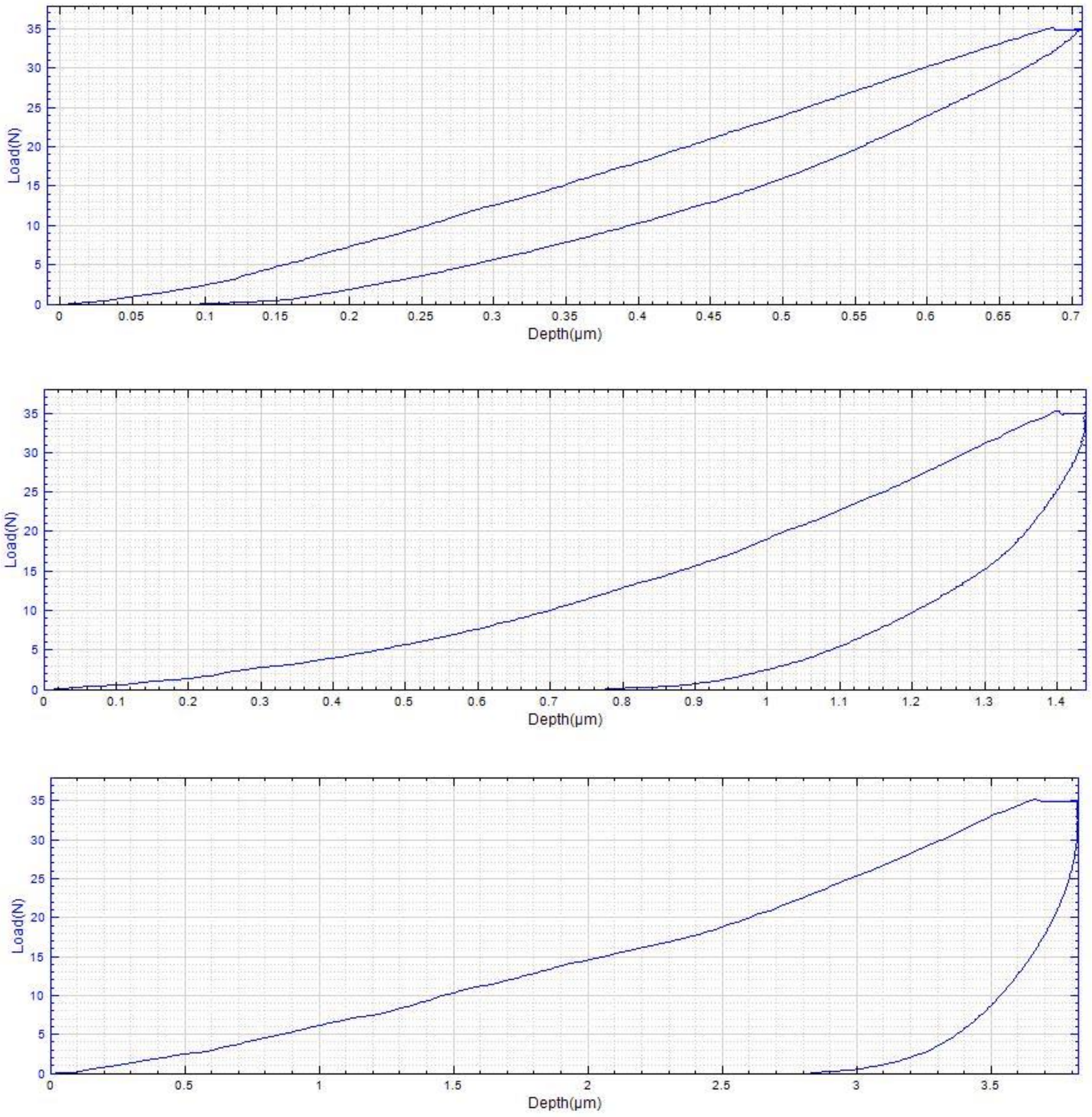

Fig. E.1. Examples of the loading-unloading curve on minerals with different mechanical properties. Top: highly elastic material (pressure ~400k psi); middle: hard elastoplastic material (pressure~100k psi); bottom: soft elastoplastic material (pressure~14k psi). All of them are above the yield strength of the rock in the stain hardening region

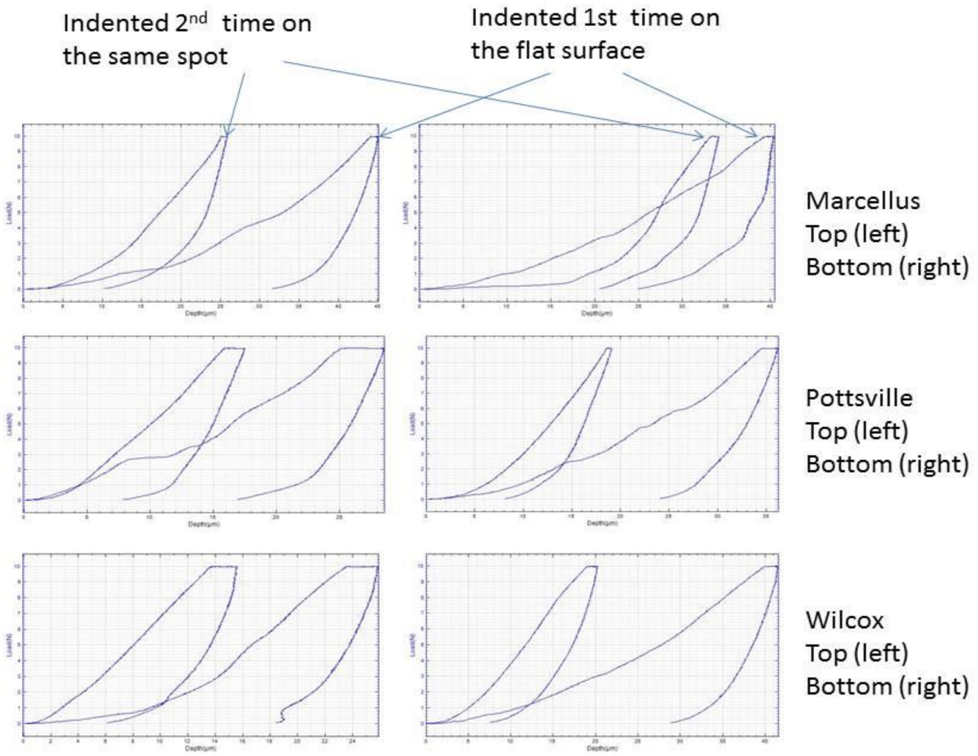

Fig. E.2. Examples of Loading-unloading curves on six different samples from the top and bottom portion of three shale formations. The two curves in the same graph represent the 1^{st} time indented on the flat surface and 2^{nd} time indented on the same spot.

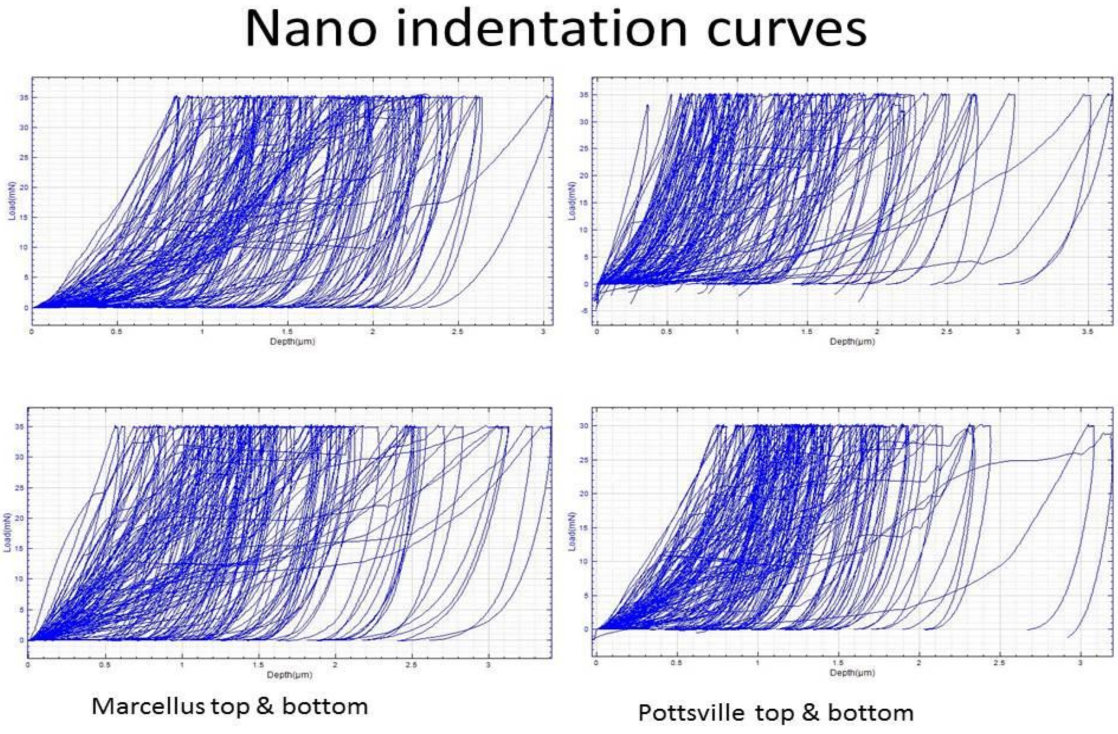

Marcellus top & bottom

Pottsville top & bottom

Fig. E.3. Nano indentation loading-unloading curves of Marcellus and Pottsville samples.

APPENDIX F. SHALE, CEMENT, AND LAB-MADE SAMPLES

Table F.1. Typical Petrophysical Properties Ranges of Clay and C-S-H

Properties	Materials and units	Value	References
Porosity	Clay (%)	34 – 57	McWhorter, D.B. and Sunada, D.K, 1977
	C-S-H (%)	31 – 61	Thomas, J., and Jennings, H, 2014
Effective porosity	Clay (%)	1 – 18	McWhorter, D.B. and Sunada, D.K, 1977
	C-S-H (%)	3 – 44	Thomas, J., and Jennings, H, 2014
Interlayer space	Clay (nm)	0.8 - 2	Nelson, P. H., 2009
	C-S-H (nm)	0.3 - 4	Jennings, H., et al., 2008
Particle size	Clay (um)	1 - 4	Nelson, P. H., 2009
	C-S-H (um)	0.5 - 3	Jennings, H., et al., 2008
Density	Clay (g/cc)	1.6 - 1.8	Bulk Materials Densities*
	C-S-H (g/cc)	1.75 - 2.2	Bullard, J. W. 2008

* Data from website http://www.simetric.co.uk/si_materials.htm

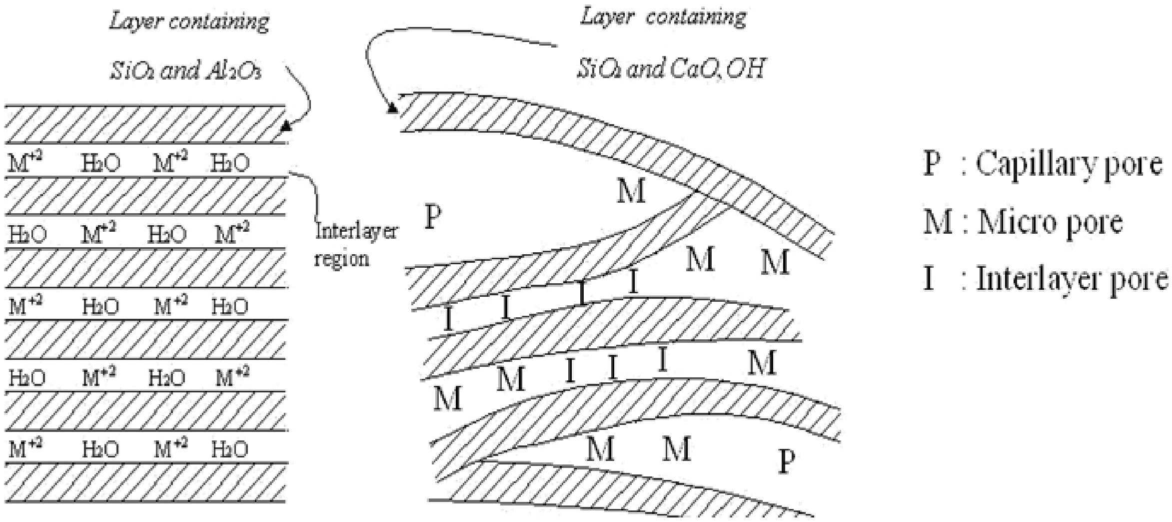

Fig. F.1. Schematics of a) well-crystallized clay mineral (left), and b) poorly crystallized C-S-H (right) [Figure reproduced from the "Portland Cement Hydration" PowerPoint of Dr. Kimberly Kurtis, Georgia Institute of Technology]

Table F.2. Comparison of natural rocks, lab-made samples and wellbore cement

	Natural shale	Lab-made sample	Wellbore cement
Depositional environment	Particles slowly deposited through suspension in calm waters. Both physical and chemical weathering at varies temperature (T) & pressure.	Lab-made environment with particles suspension in calm water, force applied vertically to mimic the overburden pressure, constant T	Particles suspension in calm water, chemical reaction between particles and water. constant T
Composition	quartz, K-feldspar, carbonates and clay minerals in varying proportions	Quartz, calcite, and clays(kaolinite, illite, and smectite)	CSH, CH, ettringite
Cementation/ binder	clay; authigenic quartz (released from the smectite illitization); carbonates	calcite	CSH
Microstructure	Dense, well compacted, laminated. Clay layers composed of silica and aluminate sheets that are stacked in a specific orientation, water, and metal ion were present between the layers.	weakly compacted, weakly developed laminae composed of stacked clay with visible pore space and fracture	Layers comprised of infinite Ca-O sheets, ribbed with silicate chains. Between the composite layers lie interlayer Ca ions and associated water molecules.
Micromechanics	clay content, distribution of the minerals	dominated by clay content and solution salinity	amount of water, salinity, degree of hydration
Durability	Stable at subsurface condition, fracture self-healing due to mineral dissolution and re-participation (with the present of water and confinement)	visible dissolution when present in water without confinement	varies with design (w/c, additives), self-healing due to rehydration (with the present of water and confinement)

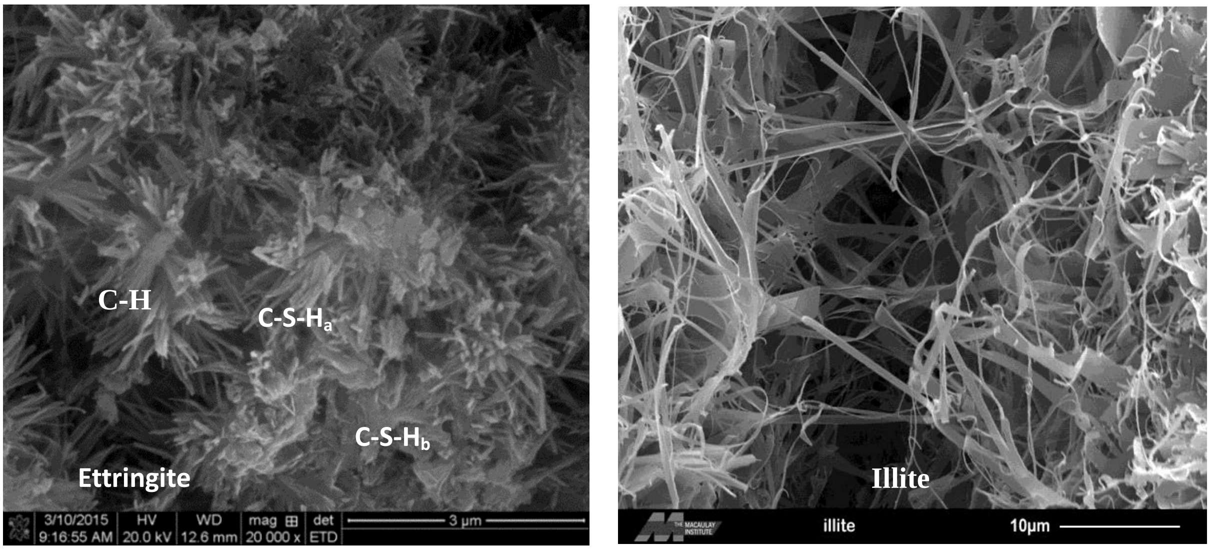

a) SEM micrograph of 0.38 w/c ratio neat cement fracture surface. C-S-H_a has a higher porosity and shows spines like structure; C-S-H_b appeared to be much denser.

b) SEM micrograph of Illite, it has a fibrous net structure that contains a matrix just like cement. (Mineralogical society).

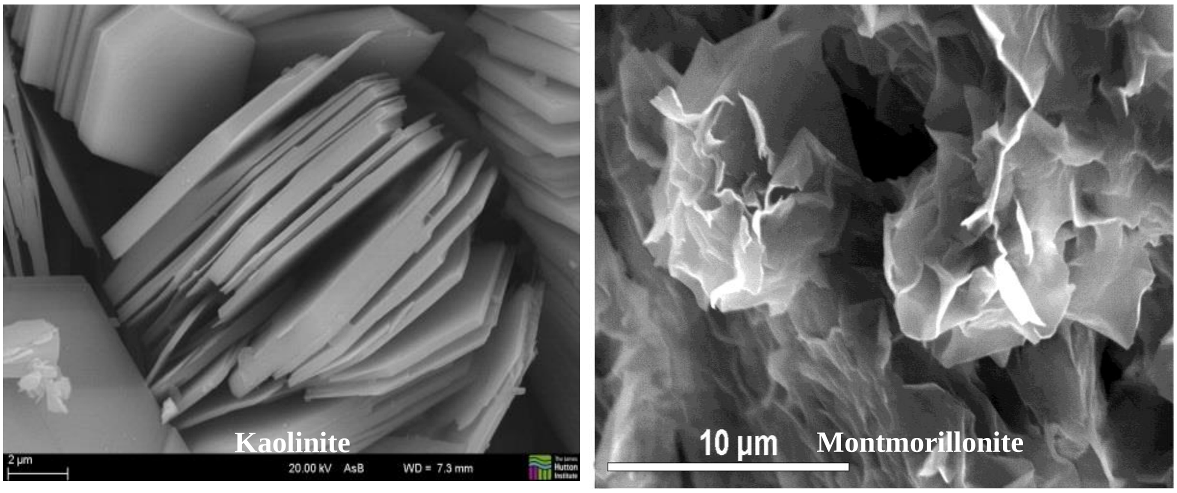

c) SEM micrograph of Kaolinite which has thin idiomorphic platelets and perfectly overlying each other (Mineralogical society).

d) SEM micrograph of Montmorillonite, showing a rose like texture (Mineralogical society).

Fig. F.2. SEM micrographs of cement and clay minerals which commonly seen in shale: a) cement, b) Illite, c) Kaolinite, and d) Montmorillonite. (Clay mineral Images reproduced from the 'Images of Clay Archive' of the Mineralogical Society of Great Britain & Ireland and The Clay Minerals Society) [Du et al., 2017a]

APPENDIX G. INDENTATION IMPRINTS

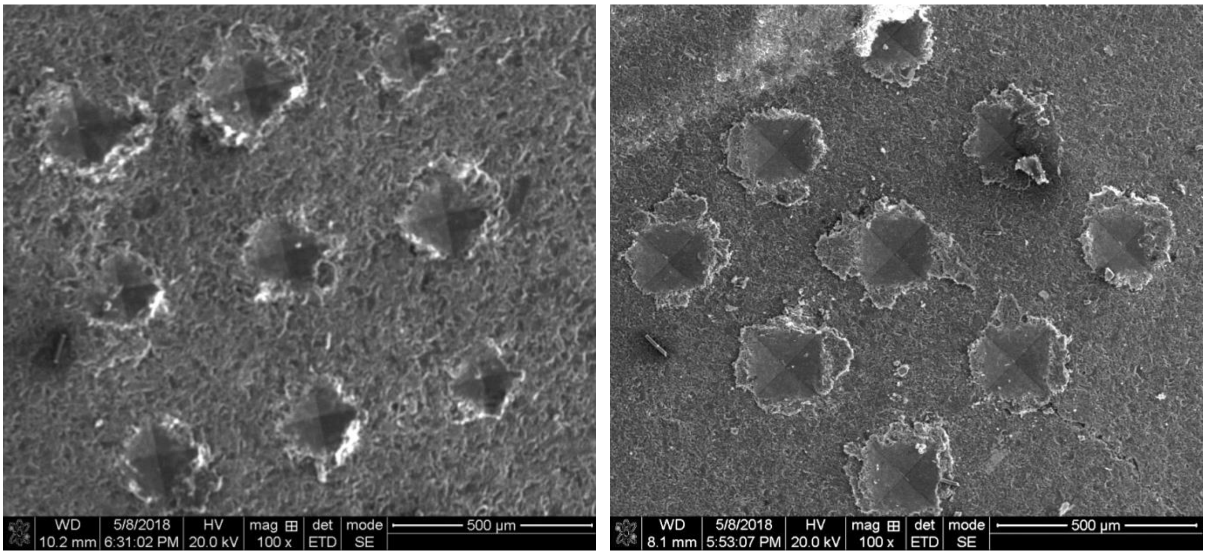

Fig. G.1. SEM micrographs of imprints of micro indentation on Pottsville top (Left) and Marcellus top (Right) shale

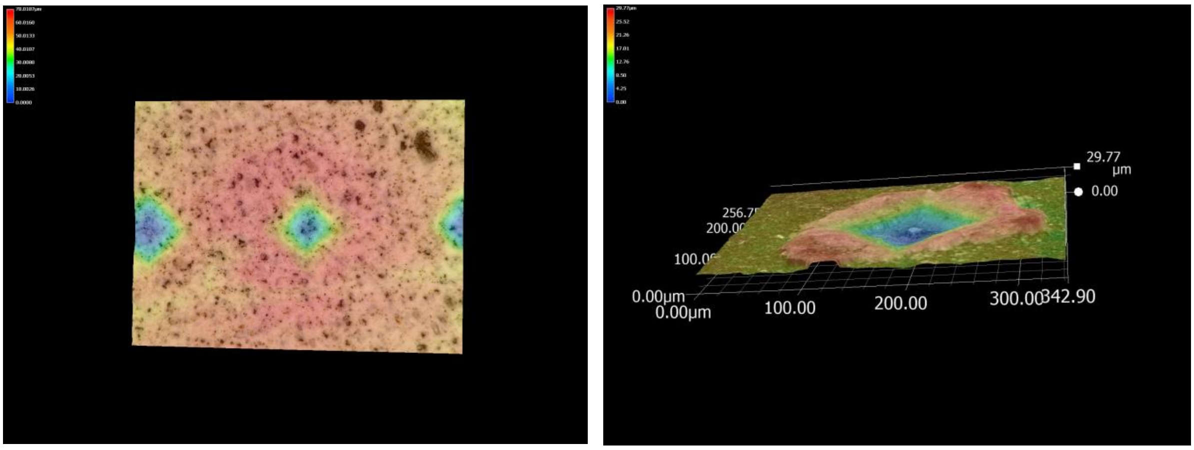

Fig. G.2. Surface profile of the micro indentation imprints on cement (left) and Marcellus shale (right).

REFERENCES

1. Ag Source Laboratories, (2017). Soil Cation Exchange Capacity (CEC). Web, last access by 2019.

2. Agbasimalo, N., Radonjic, M. (2014). *Perimental Study of the Impact of Drilling Fluid Contamination on the Integrity of Cement-Formation Interface*. Journal of Energy Resources Technology (JERT), Vol. 136, No. 3, 2014.

3. Ahmadov, R., T. Vanorio, and G. Mavko, (2009). *Confocal laser scanning and atomic-force microscopy in estimation of elastic properties of the organic-rich Bazhenov Formation*. The Leading Edge, 28, 18– 23

4. AL-Bazali, T.M., Zhang, J., Chenevert, M.E., and Sharma, M.M., (2017). *Measurement of the Sealing Capacity of Shale Caprocks.* Paper SPE 96100.

5. Alemu, B. L., P. Aagaard., I. A. Munz., and E. Skurtveit., (2011). *Caprock interaction with CO2: A laboratory study of reactivity of shale with supercritical CO2 and brine.* Appl. Geochem, 26, 1975-1989.

6. Ambrose, J. (2014). *Failure of Anisotropic Shales under Triaxial Stress Conditions.* Thesis. Imperial College London

7. Angeli, M., M. Soldal., E. Skurtveit., and E. Aker., (2009). *Experimental percolation of supercritical CO2 through a caproc*k. Energy Procedia, 1, 3351-3358.

8. Anovitz, L., and Cole, D. (2015). *Characterization and Analysis of Porosity and Pore Structures*. Mineralogy & Geochemistry Vol. 80 pp. 61-164.

9. Anstis, G., P. Chantikul, B. Lawn, and D. Marshall (1981). *A Critical Evaluation of Indentation Techniques for Measuring Fracture Toughness: I, Direct Crack Measurements*, J. Am. Ceram. Soc., 64 [9] 533-538.

10. API Recommended Practice 10B. (1977). Recommended Practice For Testing Oil-Well Cements And Cement Additives, American Petroleum Institute, April, 1977.

11. Avary, L. K., (last accessed 2019). The Geology of the Marcellus Shale, available online: http://www.wvgs.wvnet.edu/www/datastat/WVGES_GeologyMarcellusShale.pdf.

12. Bai, B.; M. Elgmati., H. Zhang., and M. Wei., (2013). *Rock characterization of Fayetteville shale gas plays*. Fuel, Vol. 105, p.645-652.

13. Bereskin, S. R. and J. McLennan., (2008). *Hydrocarbon Potential of Pennsylvanian Black Shale Reservoirs, Paradox Basin, Southeastern Utah.* Open-file report 534, Utah Geological Society, Salt Lake City.

14. Bergaya, F. and Lagaly, G. (Eds.), (2013). Handbook of Clay Science, Volume 5, 2nd Edition, Elsevier, Amsterdam, Netherlands.

15. Bhattacharyya, KG; Gupta, SS (2008). *Adsorption of a few heavy metals on natural and modified kaolinite and montmorillonite: a review*. Advances in Colloid and Interface Science. **140** (2): 114–31

16. Boukhelifa, L., Moroni, N., James, S.G., Le Roy-Delange, S., Thiercelin, M.J., Lemaire, G. (2004). *Evaluation of Cement Systems for Oil and Gas Well Zonal Isolation in a Full-Scale Annular Geometry.* Paper SPE 87195 presented at the IADC/SPE Drilling Conference, Dallas, Texas, 2-4 March.

17. Bourg, Ian C., (2015). *Sealing Shales versus Brittle Shales: A Sharp Threshold in the Material Properties and Energy Technology Uses of Fine-Grained Sedimentary Rocks*, Journal of Environmental Science & Technology Letters, 2(10), pp. 255-259.

18. Brigatti, M.F., Guggenheim, S., (2002). *Mica crystal chemistry and the influence of pressure, temperature, and solid solution on atomistic models. In: Mottana, A., Sassi, F.P., Thompson, J.B., Guggenheim, S. (Eds.), Micas: Crystal Chemistry and Metamorphic Petrology.* Reviews in Mineralogy and Geochemistry, vol. 46. Mineralogical Society of America, Washington, DC, pp. 1–97.S.

19. Brindley, G.W., Brown, G. (Eds.), (1980). Crystal Structures of Clay minerals and Their X-ray Identification. Mineralogical Society, London.

20. Bruno, M.S., K. Lao., J. Diessl., B. Childers, J. Xiang., N. White., and E. van der Veer., (2013). *Development of improved caprock integrity analysis and risk assessment techniques*. Energy Procedia Vol 63: p. 4708-4744.

21. Bullard, J. W. (2008). *A Determination of Hydration Mechanisms for Tricalcium Silicate using a Kinetic Cellular Automation Model*. Submitted to the Journal of American Ceramic Society.

22. Busch, A.; S. Alles., Y. Gensterblum., D. Prinz., D. N. Dewhurst., M. D. Raven., H. Stanjek., and B. M. Krooss., (2008). *Carbon dioxide storage potential of shales*. Int. J. Greenhouse Gas Control, Vol.2, p. 297-308.

23. Cate, A.S., (1963). *Lithostratigraphy of some Middle and Upper Devonian rocks in the subsurface of southwestern Pennsylvania*, in Shepps, V.C. (Ed.), Symposium on Middle and Upper Devonian stratigraphy of Pennsylvania and adjacent states: Pennsylvania Geological Survey General Geology Report, 4th series, no. 39, pp. 229-240.

24. Chalmers, G. R.; R. M. Bustin., and I. M. Power., (2012). *Characterization of gas shale pore systems by porosimetry, pycnometry, surface area, and field emission scanning electron microscopy/transmission electron microscopy image analyses: Examples from the Barnett, Woodford, Haynesville, Marcellus, and Doig units*. AAPG Bull, Vol.96, p.1099-1119.

25. Chapman, D. L., (1913). LI. A contribution to the theory of electrocapillarity, The London, Edinburgh, and Dublin Philosophical Magazine and Journal of Science, 25:148, p. 475-481

26. Chilingar, G. V. Haroun, M., Shojaei, H., and Shin, S. (2014). *Introduction to Electrokinectics, Electrokinetics for Petroleum and Environmental Engineers*. Scrivener Publishing.

27. Clarkson, C.R., Haghshenas, B., Ghanizadeh, A., Qanbari, F., Williams-Kovacs, J.D., Riazi, N., Debuhr, C., Deglint, H.J., (2016). *Nanopores to megafractures: current challenges and methods for shale gas reservoir and hydraulic fracture characterization*. J. Nat. Gas Sci. Eng. 31, 612-657.

28. Coffman, V.R. (2007). *Macroscopic Effects of Atomic Scale Defects in Crystals: Grain Boundary Fracture and Brittle-Ductile Transitions.* Cornell University, Doctoral Dissertation

29. Cosenza, P., A. Ghorbani, A. Revil, M. Zamora, M. Schmutz, D. Jougnot, and N. Florsch (2008). *A physical model of the low-frequency electrical polarization of clay-rocks, J. Geophys. Res.*, **113**,

30. Cosenza, P., A. Ghorbani, N. Florsch, and A. Revil, (2007). *Effects of drying on the low-frequency electrical properties of Tournemire argillites,* Pure Appl. Geophys., **164**(10), 2043–2066.

31. Cosenza, P., D. Prêt, and M. Zamora, (2015). *Effect of the local clay distribution on the effective electrical conductivity of clay rocks*, J. Geophys. Res. Solid Earth, 120, 145–168

32. Curtis, M., Cardott, B., Sondergeld, C., and Rai, C., (2012). *Development of organic porosity in the Woodford Shale with increasing thermal maturity*. International Journal of Coal Geology. 103. 26–31.

33. Day-Stirrat, R.J., P.B. Flemings., Y. You., and A.C. Aplin., (2012). *The Fabric of Consolidation in Gulf of Mexico Mudstones,* Marine Geology 295-298, pp. 77–85.

34. Deirieh A, Ortega JA, Ulm F-J, Abousleiman YN., (2012). *Nanochemomechanical assessment of shale: a coupled WDS-indentation analysis*. Acta Geotech. 2012;7(4):271-295

35. Delafargue, A., and F. J. Ulm., (2004). *Explicit approximations of the indentation modulus of elastically orthotropic solids for conical indenters.* International Journal of Solids and Structures, 41(26), 7351-7360.

36. Denry, I.L., Holloway, J.A., (2004). *Elastic constants, Vickers hardness, and fracture toughness of fluorrichterite-based glass-ceramics*. Dental Materials 20 (3), 213–219.

37. Derjaguin, B. and Landau, L. (1941). T*heory of the stability of strongly charged*

lyophobic sols and of the adhaension of strongly charged particles in solutions of electrolytes. Acta Physicochimica U.R.S.S., 15(6), 633-662.

38. Dewhurst, D.N., Aplin, A.C. and Sarda, J.P., (1999). *Influence of clay fraction on pore-scale properties and hydraulic conductivity of experimentally compacted mudstones*, Journal of Geophysical Research, 104(B12), pp. 29261–29274.

39. Dewhurst, D.N., Aplin, A.C., Sarda, J.-P. and Yang, Y., (1998). *Compaction-driven evolution of porosity and permeability in natural mudstones: An experimental study,* Journal of Geophysical Research: Solid Earth,103, pp. 651–661.

40. Dewhurst, D.N., Siggins, A.F., Kuila, U., Clennell, M.B., Raven, M.D., Nordgård-Bolås, H.M., (2008). *Elastic, geomechanical and petrophysical properties of shales,* Proceedings of American Rock Mechanics Association Symposium. Paper ARMA 08-208, 12p.

41. Diaz-Perez, A., Cortes-Monroy, I., Roegiers, J.C., (2007). *The role of water/clay interaction in the shale characterization*. Journal of Petroleum Science and Engineering, 58(1-2), pp. 83-98.

42. Dornberger-Schiff, K., Durovic, S., (1975). *OD [order–disorder]-interpretation of kaolinite-type structures. I. Symmetry of kaolinite packets and their stacking possibilities*. Clays and Clay Minerals 23, 219–229.

43. Drever, J. I., (1982). *The geochemistry of natural waters. Prentice-Hall, Inc., Englewood Cliffs,* N.J. 388 p, Limnology and Oceanography, 28.

44. Du, H., and M. Radonjic, (2018). *Comparison of Micro/Nano-Indentation Results for Pottsville and Marcellus Shale.* Paper 18-805 prepared for 52nd US Rock Mechanics/Geomechanics Symposium, 17-20 June, Seattle, Washington

45. Du, H., and M. Radonjic, (2019). *The Mechanism of Fracture Initiation and Propagation in Shale.* Paper prepared for presentation at the 53rd US Rock Mechanics / Geomechanics Symposium held in New York City, USA, 23–26 June 2019.

46. Du, H., M. Radonjic., and A. Olabode, (2017a). *Impact of Clay Mineralogy on Micro Geomechanics of Shale Caprocks*. Paper ARMA 17-700 prepared to present at the 51th US Rock Mechanics / Geomechanics Symposium held in San Francisco, CA, USA, 25-28 June 2017.

47. Du, H., K. Carpenter, D. Hui, and M. Radonjic, (2017b). *Microstructure and Micromechanics of Shale Rocks: Case Study of Marcellus Shale*. Facta Universitatis, Series: Mechanical Engineering, Vol. 15 Issue 2, p331-340. 10p.

48. Du, H., R. Guo, and M. Radonjic, (2015). *Microstructure and Micromechanics of Wellbore Cements under Compression and Thermal Loading.* Paper ARMA 15-498 prepared to present at the 49th US Rock Mechanics / Geomechanics Symposium held in San Francisco, CA, USA, 28 June- 1 July 2015.

49. Elston, H. (2014). *Mineralogical and Geochemical Assessment of the Eagle Ford Shale*. Thesis. The Ohio State University

50. Emmanuel, S., L.M. Anovitz, and R.J. Day-Stirrat, (2015). *Effects of Coupled Chemo-Mechanical Processes on the Evolution of Pore-Size Distributions in Geological Media.* Rev Mineral Geochem, 2015. 80: p. 45-60.

51. Ettensohn, F.R., and Barron, L.S., (1982). *A tectonic-climatic approach to the deposition of the Devonian-Mississippian black-shale sequence of North America*; Proceedings of the 1982 Eastern oil shale symposium: Proceedings - Eastern Oil Shale Symposium, v. 1982, pp. 5-37.

52. Ferrari, A.F. Gualtieri, (2006). *The use of illitic clays in the production of stoneware tile ceramics*, Applied Clay Science, Volume 32, Issues 1–2, Pages 73-81.

53. Finkin E.F. (1974). E*xamination of abrasion Resistance Criteria for Some Ductile Metals*. Journal of Lubrication Technology 1974;96(2) 210-214.

54. Fisher, G. W., Pettijohn, F. J., Reed Jr., J.C., and Weaver, K. N. (Eds.), (1970). Studies on Appalachian Geology: Central and Southern, Interscience (Wiley), New York, US, p. 460.

55. Gaus, I., (2010). *Role and impact of CO2-rock interactions during CO2 storage in sedimentary rocks*: International Journal of Greenhouse Gas Control, v. 4, p. 73-89.

56. George W., (2016). *Frac Fluids on Organic Shales: What We Know, What We Don't, and What Can We Do About It*. SPE Asia Pacific Hydraulic Fracturing Conference

57. Glinicki, M., Zielinski, M. (2004). *Depth-sensing Indentation Method for Evaluation of Efficiency of Secondary Cementitious Materials.* Cement and Concrete Research 34: 721–724.

58. Global CCS Institute, (2015). The Global Status of CCS: 2015, Summary Report, Melbourne, Australia.

59. Global CCS Institute, (2019). The Global Status of CCS: 2019, Summary Report, Madrid, Spain.

60. Gong, J.; Lipomi, D. J.; Deng, J.; Nie, Z.; Chen, X.; Randall, N. X.; Nair, R.; Whitesides, G. M. (2010). *Micro- and Nanopatterning of Inorganic and Polymeric Substrates by Indentation Lithography*, Nano Lett, 10, 2702.

61. Gouy. M., (1910). *Sur la constitution de la charge électrique à la surface d'un électrolyte*. J. Phys. Theor. Appl., 9 (1), pp.457-468

62. Goodwin, K.J., Crook, R.J. (1992). *Cement Sheath Stress Failure*. SPE Drill & Compl 7 (4): 291-296. SPE 20453-PA.

63. Heath, J. E., T. A. Dewers., B. J. O. L McPherson., R. Petrusak., T. C. Chidsey. Jr., A. J. Rinehart., and P. S. Mozley., (2011). *Pore networks in continental and marine mudstones: Characteristics and controls on sealing behavior.* Geosphere 7, 429-454.

64. Heath, J. E., T. A. Dewers., B. J. O. L. McPherson., M. B. Nemer., and P. G. Kotula., (2012). *Pore-lining phases and capillary breakthrough pressure of mudstone caprocks: Sealing efficiency of geologic CO2 storage sites*. Int. J. Greenhouse Gas Control, 11, 204-220.

65. Hentz, T. F., Ambrose, W. A., and Smith, D. C., (2014). *Eaglebine play of the southwestern East Texas basin: Stratigraphic and depositional framework of the Upper Cretaceous (Cenomanian-Turonian) Woodbine and Eagle Ford Groups*: AAPG Bulletin, v. 98, p. 2551-2580.

66. Hise, Charles Richard Van., (1896). *Principles of North American Pre-Cambrian Geology*. U.S. Government Printing Office.

67. Ho, N.C., D.R. Peacor., and B.A. Van der Pluijm., (1995). *Reorientation mechanisms of phyllosilicates in the mudstone-to-slate transition at Lehigh Gap, Pennsylvania.* Journal of Structural Geology, 17, 345-356.

68. Hosterman, J.W. and S.H. Patterson. (1992). *Bentonite and Fuller's earth resources of the United States*. U.S. Geological Survey Professional Paper 1522. United States Government Printing Office, Washington D.C., USA.

69. Hosterman, J.W., Whitlow, S.I., (1983). *Clay Mineralogy of Devonian Shales in the Appalachian Basin,* Geological Survey Professional Paper 1298, United States Government Printing Office, Washington, 31p.

70. Howard, J.J. (1981). *Lithium and potassium saturation of illite–smectite clays from interlaminated shales and sandstones*. Clay and Clay Mineral., 29, 136–142

71. Hudson, J.A., (2008). *The future for rock mechanics and the ISRM*. Proceedings of the 5th Asian Rock Mech. Symposium (ARMS5), 25–26 Nov. 2008, Tehran, Iran, p. 105-118.

72. Hussain, S.A., Demirci, S., and Özbayoğlu, G., (1996). *Zeta Potential Measurements on Three Clays from Turkey and Effects of Clays on Coal Flotation*, Journal of Colloid and Interface Science, Volume 184, Issue 2, 1996, Pages 535-541,

73. Iverson, B., Darbe, R., McMechan, D. (2008). *Evaluation of Mechanical Properties of Cements*. Paper ARMA-08-293 presented at 42nd US Rock Mechanics Symposium, San Francisco, CA.

74. Jennings, H., Bullard, J., Thomas, J., Andrade, J., Chen, J., and Scherer, G., (2008). *Characterization and Modeling of Pores and Surfaces in Cement Paste: Correlation to Processing and Properties*. Journal of Advanced Concrete Technology. Vol.6, No. 1, p.5-29..

75. Jennings, H., Thomas, J., Gevrenov, J., Constantinides, G., Ulm, F., (2007). *A multi-technique investigation of nanoporosity of cement paste*. Cement and Concrete Research 37 (2007) 329 – 336.

76. Jo, H., Gray, K.E., (2010). *Mechanical Behavior of Concentric Casing, Cement, and Formation Using Analytical and Numerical Method*s. Paper ARMA 10-142 presented at the 44th US Rock Mechanics Symposium and 5th U.S.-Canada Rock Mechanics Symposium, Salt Lake City, UT.

77. Josh, M., L. Esteban., C. Delle Piane., J. Sarout., D.N. Dewhurst., and M.B. Clennell., (2012). *Laboratory characterization of shale properties*, Journal of Petroleum Science and Engineering, Volumes 88–89, Pages 107-124

78. Katsube, T., and Klassen, R., Das, Y., Ernst, R., Calvert, T., Cross, G., Best, M.E., DiLabio, R., Connell, S., (2003). *Prediction and validation of soil electromagnetic characteristics for application in landmine detection.* Proceedings of SPIE - The International Society for Optical Engineering

79. Khilar, K. C. and Fogler, H. S., (1998). Migration of Fines in porous media, Kluwer Academic Publishers.

80. Khor, K.A., Li, H., Cheang, P., (2003). *Processing-microstructureproperty relations in HVOF sprayed calcium phosphate based bioceramic coatings*. Biomaterials 24 (13), 2233–2243

81. King, H.(last accessed 2019) Hydraulic Fracturing of Oil & Gas Wells Drilled in Shale. Online article. https://geology.com/articles/hydraulic-fracturing/

82. King, H.(last accessed 2019) Shale is the most abundant sedimentary rock and is in sedimentary basins worldwide. Online article. https://geology.com/rocks/shale.shtml

83. Koteeswaran, S., Habibpour, M., Puckette, J., Pashin, J., and Clark, P., (2018). *Characterization of shale–fluid interaction through a series of immersion tests and rheological studies*. J Petrol Explor Prod Technol 8: 1273.

84. Kruzic, J.J. D.K. Kim, K.J. Koester, R.O. Ritchie, (2009). *Indentation techniques for evaluating the fracture toughness of biomaterials and hard tissues*, Journal of the Mechanical Behavior of Biomedical Materials, Volume 2, Issue 4,2009, Pages 384-395,

85. Kumar, V., C. H. Sondergeld., and C. S. Rai., (2012). *Nano to macro mechanical characterization of shale*: Presented at SPE Annual Technical Conference and Exhibition, SPE 159804

86. Kupresan, D., Heathman, J., Radonjic, M. (2013). *Application of a New Physical Model of Expandable Casing Technology in Mitigation of Wellbore Leaks.* Journal of Canadian Energy Technology & Innovation (CETI), Vol. 1, No. 5.

87. Kupresan, D., Heathman, J., Radonjic, M. (2014). *Casing Expansion as a Promising*

Solution for Microannular Gas Migration. SPE Drilling & Completion, 168056-PA.

88. Kupresan, D, (2014). *Experimental assessment of expandable casing technology as a solution for microannular gas flow*. LSU Master's Theses. *1265.*

89. Lal, M. (1999). *Shale stability: drilling fluid interaction and shale strength*. Paper presented at the SPE Asia Pacific oil and gas conference and exhibition, Jakarta, Indonesia

90. Laugier, M.T., (1985). *The elastic plastic indentation of ceramics*. Journal of Materials Science Letters 4 (12), 1539–1541.

91. Laugier, M.T., (1987). *New formula for indentation toughness in ceramics.* Journal of Materials Science Letters 6 (3), 355–356.

92. Lawn, B.R., Evans, A.G., Marshall, D.B., (1980). *Elastic/plastic indentation damage in ceramics: The median/radial crack system*. Journal of the American Ceramic Society 63 (9-10), 574–581.

93. Li, D., and B. Altstatt. (2014). *Elastic-Plastic Response of Polymer Coating under Repetitive Impact*. Nanovea

94. Li, Qinghui., M. Chen., Y. Zhou., Y. Jin., F. P. Wang., and R. Zhang., (2013). *Rock Mechanical Properties of Shale Gas Reservoir and their Influences on Hydraulic Fracture.* International Petroleum Technology Conference held in Beijing, China, 26–28 March 2013.

95. Li, Z., A. Ghosh, A. S. Kobayashi, and R. C. Bradt, (1989). *Indentation Fracture Toughness of Sintered Silicon Carbide in the Palmqvist Crack Regime*, J. Amer. Ceram. Soc., 72 [6] (1989) 904-911.

96. Lindgreen H, Jacobsen H, Jakobsen HJ. (1991). *Diagenetic structural transformations in North Sea Jurassic illite/smectite*. Clays Clay Miner 39:54-69.

97. Liu, K., M. Ostadhassan., and B. Bubach., (2016). *Applications of nano-indentation methods to estimate nanoscale mechanical properties of shale reservoir rocks,* Journal of Natural Gas Science and Engineering, Volume 35, Part A, Pages 1310-1319,

98. Lonardelli, I., W. Hans-Rudolf., and Y. Ren., (2007). *Preferred orientation and elastic anisotropy in shale.* Geophysics 72:2, D33-D40

99. Lynch, F.L. (1997). *Frio shale mineralogy and the stoichiometry of the smectite-to-illite reaction: the most important reaction in clastic sedimentary diagenesis.* Clays and Clay Minerals, 45, 618_631.

100. Ma, D.J., Sun, L., and Wang, L.Z. (2018). *A New Formula for Evaluating Indentation Toughness in Ceramics,* Exp Mech 58: pp 177–182

101. MacFarlane, James R. (1890). *An American Geological Railway Guide, giving the Geological Formation at every Railway Station; with Notes on interesting Places on the Routes, and a Description of each of the Formations*. Nature **19,** 287

102. Mares, V.M., and A.K. Kronenberg., (1993). *Experimental deformation of muscovite.* J. Struct. Geol. 15, 1061–1075.

103. Mavko, G., T. Mukerji., and J. Dvorkin., (2009). The rock physics handbook, 2nd ed.: Cambridge University Press.

104. Mbia, E. N., P. Frykman., C. M. Nielsen., I. L. Fabricius., G..E. Pickup., and C. Bernstone., (2014). *Caprock compressibility and permeability and the consequences for pressure development in CO2 storage sites*. Int. J. Greenhouse Gas Control, 22, 139-153

105. McColm, I. J, (2013). *Ceramic Hardness.* Springer Science & Business Media.

106. McWhorter, D. B., and Sunada, D. K., (1977). *Ground-Water Hydrology and Hydraulics. Water Resources Publications*, Highlands Ranch, Colorado..

107. Meier, L.P., Kahr, G., (1999). *Determination of the Cation Exchange Capacity of clay minerals based on the Complexes of the Copper(II) ion with Triethylenetetramine and Tetraethylenepentamine*, Clays and Clay Miner., 47, 3, 386–388.

108. Mesri, G. and Olson, R.E., (1971). *Mechanisms Controlling the Permeability of Clays*, Clays and Clay Minerals, 19, pp. 151-158.

109. Mighani, S., C. Sondergeld., and C. Rai., (2016). *Observations of Tensile Fracturing of Anisotropic Rocks*. SPE Journal. 10.2118/1934272-PA.

110. Miller, C. K., Waters, G. A., and Rylander, E. I., (2011). *Evaluation of Production Log Data from Horizontal Wells Drilled in Organic Shales*. Society of Petroleum Engineers 144326.

111. Missana, T., and Adell, A., (2000). *On the Applicability of DLVO Theory to the Prediction of Clay Colloids Stability*, In Journal of Colloid and Interface Science, Volume 230, Issue 1, 2000, Pages 150-156

112. Mitchell, J.K., (1993). Fundamentals of Soil Behavior. John Wiley & Sons, Inc., 2nd Edition, New York, Chichester, Brisbane, Toronto, Singapore, 437 p.

113. Mitchell, J.K. and Soga, K., (2005). Fundamentals of Soil Behavior, 3rd. John Wiley & Sons, Inc., Hoboken, NJ.

114. Mojid M.A. (2011) *Diffuse Double Layer (DDL)*. In: Gliński J., Horabik J., Lipiec J. (eds) Encyclopedia of Agrophysics. Encyclopedia of Earth Sciences Series. Springer, Dordrecht.

115. Mondol, N.H., Jahren, J., Bjorlykke, K., and Brevik, I., (2008), *Elastic properties of clay minerals*, The Leading Edge, 27, pp. 758-770.

116. Moore, D.M., Reynolds, R.C. Jr., (1989). *X-Ray Diffraction and the Identification and Analysis of Clay Minerals*. Oxford University Press, New York.

117. Mueller, M., and Amro, M. (2015). *Indentaion Hardness for Improved Proppant Embedment Prediction in Shale Formations*. Society of Petroleum Engineers

118. Murtey, M. D., and P. Ramasamy., (2016). *Sample preparations for scanning electron microscopy—life sciences*. In: Modern Electron Microscopy in Physical and Life Sciences, edited by M. Janecek. InTech.

119. Mutschler, T., T. Triantafyllidis., and K. Balthasar., (2009). *Geotechnical investigations of cap rocks above CO2-reservoirs*. Energy Procedia, 1, 3375-3382.

120. Naik, G. (2007). Tight Gas Reservoirs-An Unconventional Natural Energy Source for the Future, from WWW.SUBLETTE-SE.ORG.

121. Nakagawa, S., J. Rutqvist, T. Kneafsey, and K. Kim (2017). *Sustainability of Hydraulic Fracture Conductivity in Ductile and Expanding Shales* Carbon Storage and Oil and Natural Gas Technologies Review Meeting August 1-3, 2017

122. Nasrazadani, S., and S. Hassani, (2016). *Modern analytical techniques in failure analysis of aerospace, chemical, and oil and gas industries*, Handbook of Materials Failure Analysis with Case Studies from the Oil and Gas Industry

123. Neasham, J. W. (1977). *The Morphology of Dispersed Clay in Sandstone Reservoirs and Its Effect on Sandstone Shaliness, Pore Space and Fluid Flow Properties*. Society of Petroleum Engineers. SPE-6858-MS

124. Nelson, E.B., Guillot, D. (2006). Well Cementing, second edition. Schlumberger, TX.

125. Nelson, P. H., (2009). *Pore-throat sizes in sandstones, tight sandstones, and shales*. The American Association of Petroleum Geologists. AAPG Bulletin, Vol. 93, No. 3, p. 329–340

126. Nelson, S. A.,(2015). *Phyllosilicates (Micas, Chlorite, Talc, & Serpentine).* Mineralogy, EENS 2110. Tulane University

127. Nemecz, E., (1981). Clay Minerals. Akademiai Kiado, Budapest.

128. Nordquist, J.W. (1953). *Mississippian stratigraphy of northern Montana,*Billings Geological Society, 4th Annual Field Conference Guidebook, pp. 68–82.

129. Olabode, A. and M. Radonjic, (2017). *Fracture Conductivity Modelling in Experimental Shale Rock Interactions with Aqueous CO2*, Energy Procedia, Volume 114,

Pages 4494-4507,

130. Olabode, Abiola Olukola, (2017). *Diagenesis and Formation Stress in Fracture Conductivity of Shaly Rocks; Experimental-Modelling Approach in CO2-Rock Interactions*. LSU Doctoral Dissertations. 4105.

131. Oliver, W. and Pharr, G., (1992). *An improved technique for determining hardness and elastic modulus using load and displacement sensing indentation experiments*, Journal of Materials Research, 7(6), pp. 1564-1583.

132. Oliver, W., and G. Pharr., (2004). *Measurement of hardness and elastic modulus by instrumented indentation: Advances in understanding and refinements to methodology*. Journal of Materials Research, 19(1), pp. 3-20.

133. Pant, R.R., (2013). *Nanoindentation Characterization of Clay Minerals and Clay-Based Hybrid Bio-Geomaterials.* Ph.D. Thesis. Louisiana State University; Baton Rouge, LA,

134. Pawley, A.R., Clark, S.M., and Chinnery, N.J., (2002). *Equations of state measurements of chlorite, pyrophyllite, and talc*, American Mineralogist, 87(8-9), pp. 1172-1182.

135. Perry, E. A., Jr, and Hower, J., (1970). *Burial diagenesis in Gulf Coast pelitic sediments*: Clays & Clay Minerals, v. 18, p. 165-177

136. Perry, E. A., Jr, and Hower, J., (1972). L*ate-stage dehydration in deeply buried pelitic sediments:* American Association of Petroleum Geologists Bulletin, v. 56, p. 2013-2021.

137. Pintaude, G., (2013). *Introduction of the Ratio of the Hardness to the Reduced Elastic Modulus for Abrasion.* Tribology - Fundamentals and Advancements, Edition:1 . Publisher: Intech.

138. Pitman, J.K., Pashin, J.C., Hatch, J.R, Goldhaber, M.B, (2003). *Origin of minerals in joint and cleat systems of the Pottsville Formation, Black Warrior basin, Alabama: Implications for coalbed methane generation and production*. AAPG Bulletin, 2003. 87(5): p. 713-731.

139. Plancon, A., Giese, R.F. Jr., Snyder, R., Drits, V.A., Bukin, A.S., (1989). *Stacking faults in the kaolin-group minerals: defect structures of kaolinite*. Clays and Clay Minerals 37, 203–210.

140. Ponton, C. B., and R. D. Rawlings, (1989). *Dependence of the Vickers Indentation Fracture Toughness on the Surface Crack Length*, Br. Ceram. Trans. J., 88 (1989) 83-90.

141. Pusch, R. and Yong, R.N., (2006). *Microstructure of Smectite Clays and Engineering Performance*. Taylor & Francis, London & New York.

142. Quinn, G. (2006). *Fracture Toughness of Ceramics by the Vickers Indentation Crack Length Method: A Critical Review.* Ceramic Engineering and Science Proceedings 27(3):45 – 62

143. Quinn, G. D., and Salem, J. A., (2002). *Effect of Lateral Cracks Upon Fracture Toughness Determined by the Surface Crack in Flexure Method*, J. Am. Ceram. Soc., 85 [4] (2002) pp. 873-80.

144. Quinn, G.D., and Bradt, R.C., (2007). *On the Vickers indentation fracture toughness test.* Journal of the American Ceramic Society 90 (3), 673–680

145. Radonjic, M., Kupresan, D. (2014). *Mechanical Expansion of Steel Tubing as a Solution to Leaky Wellbores*. Journal of Visualized Experiments.

146. Radonjic, M., H. Du, D. Kupresan and A. Olabode., (2015). *Preliminary Comparative Evaluation of Wellbore Cement and Shale as the Major Subsurface Hydraulic Barriers: Micromechanics and Microstructures.* 14th International Congress on the Chemistry of Cement (ICCC), Beijing, China.

147. Randall, N., Vandamme, M., and Ulm, F. (2009). *Nanoindentation analysis as a two-dimensional tool for mapping the mechanical properties of complex surfaces*. Journal of Materials Research, *24*(3), 679-690.

148. Raysoni, N., and Weaver, J. (2013). *Understanding Geochemical Interaction of Proppant-Formation For Improved Conductivity of Hydraulic Fractures*. American Rock Mechanics Association.

149. Rickman, R., Mullen, M. J., Petre, J. E., Grieser, W. V., and Kundert, D. (2008). *A Practical Use of Shale Petrophysics for Stimulation Design Optimization: All Shale Plays Are Not Clones of the Barnett Shale.* Society of Petroleum Engineers.

150. Ross, D., and Bustin, R. M. (2009). T*he importance of shale composition and pore structure upon gas storage potential of shale gas reservoirs*. Marine and Petroleum Geology - MAR PETROL GEOL. 26. 916-927

151. Ryan, J. N., and Gschwend, P.M., (1992). *Effect of iron diagenesis on the transport of colloidal clay in an unconfined sand aquifer,* Geochimica et Cosmochimica Acta, Volume 56, Issue 4, Pages 1507-1521

152. Rybacki, E., A. Reinicke., T. Meier., M. Makasi., G. Dresen., (2015). *What controls the mechanical properties of shale rocks? – Part I: Strength and Young's modulus,* Journal of Petroleum Science and Engineering, Volume 135, Pages 702-722,

153. Şakar-Deliormanli, A., and Güden, M., (2005). *Microhardness and fracture toughness of dental materials by indentation method,* J. Biomed. Mater. Res., 76B: 257-264.

154. Samsuri, A.B., Shadizadeh, S.R., and Zoveidavianpoor, M. (2012). *A Review on Conventional Candidate-well Selection for Hydraulic Fracturing in Oil and Gas Wells*. International Journal of Engineering and Technology Volume 2 No. 1.

155. Santamarina, J. C., Klein, K. A. and Fam, M. A., (2001). Soils and Waves. John Wiley & Sons, New York.

156. Schoonheydt, R.A., and Johnston, C.T., (2006). Chapter 3 Surface and Interface Chemistry of Clay Minerals, Editor(s): Faïza Bergaya, Benny K.G. Theng, Gerhard Lagaly, In Developments in Clay Science, Elsevier, Volume 1, 2006, Pages 87-113,

157. Shaw, D. B. and C. E. Weaver., (1965). *The Mineralogical Composition of Shales*. Journal of Sedimentary Petrology 35: 213–222.

158. Somasundaran, P., and Agar, G.E. (1967). *The zero point of charge of calcite*, Journal of Colloid and Interface Science, Volume 24, Issue 4,1967, Pages 433-440.

159. Sone, H., and M. D. Zoback., (2013). *Mechanical properties of shale gas reservoir rocks — Part 1: Static and dynamic elastic properties and anisotropy*. Geophysics, 78, D381–D392

160. Sposito, G., (1989). The Chemistry of Soils. Oxford University Press, New York.

161. Stephens, M., Gomez-Nava, S., Churan, M. (2009). *Laboratory Methods To Assess Shale Reactivity With Drilling Fluids.* National Technical Conference & Exhibition (AADE), New Orleans, LA.

162. Stern, O. *Z.* (1924). *Electrochem*, 30, 508

163. Suarez-Rivera, R., and E. Fjær., (2013). *Evaluating the poroelastic effect on anisotropic, organic-rich, mudstone systems*. Rock Mech. Rock Eng., 46(3), 569-580.

164. Taylor, H. (1997). Cement Chemistry, second edition. Thomas Telford, London.

165. The clay mineral group, Website. (Last access: Jan.2018). http://www.galleries.com/Clays_Group

166. Thiercelin, J., Dargaud, B., Baret, J., and J. Rodriquez, W., (1998). *Cement Design Based on Cement Mechanical Response. SPE Drilling & Completion* - SPE DRILL COMPLETION. 13. 266-273.

167. Thomas, J., and Jennings, H., (2003). *Changes in the size of pores during shrinkage (or expansion) of cement paste and concrete*. Cement and Concrete Research 33, 1897-1900.

168. Tournassat, C., Bourg, I. C., Bergaya, F., & Steefel, C. I., (2015). *Natural and Engineered Clay Barriers*. Elsevier.

169. Towe, K.M. (1962). *Clay mineral diagenesis as a possible source of silica cement in sedimentary rocks*. Journal of Sedimentary Petrology, 32, 26_28.

170. Ulm, F.-J., and Y. Abousleiman., (2006). *The nanogranular nature of shale*. Acta Geotechnica, 1(2), 77-88.

171. University of Alabama: (2009). *Site Characterization for CO2 Storage from Cola-fired Power Facilities in the Black Warrior Basin of Alabama*. Recovery Act Proposal. 2009: p. 41.

172. U.S. Geological Survey Black Warrior Basin Province Assessment Team, National Assessment Of Oil And Gas Project, U. S. & Geological Survey, U. S. (2007) Geologic assessment of undiscovered oil and gas resources of the Black Warrior Basin Province, Alabama and Mississippi. Reston, Va.: U.S. Geological Survey, Retrieved from the Library of Congress

173. Van de Kamp, P. C. (2008). *Smectite-illite-muscovite transformations, quartz dissolution, and silica release in shales.* Clays and Clay Minerals *;* 56 (1): 66–81.

174. Van Olphen, H. and Fripiat, J.J. (1979). *Data Handbook for Clay Materials and Other Non-Metallic Minerals*. Pergamon Press, Oxford.

175. Van Olphen, H., (1963). *An Introduction to Colloid Chemistry,* John Wiley and Sons Inc., New York

176. Van Oort, E. (2003). *On the physical and chemical stability of shales*. J Petrol Sci Eng 38(3):213–235

177. Van Oort, E., Hale, A.H., Mody, F.K., (1995). *Manipulation of coupled osmotic flows for stabilisation of shales exposed to water-based drilling fluids*. Paper presented at the SPE annual technical conference and exhibition

178. Velez, K., S. Maximilien., D. Damidot., G. Fantozzi., and F. Sorrentino., (2001). *Determination by nanoindentation of elastic modulus and hardness of pure constituents of Portland cement clinker.* Cement and Concrete Research, 31(4), 555-561.

179. Vernik, L., and A. Nur., (1992). *Ultrasonic velocity and anisotropy of hydrocarbon source rocks.* Geophysics, 57, 727–735

180. Vernik, L., and X. Liu., (1997). *Velocity anisotropy in shales: a petrophysical study.* Geophysics, 62, 521–32

181. Verwey, E. J. W., Overbeek, J. T. G. and Nes, K. V., (1948). *Theory of the stability of lyophobic colloids; the interaction of sol particles having an electric double layer*. Elsevier Pub. Co., New York,.

182. Veytskin, Y.B., Vamsi K. Tammina, Christopher P. Bobko, Patrick G. Hartley, Michael B. Clennell, David N. Dewhurst, Raymond R. Dagastine, (2017).

Micromechanical characterization of shales through nanoindentation and energy dispersive x-ray spectrometry, Geomechanics for Energy and the Environment, Volume 9, 2017, Pages 21-35.

183. Vlassak, J. (1993). *Indentation modulus of elastically anisotropic half spaces*. Philosophical Magazine A, 67(5), 1045-1056.

184. Wang, Z., H. Wang., and M.E. Cates., (2001). *Effective elastic properties of clays*: Geophysics, 66, 428–440.

185. Wayne M. Bundy, Joseph N. Ishley, (1991). *Kaolin in paper filling and coating,* Applied Clay Science, Volume 5, Issues 5–6, 1991, Pages 397-420,

186. Weaver, J. D., Rickman, R. D., Luo, H., and Logrhy, R. (2009). *A Study of Proppant Formation Reactions*. Society of Petroleum Engineers

187. Wilford, John Noble. (1998). *Revolutions in Mapping*. National Geographic (February 1998): 6-39

188. Williams, K., (2012). *The Permeability of Overpressure Shale Seals and of Source Rock Reservoirs is the Same*. AAPG 2012 Annual Convention and Exhibition, Long Beach, California, 22-25 April

189. Worden, R.H., D. Charpentier., Q. Fisher., A.C.. Aplin., (2005). *Fabric development and the smectite to illite transition in Upper Cretaceous mudstones from the North Sea: an image analysis approach. In: Shaw, R.P. (Ed.), Understanding the Micro to Macro Behaviour of Rock–Fluid Systems*. Geological Society Special Publication, 249, pp. 103–114

190. Xie, Q., Saeedi, A., Pooryousefy, E., and Liu, Y., (2016). *Extended DLVO-based estimates of surface force in low salinity water flooding*, Journal of Molecular Liquids, Volume 221, 2016, Pages 658-665,

191. Xu, J.G., Z. Qiu., X. Zhao., Y. Zhang., G. Li., and W. Huang., (2018). *Application of nanopolymer emulsion for inhibiting shale self-imbibition in water-based drilling fluids*. Journal of Surfactant and Detergent, Vol 21, pages 155–164

192. Yang, Y. and Aplin, A.C., (2007). *Permeability and petrophysical properties of 30 natural mudstones*, Journal of Geophysical Research, 112(B3), B03206.

193. Yin, X., Yan, L., Liu, J., Xu, Z., and Miller, J.D., (2013). *Anisotropic Surface Charging of Chlorite Surfaces*. Clays and Clay Minerals ; 61 (2): 152–164

194. Yu, M., Zhou, S., Li, J., Li, Y., Chen, K., Zhang, Y., Fu, D. (2017). *Pyrolysis characteristics analysis of Chang-7 oil shale using thermal analysis and pyrolysis-gas chromatograph-mass spectrometry*. Energy Exploration & Exploitation.

195. Zendehboudi, S., and Bahadori, A., (2016). Shale Oil and Gas Handbook: Theory,

Technologies, and Challenges.

196. Zhang, J., (2014). *Fracture Conductivity Damage by Water in Shale Formations*. Society of Petroleum Engineers.

197. Zhao, L., Qin, X., Han, D., Geng, J., Yang, Z., and Cao, H., (2016). *Rock-physics modeling for the elastic properties of organic shale at different maturity stages*. Geophysics 81(5):D527–D541

198. Zhao, H., Givens, N., and Curtis, B., (2007). T*hermal maturity of the Barnett Shale determined from well-log analysis*. Aapg Bulletin - AAPG BULL. 91. 535-549.

199. Zvyagin, B.B., and Drits, V.A., (1996). *Interrelated features of structure and stacking of kaolin mineral layers*. Clays and Clay Minerals 44, 297–303.

VITA

Hui Du was born in Weinan, Shaanxi, China on July 9th, 1988. He graduated with a Bachelor of Science degree in Petroleum Engineering from both China University of Petroleum Beijing and University of Alaska Fairbanks in July 2011. In addition, he obtained a Master of Science degree in Petroleum Engineering from Missouri University of Science and Technology in May 2013.

Hui Du joined the Ph.D. program of the Craft & Hawkins Department of Petroleum Engineering at Louisiana State University in January 2014 as a Graduate Research and Teaching Assistant. His research is focused on the mechanical characterization of hydraulic barrier materials including wellbore cement and shales. Mr.. Du expects to finish his study and receive the degree of Doctor of Philosophy in Petroleum Engineering in spring 2020.